

# Directional Search for Persistent Gravitational Waves: Results from the First Part of LIGO-Virgo-KAGRA's Fourth Observing Run

A. G. Abac<sup>1</sup>, I. Abouelfettouh,<sup>2</sup> F. Acernese,<sup>3,4</sup> K. Ackley<sup>5</sup>, C. Adamcewicz<sup>6</sup>, S. Adhicary<sup>7</sup>,  
D. Adhikari,<sup>8,9</sup> N. Adhikari<sup>10</sup>, R. X. Adhikari<sup>11</sup>, V. K. Adkins,<sup>12</sup> S. Afroz<sup>13</sup>, A. Agapito,<sup>14</sup> D. Agarwal<sup>15</sup>,  
M. Agathos<sup>16</sup>, N. Aggarwal,<sup>17</sup> S. Aggarwal,<sup>18</sup> O. D. Aguiar<sup>19</sup>, I.-L. Ahrend,<sup>20</sup> L. Aiello<sup>21,22</sup>, A. Ain<sup>23</sup>,  
P. Ajith<sup>24</sup>, T. Akutsu<sup>25,26</sup>, S. Albanesi<sup>27,28</sup>, W. Ali,<sup>29,30</sup> S. Al-Kersh, <sup>8,9</sup> C. Alléné,<sup>31</sup> A. Allocca<sup>32,4</sup>,  
S. Al-Shammari,<sup>33</sup> P. A. Altin<sup>34</sup>, S. Alvarez-Lopez<sup>35</sup>, W. Amar,<sup>31</sup> O. Amarasinghe,<sup>33</sup> A. Amato<sup>36,37</sup>,  
F. Amicucci<sup>38,39</sup>, C. Amra,<sup>40</sup> A. Ananyeva,<sup>11</sup> S. B. Anderson<sup>11</sup>, W. G. Anderson<sup>11</sup>, M. Andia<sup>41</sup>,  
M. Ando,<sup>42</sup> M. Andrés-Carcasona<sup>43</sup>, T. Andrić<sup>44,45,8,9</sup>, J. Anglin,<sup>46</sup> S. Ansoldi<sup>47,48</sup>, J. M. Antelis<sup>49</sup>,  
S. Antier<sup>41</sup>, M. Aoumi,<sup>50</sup> E. Z. Appavuravther,<sup>51,52</sup> S. Appert,<sup>11</sup> S. K. Apple<sup>53</sup>, K. Arai<sup>11</sup>, A. Araya<sup>42</sup>,  
M. C. Araya<sup>11</sup>, M. Arca Sedda<sup>44,45</sup>, J. S. Areeda<sup>54</sup>, N. Aritomi,<sup>2</sup> F. Armato<sup>29,30</sup>, S. Armstrong<sup>55</sup>,  
N. Arnaud<sup>56</sup>, M. Arogeti<sup>57</sup>, S. M. Aronson<sup>12</sup>, G. Ashton<sup>58</sup>, Y. Aso<sup>25,59</sup>, L. Asprea,<sup>28</sup> M. Assiduo,<sup>60,61</sup>  
S. Assis de Souza Melo,<sup>62</sup> S. M. Aston,<sup>63</sup> P. Astone<sup>38</sup>, F. Attadio<sup>39,38</sup>, F. Aubin<sup>64</sup>, K. AultONeal<sup>65</sup>,  
G. Avallone<sup>66</sup>, E. A. Avila<sup>49</sup>, S. Babak<sup>20</sup>, C. Badger,<sup>67</sup> S. Bae<sup>68</sup>, S. Bagnasco<sup>28</sup>, L. Baiotti<sup>69</sup>,  
R. Bajpai<sup>70</sup>, T. Baka,<sup>71,37</sup> A. M. Baker,<sup>6</sup> K. A. Baker,<sup>72</sup> T. Baker<sup>73</sup>, G. Baldi<sup>74,75</sup>, N. Baldicchi<sup>76,51</sup>,  
M. Ball,<sup>77</sup> G. Ballardini,<sup>62</sup> S. W. Ballmer,<sup>78</sup> S. Banagiri<sup>6</sup>, B. Banerjee<sup>44</sup>, D. Bankar<sup>79</sup>, T. M. Baptiste,<sup>12</sup>  
P. Baral<sup>10</sup>, M. Baratti<sup>80,81</sup>, J. C. Barayoga,<sup>11</sup> B. C. Barish,<sup>11</sup> D. Barker,<sup>2</sup> N. Barman,<sup>79</sup> P. Barneo<sup>82,83,84</sup>,  
F. Barone<sup>85,4</sup>, B. Barr<sup>86</sup>, L. Barsotti<sup>35</sup>, M. Barsuglia<sup>20</sup>, D. Barta<sup>87</sup>, A. M. Bartoletti,<sup>88</sup> M. A. Barton<sup>86</sup>,  
I. Bartos,<sup>46</sup> A. Basalaeu<sup>8,9</sup>, R. Bassiri<sup>89</sup>, A. Basti<sup>81,80</sup>, M. Bawaj<sup>76,51</sup>, P. Baxi,<sup>90</sup> J. C. Bayley<sup>86</sup>,  
A. C. Baylor<sup>10</sup>, P. A. Baynard II,<sup>57</sup> M. Bazzan,<sup>91,92</sup> V. M. Bedakihalé,<sup>93</sup> F. Beirnaert<sup>94</sup>, M. Bejger<sup>95</sup>,  
D. Belardinelli<sup>22</sup>, A. S. Bell<sup>86</sup>, D. S. Bellie,<sup>96</sup> L. Bellizzi<sup>80,81</sup>, W. Benoit<sup>18</sup>, I. Bentara<sup>56</sup>, J. D. Bentley<sup>97</sup>,  
M. Ben Yaala,<sup>55</sup> S. Bera<sup>98,99</sup>, F. Bergamin<sup>33</sup>, B. K. Berger<sup>89</sup>, S. Bernuzzi<sup>27</sup>, M. Beroiz<sup>11</sup>, D. Bersanetti<sup>29</sup>,  
T. Bertheas,<sup>100</sup> A. Bertolini,<sup>37,36</sup> J. Betzwieser<sup>63</sup>, D. Beveridge<sup>72</sup>, G. Bevilacqua<sup>101</sup>, N. Bevens<sup>102</sup>,  
R. Bhandare,<sup>103</sup> R. Bhatt,<sup>11</sup> D. Bhattacharjee<sup>104,105</sup>, S. Bhattacharyya,<sup>106</sup> S. Bhaumik<sup>46</sup>, V. Biancalana<sup>101</sup>,  
A. Bianchi,<sup>37,107</sup> I. A. Bilenko,<sup>108</sup> G. Billingsley<sup>11</sup>, A. Binetti<sup>109</sup>, S. Bini<sup>11,74,75</sup>, C. Binu,<sup>110</sup> S. Biot,<sup>111</sup>  
O. Birnholtz<sup>112</sup>, S. Biscoveanu<sup>96</sup>, A. Bisht,<sup>9</sup> M. Bitossi<sup>62,80</sup>, M.-A. Bizouard<sup>113</sup>, S. Blaber,<sup>114</sup>  
J. K. Blackburn<sup>11</sup>, L. A. Blagg,<sup>77</sup> C. D. Blair,<sup>72,63</sup> D. G. Blair,<sup>72</sup> N. Bode<sup>8,9</sup>, N. Boettner,<sup>97</sup> G. Boileau<sup>113</sup>,  
M. Boldrini<sup>38</sup>, G. N. Bolingbroke<sup>115</sup>, A. Bolliand,<sup>116,40</sup> L. D. Bonavena<sup>46</sup>, R. Bondarescu<sup>82</sup>, F. Bondu<sup>117</sup>,  
E. Bonilla<sup>89</sup>, M. S. Bonilla<sup>54</sup>, A. Bonino,<sup>118</sup> R. Bonnand<sup>31,116</sup>, A. Borchers,<sup>8,9</sup> S. Borhanian,<sup>7</sup> V. Boschi<sup>80</sup>,  
S. Bose,<sup>119</sup> V. Bossilkov,<sup>63</sup> Y. Bothra<sup>37,107</sup>, A. Boudon,<sup>56</sup> L. Bourg,<sup>57</sup> M. Boyle,<sup>120</sup> A. Bozzi,<sup>62</sup> C. Bradaschia,<sup>80</sup>  
P. R. Brady<sup>10</sup>, A. Branch,<sup>63</sup> M. Branchesi<sup>44,45</sup>, I. Braun,<sup>104</sup> T. Briant<sup>121</sup>, A. Brillet,<sup>113</sup> M. Brinkmann,<sup>8,9</sup>  
P. Brockill,<sup>10</sup> E. Brockmueller<sup>8,9</sup>, A. F. Brooks<sup>11</sup>, B. C. Brown,<sup>46</sup> D. D. Brown,<sup>115</sup> M. L. Brozzetti<sup>76,51</sup>,  
S. Brunett,<sup>11</sup> G. Bruno,<sup>15</sup> R. Bruntz<sup>122</sup>, J. Bryant,<sup>118</sup> Y. Bu,<sup>123</sup> F. Bucci<sup>61</sup>, J. Buchanan,<sup>122</sup>  
O. Bulashenko<sup>82,83</sup>, T. Bulik,<sup>124</sup> H. J. Bulten,<sup>37</sup> A. Buonanno<sup>125,1</sup>, K. Burtnyk,<sup>2</sup> R. Busicchio<sup>126,127</sup>,  
D. Buskulic,<sup>31</sup> C. Buy<sup>100</sup>, R. L. Byer,<sup>89</sup> G. S. Cabourn Davies<sup>73</sup>, R. Cabrita<sup>15</sup>, V. Cáceres-Barbosa<sup>7</sup>,  
L. Cadonati<sup>57</sup>, G. Cagnoli<sup>128</sup>, C. Cahillane<sup>78</sup>, A. Calafat,<sup>98</sup> T. A. Callister,<sup>129</sup> E. Calloni,<sup>32,4</sup> S. R. Callos<sup>77</sup>,  
G. Caneva Santoro<sup>43</sup>, K. C. Cannon<sup>42</sup>, H. Cao,<sup>35</sup> L. A. Capistran,<sup>130</sup> E. Capocasa<sup>20</sup>, E. Capote<sup>2,11</sup>,  
G. Capurri<sup>81,80</sup>, G. Carapella,<sup>66,131</sup> F. Carbognani,<sup>62</sup> M. Carlassara,<sup>8,9</sup> J. B. Carlin<sup>123</sup>, T. K. Carlson,<sup>132</sup>  
M. F. Carney,<sup>104</sup> M. Carpinelli<sup>126,62</sup>, G. Carrillo,<sup>77</sup> J. J. Carter<sup>8,9</sup>, G. Carullo<sup>118,133</sup>, A. Casallas-Lagos,<sup>134</sup>  
J. Casanueva Diaz<sup>62</sup>, C. Casentini<sup>135,22</sup>, S. Y. Castro-Lucas,<sup>136</sup> S. Caudill,<sup>132</sup> M. Cavaglià<sup>105</sup>,  
R. Cavalieri<sup>62</sup>, A. Ceja,<sup>54</sup> G. Cella<sup>80</sup>, P. Cerdá-Durán<sup>137,138</sup>, E. Cesarini<sup>22</sup>, N. Chabbra,<sup>34</sup> W. Chaibi,<sup>113</sup>  
A. Chakraborty<sup>13</sup>, P. Chakraborty<sup>8,9</sup>, S. Chakraborty,<sup>103</sup> S. Chalathadka Subrahmanya<sup>97</sup>, J. C. L. Chan<sup>139</sup>,  
M. Chan,<sup>114</sup> K. Chang,<sup>140</sup> S. Chao<sup>141,140</sup>, P. Charlton<sup>142</sup>, E. Chassande-Mottin<sup>20</sup>, C. Chatterjee<sup>143</sup>,  
Debarati Chatterjee<sup>79</sup>, Deep Chatterjee<sup>35</sup>, M. Chaturvedi,<sup>103</sup> S. Chaty<sup>20</sup>, K. Chatziioannou<sup>11</sup>, A. Chen<sup>144</sup>,  
A. H.-Y. Chen,<sup>145</sup> D. Chen<sup>146</sup>, H. Chen,<sup>141</sup> H. Y. Chen<sup>147</sup>, S. Chen,<sup>143</sup> Yanbei Chen,<sup>148</sup> Yitian Chen<sup>120</sup>,  
H. P. Cheng,<sup>149</sup> P. Chessa<sup>76,51</sup>, H. T. Cheung<sup>90</sup>, S. Y. Cheung,<sup>6</sup> F. Chiadini<sup>150,131</sup>, G. Chiarini,<sup>8,9,92</sup>  
A. Chiba,<sup>151</sup> A. Chincarini<sup>29</sup>, M. L. Chiofalo<sup>81,80</sup>, A. Chiummo<sup>4,62</sup>, C. Chou,<sup>145</sup> S. Choudhary<sup>72</sup>,  
N. Christensen<sup>113,152</sup>, S. S. Y. Chua<sup>34</sup>, G. Ciani<sup>74,75</sup>, P. Ciecielag<sup>95</sup>, M. Cieřlar<sup>124</sup>, M. Cifaldi<sup>22</sup>,  
B. Cirotk,<sup>153</sup> F. Clara,<sup>2</sup> J. A. Clark<sup>11,57</sup>, T. A. Clarke<sup>6</sup>, P. Clearwater,<sup>154</sup> S. Clesse,<sup>111</sup> F. Cleva,<sup>113,116</sup>  
E. Coccia,<sup>44,45,43</sup> E. Codazzo<sup>155,156</sup>, P.-F. Cohadon<sup>121</sup>, S. Colace<sup>30</sup>, E. Colangeli,<sup>73</sup> M. Colleoni<sup>98</sup>,  
C. G. Collette,<sup>157</sup> J. Collins,<sup>63</sup> S. Colloms<sup>86</sup>, A. Colombo<sup>158,127</sup>, C. M. Compton,<sup>2</sup> G. Connolly,<sup>77</sup> L. Conti<sup>92</sup>,  
T. R. Corbitt<sup>12</sup>, I. Cordero-Carrión<sup>159</sup>, S. Corezzi<sup>76,51</sup>, N. J. Cornish<sup>160</sup>, I. Coronado,<sup>161</sup> A. Corsi<sup>162</sup>

- R. Cottingham,<sup>63</sup> M. W. Coughlin<sup>18</sup> A. Couineaux,<sup>38</sup> P. Couvares<sup>11,57</sup> D. M. Coward,<sup>72</sup> R. Coyne<sup>163</sup>  
 A. Cozzumbo,<sup>44</sup> J. D. E. Creighton<sup>10</sup> T. D. Creighton,<sup>164</sup> P. Cremonese<sup>98</sup> S. Crook,<sup>63</sup> R. Crouch,<sup>2</sup>  
 J. Csizmazia,<sup>2</sup> J. R. Cudell<sup>165</sup> T. J. Cullen<sup>11</sup> A. Cumming<sup>86</sup> E. Cuoco<sup>166,167</sup> M. Cusinato<sup>137</sup>  
 L. V. Da Conceição<sup>168</sup> T. Dal Canton<sup>41</sup> S. Dal Pra<sup>169</sup> G. D'Álya<sup>100</sup> B. D'Angelo<sup>29</sup> S. Danilishin<sup>36,37</sup>  
 S. D'Antonio<sup>38</sup> K. Danzmann,<sup>9,8,9</sup> K. E. Darroch,<sup>122</sup> L. P. Dartez<sup>63</sup> R. Das,<sup>106</sup> A. Dasgupta,<sup>93</sup> V. Dattilo<sup>62</sup>  
 A. Daumas,<sup>20</sup> N. Davari,<sup>170,171</sup> I. Dave,<sup>103</sup> A. Davenport,<sup>136</sup> M. Davier,<sup>41</sup> T. F. Davies,<sup>72</sup> D. Davis<sup>11</sup> L. Davis,<sup>72</sup>  
 M. C. Davis<sup>18</sup> P. Davis<sup>172,173</sup> E. J. Daw<sup>174</sup> M. Dax<sup>1</sup> J. De Bolle<sup>94</sup> M. Deenadayalan,<sup>79</sup> J. Degallaix<sup>175</sup>  
 M. De Laurentis<sup>32,4</sup> F. De Lillo<sup>23</sup> S. Della Torre<sup>127</sup> W. Del Pozzo<sup>81,80</sup> A. Demagny,<sup>31</sup> F. De Marco<sup>39,38</sup>  
 G. Demasi,<sup>176,61</sup> F. De Matteis<sup>21,22</sup> N. Demos,<sup>35</sup> T. Dent<sup>177</sup> A. Depasse<sup>15</sup> N. DePergola,<sup>102</sup>  
 R. De Pietri<sup>178,179</sup> R. De Rosa<sup>32,4</sup> C. De Rossi<sup>62</sup> M. Desai<sup>35</sup> R. DeSalvo<sup>180</sup> A. DeSimone,<sup>181</sup>  
 R. De Simone,<sup>150,131</sup> A. Dhani<sup>1</sup> R. Diab,<sup>46</sup> M. C. Díaz<sup>164</sup> M. Di Cesare<sup>32,4</sup> G. Dideron,<sup>182</sup> T. Dietrich<sup>1</sup>  
 L. Di Fiore,<sup>4</sup> C. Di Fronzo<sup>72</sup> M. Di Giovanni<sup>39,38</sup> T. Di Girolamo<sup>32,4</sup> D. Diksha,<sup>37,36</sup> J. Ding<sup>20,183</sup>  
 S. Di Pace<sup>39,38</sup> I. Di Palma<sup>39,38</sup> D. Di Piero,<sup>184,48</sup> F. Di Renzo<sup>56</sup> Divyajyoti<sup>33</sup> A. Dmitriev<sup>118</sup>  
 J. P. Docherty,<sup>86</sup> Z. Doctor<sup>96</sup> N. Doerken<sup>168</sup> E. Dohmen,<sup>2</sup> A. Doke,<sup>132</sup> A. Domiciano De Souza,<sup>185</sup>  
 L. D'Onofrio<sup>38</sup> F. Donovan,<sup>35</sup> K. L. Dooley<sup>33</sup> T. Dooney,<sup>71</sup> S. Doravari<sup>79</sup> O. Dorosh,<sup>186</sup> W. J. D. Doyle,<sup>122</sup>  
 M. Drago<sup>39,38</sup> J. C. Driggers<sup>2</sup> L. Dunn<sup>123</sup> U. Dupletsa,<sup>44</sup> P.-A. Duverne<sup>20</sup> D. D'Urso<sup>170,155</sup>  
 P. Dutta Roy<sup>46</sup> H. Duval<sup>187</sup> S. E. Dwyer,<sup>2</sup> C. Eassa,<sup>2</sup> M. Ebersold<sup>188,31</sup> T. Eckhardt<sup>97</sup> G. Eddolls<sup>78</sup>  
 A. Effler<sup>63</sup> J. Eichholz<sup>34</sup> H. Einsle,<sup>113</sup> M. Eisenmann,<sup>25</sup> M. Emma<sup>58</sup> K. Endo,<sup>151</sup> R. Enficiaud<sup>1</sup>  
 L. Errico<sup>32,4</sup> R. Espinosa,<sup>164</sup> M. Esposito<sup>4,32</sup> R. C. Essick<sup>189</sup> H. Estellés<sup>1</sup> T. Etzel,<sup>11</sup> M. Evans<sup>35</sup>  
 T. Evstafyeva,<sup>182</sup> B. E. Ewing,<sup>7</sup> J. M. Ezquiaga<sup>139</sup> F. Fabrizi<sup>60,61</sup> V. Fafone<sup>21,22</sup> S. Fairhurst<sup>33</sup>  
 A. M. Farah<sup>129</sup> B. Farr<sup>77</sup> W. M. Farr<sup>190,191</sup> G. Favaro<sup>91</sup> M. Favata<sup>192</sup> M. Fays<sup>165</sup> M. Fazio<sup>55</sup>  
 J. Feicht,<sup>11</sup> M. M. Fejer,<sup>89</sup> R. Felicetti<sup>184,48</sup> E. Fenyvesi<sup>87,193</sup> J. Fernandes,<sup>194</sup> T. Fernandes<sup>195,137</sup>  
 D. Fernando,<sup>110</sup> S. Ferraiuolo<sup>196,39,38</sup> T. A. Ferreira,<sup>12</sup> F. Fidencaro<sup>81,80</sup> P. Figura<sup>95</sup> A. Fiori<sup>80,81</sup>  
 I. Fiori<sup>62</sup> M. Fishbach<sup>189</sup> R. P. Fisher,<sup>122</sup> R. Fittipaldi<sup>197,131</sup> V. Fiumara<sup>198,131</sup> R. Flaminio,<sup>31</sup>  
 S. M. Fleischer<sup>199</sup> L. S. Fleming,<sup>200</sup> E. Floden,<sup>18</sup> H. Fong,<sup>114</sup> J. A. Font<sup>137,138</sup> F. Fontinele-Nunes,<sup>18</sup> C. Foo,<sup>1</sup>  
 B. Fornal<sup>201</sup> K. Franceschetti,<sup>178</sup> F. Frappez,<sup>31</sup> S. Frasca,<sup>39,38</sup> F. Frasconi<sup>80</sup> J. P. Freed,<sup>65</sup> Z. Frei<sup>202</sup>  
 A. Freise<sup>37,107</sup> O. Freitas<sup>195,137</sup> R. Frey<sup>77</sup> W. Frischhertz,<sup>63</sup> P. Fritschel,<sup>35</sup> V. V. Frolov,<sup>63</sup> G. G. Fronzé<sup>28</sup>  
 M. Fuentes-García<sup>11</sup> S. Fujii,<sup>203</sup> T. Fujimori,<sup>204</sup> P. Fulda,<sup>46</sup> M. Fyffe,<sup>63</sup> B. Gadre<sup>71</sup> J. R. Gair<sup>1</sup>  
 S. Galaudage<sup>185</sup> V. Galdi,<sup>205</sup> R. Gamba,<sup>7</sup> A. Gamboa<sup>1</sup> S. Gamoji,<sup>180</sup> D. Ganapathy<sup>206</sup> A. Ganguly<sup>79</sup>  
 B. Garaventa<sup>29</sup> J. García-Bellido<sup>207</sup> C. García-Quirós<sup>188</sup> J. W. Gardner<sup>34</sup> K. A. Gardner,<sup>114</sup> S. Garg,<sup>42</sup>  
 J. Gargiulo<sup>62</sup> X. Garrido<sup>41</sup> A. Garron<sup>98</sup> F. Garufi<sup>32,4</sup> P. A. Garver,<sup>89</sup> C. Gasbarra<sup>21,22</sup>  
 B. Gateley,<sup>2</sup> F. Gautier<sup>208</sup> V. Gayathri<sup>10</sup> T. Gayer,<sup>78</sup> G. Gemme<sup>29</sup> A. Gennai<sup>80</sup> V. Gennari<sup>100</sup>  
 J. George,<sup>103</sup> R. George<sup>147</sup> O. Gerberding<sup>97</sup> L. Gergely<sup>153</sup> Archisman Ghosh<sup>94</sup> Sayantan Ghosh,<sup>194</sup>  
 Shaon Ghosh<sup>192</sup> Shrobana Ghosh,<sup>8,9</sup> Suprovo Ghosh<sup>209</sup> Tathagata Ghosh<sup>79</sup> J. A. Giaime<sup>12,63</sup>  
 K. D. Giardina,<sup>63</sup> D. R. Gibson,<sup>200</sup> C. Gier<sup>55</sup> S. Gkaitatzis<sup>81,80</sup> J. Glanzer<sup>11</sup> F. Glotin<sup>41</sup> J. Godfrey,<sup>77</sup>  
 R. V. Godley,<sup>8,9</sup> P. Godwin<sup>11</sup> A. S. Goettel<sup>33</sup> E. Goetz<sup>114</sup> J. Golomb,<sup>11</sup> S. Gomez Lopez<sup>39,38</sup>  
 B. Goncharov<sup>44</sup> G. González<sup>12</sup> P. Goodarzi<sup>210</sup> S. Goode,<sup>6</sup> A. W. Goodwin-Jones<sup>15</sup> M. Gosselin,<sup>62</sup>  
 R. Gouaty<sup>31</sup> D. W. Gould,<sup>34</sup> K. Govorkova,<sup>35</sup> A. Grado<sup>76,51</sup> V. Graham<sup>86</sup> A. E. Granados<sup>18</sup>  
 M. Granata<sup>175</sup> V. Granata<sup>211,131</sup> S. Gras,<sup>35</sup> P. Grassia,<sup>11</sup> J. Graves,<sup>57</sup> C. Gray,<sup>2</sup> R. Gray<sup>86</sup> G. Greco,<sup>51</sup>  
 A. C. Green<sup>37,107</sup> L. Green,<sup>212</sup> S. M. Green,<sup>73</sup> S. R. Green<sup>213</sup> C. Greenberg,<sup>132</sup> A. M. Gretarsson,<sup>65</sup>  
 H. K. Griffin,<sup>18</sup> D. Griffith,<sup>11</sup> H. L. Griggs<sup>57</sup> G. Grignani,<sup>76,51</sup> C. Grimaud<sup>31</sup> H. Grote<sup>33</sup> S. Grunewald<sup>1</sup>  
 D. Guerra<sup>137</sup> D. Guetta<sup>214</sup> G. M. Guidi<sup>60,61</sup> A. R. Guimaraes,<sup>12</sup> H. K. Gulati,<sup>93</sup> F. Gulminelli<sup>172,173</sup>  
 H. Guo<sup>144</sup> W. Guo<sup>72</sup> Y. Guo<sup>37,36</sup> Anuradha Gupta<sup>215</sup> I. Gupta<sup>7</sup> N. C. Gupta,<sup>93</sup> S. K. Gupta,<sup>46</sup>  
 V. Gupta<sup>18</sup> N. Gupte,<sup>1</sup> J. Gurs,<sup>97</sup> N. Gutierrez,<sup>175</sup> N. Guttman,<sup>6</sup> F. Guzman<sup>130</sup> D. Haba,<sup>216</sup> M. Haberland<sup>1</sup>  
 S. Haino,<sup>217</sup> E. D. Hall<sup>35</sup> E. Z. Hamilton<sup>98</sup> G. Hammond<sup>86</sup> M. Haney,<sup>37</sup> J. Hanks,<sup>2</sup> C. Hanna<sup>7</sup>  
 M. D. Hannam,<sup>33</sup> O. A. Hannuksela<sup>218</sup> A. G. Hanselman<sup>129</sup> H. Hansen,<sup>2</sup> J. Hanson,<sup>63</sup> S. Hanumasagar,<sup>57</sup>  
 R. Harada,<sup>42</sup> A. R. Hardison,<sup>181</sup> S. Harikumar<sup>186</sup> K. Haris,<sup>37,71</sup> I. Harley-Trochimczyk,<sup>130</sup> T. Harmark<sup>133</sup>  
 J. Harms<sup>44,45</sup> G. M. Harry<sup>219</sup> I. W. Harry<sup>73</sup> J. Hart,<sup>104</sup> B. Haskell,<sup>95,220,221</sup> C. J. Haster<sup>212</sup>  
 K. Haughian<sup>86</sup> H. Hayakawa,<sup>50</sup> K. Hayama,<sup>222</sup> M. C. Heintze,<sup>63</sup> J. Heinze<sup>118</sup> J. Heinzl,<sup>35</sup> H. Heitmann<sup>113</sup>  
 F. Hellman<sup>206</sup> A. F. Helmling-Cornell<sup>77</sup> G. Hemming<sup>62</sup> O. Henderson-Sapir<sup>115</sup> M. Hendry<sup>86</sup>  
 I. S. Heng,<sup>86</sup> M. H. Hennig<sup>86</sup> C. Henshaw<sup>57</sup> M. Heurs<sup>8,9</sup> A. L. Hewitt<sup>223,224</sup> J. Heynen,<sup>15</sup>  
 J. Heyns,<sup>35</sup> S. Higginbotham,<sup>33</sup> S. Hild,<sup>36,37</sup> S. Hill,<sup>86</sup> Y. Himemoto<sup>225</sup> N. Hirata,<sup>25</sup> C. Hirose,<sup>226</sup>  
 D. Hofman,<sup>175</sup> B. E. Hogan,<sup>65</sup> N. A. Holland,<sup>37,107</sup> I. J. Hollows<sup>174</sup> D. E. Holz<sup>129</sup> L. Honet,<sup>111</sup>

D. J. Horton-Bailey,<sup>206</sup> J. Hough,<sup>86</sup> S. Hourihane,<sup>11</sup> N. T. Howard,<sup>143</sup> E. J. Howell,<sup>72</sup> C. G. Hoy,<sup>73</sup> C. A. Hrishikesh,<sup>21</sup> P. Hsi,<sup>35</sup> H.-F. Hsieh,<sup>141</sup> H.-Y. Hsieh,<sup>141</sup> C. Hsiung,<sup>227</sup> S.-H. Hsu,<sup>145</sup> W.-F. Hsu,<sup>109</sup> Q. Hu,<sup>86</sup> H. Y. Huang,<sup>140</sup> Y. Huang,<sup>7</sup> Y. T. Huang,<sup>78</sup> A. D. Huddart,<sup>228</sup> B. Hughey,<sup>65</sup> V. Hui,<sup>31</sup> S. Husa,<sup>98</sup> R. Huxford,<sup>7</sup> L. Iampieri,<sup>39,38</sup> G. A. Iandolo,<sup>36</sup> M. Ianni,<sup>22,21</sup> G. Iannone,<sup>131</sup> J. Iascau,<sup>77</sup> K. Ide,<sup>229</sup> R. Iden,<sup>216</sup> A. Ierardi,<sup>44,45</sup> S. Ikeda,<sup>146</sup> H. Imafuku,<sup>42</sup> Y. Inoue,<sup>140</sup> G. Iorio,<sup>91</sup> P. Iosif,<sup>184,48</sup> M. H. Iqbal,<sup>34</sup> J. Irwin,<sup>86</sup> R. Ishikawa,<sup>229</sup> M. Isi,<sup>190,191</sup> K. S. Isleif,<sup>230</sup> Y. Itoh,<sup>204,231</sup> M. Iwaya,<sup>203</sup> B. R. Iyer,<sup>24</sup> C. Jacquet,<sup>100</sup> P.-E. Jacquet,<sup>121</sup> T. Jacquot,<sup>41</sup> S. J. Jadhav,<sup>232</sup> S. P. Jadhav,<sup>154</sup> M. Jain,<sup>132</sup> T. Jain,<sup>223</sup> A. L. James,<sup>11</sup> K. Jani,<sup>143</sup> J. Janquart,<sup>15</sup> N. N. Janthalur,<sup>232</sup> S. Jaraba,<sup>233</sup> P. Jaranowski,<sup>234</sup> R. Jaume,<sup>98</sup> W. Javed,<sup>33</sup> A. Jennings,<sup>2</sup> M. Jensen,<sup>2</sup> W. Jia,<sup>35</sup> J. Jiang,<sup>149</sup> H.-B. Jin,<sup>235,236</sup> G. R. Johns,<sup>122</sup> N. A. Johnson,<sup>46</sup> M. C. Johnston,<sup>212</sup> R. Johnston,<sup>86</sup> N. Johny,<sup>8,9</sup> D. H. Jones,<sup>34</sup> D. I. Jones,<sup>209</sup> R. Jones,<sup>86</sup> H. E. Jose,<sup>77</sup> P. Joshi,<sup>7</sup> S. K. Joshi,<sup>79</sup> G. Joubert,<sup>56</sup> J. Ju,<sup>237</sup> L. Ju,<sup>72</sup> K. Jung,<sup>238</sup> J. Junker,<sup>34</sup> V. Juste,<sup>111</sup> H. B. Kabagoz,<sup>63,35</sup> T. Kajita,<sup>239</sup> I. Kaku,<sup>204</sup> V. Kalogera,<sup>96</sup> M. Kalomenopoulos,<sup>212</sup> M. Kamiizumi,<sup>50</sup> N. Kanda,<sup>231,204</sup> S. Kandhasamy,<sup>79</sup> G. Kang,<sup>240</sup> N. C. Kannachel,<sup>6</sup> J. B. Kanner,<sup>11</sup> S. A. KantiMahanty,<sup>18</sup> S. J. Kapadia,<sup>79</sup> D. P. Kapasi,<sup>54</sup> M. Karthikeyan,<sup>132</sup> M. Kasprzack,<sup>11</sup> H. Kato,<sup>151</sup> T. Kato,<sup>203</sup> E. Katsavounidis,<sup>35</sup> W. Katzman,<sup>63</sup> R. Kaushik,<sup>103</sup> K. Kawabe,<sup>2</sup> R. Kawamoto,<sup>204</sup> D. Keitel,<sup>98</sup> L. J. Kemperman,<sup>115</sup> J. Kennington,<sup>7</sup> F. A. Kerkow,<sup>18</sup> R. Kesharwani,<sup>79</sup> J. S. Key,<sup>241</sup> R. Khadela,<sup>8,9</sup> S. Khadka,<sup>89</sup> S. S. Khadkikar,<sup>7</sup> F. Y. Khalili,<sup>108</sup> F. Khan,<sup>8,9</sup> T. Khanam,<sup>162</sup> M. Khursheed,<sup>103</sup> N. M. Khusid,<sup>190,191</sup> W. Kiendrebeogo,<sup>113,242</sup> N. Kijbunchoo,<sup>115</sup> C. Kim,<sup>243</sup> J. C. Kim,<sup>244</sup> K. Kim,<sup>245</sup> M. H. Kim,<sup>237</sup> S. Kim,<sup>246</sup> Y.-M. Kim,<sup>245</sup> C. Kimball,<sup>96</sup> K. Kimes,<sup>54</sup> M. Kinnear,<sup>33</sup> J. S. Kissel,<sup>2</sup> S. Klimenko,<sup>46</sup> A. M. Knee,<sup>114</sup> E. J. Knox,<sup>77</sup> N. Knust,<sup>8,9</sup> K. Kobayashi,<sup>203</sup> S. M. Koehlenbeck,<sup>89</sup> G. Koekoek,<sup>37,36</sup> K. Kohri,<sup>247,248</sup> K. Kokeyama,<sup>33,249</sup> S. Koley,<sup>44,165</sup> P. Kolitsidou,<sup>118</sup> A. E. Koloniari,<sup>250</sup> K. Komori,<sup>42</sup> A. K. H. Kong,<sup>141</sup> A. Kontos,<sup>251</sup> L. M. Koponen,<sup>118</sup> M. Korobko,<sup>97</sup> X. Kou,<sup>18</sup> A. Koushik,<sup>23</sup> N. Kouvatsos,<sup>67</sup> M. Kovalam,<sup>72</sup> T. Koyama,<sup>151</sup> D. B. Kozak,<sup>11</sup> S. L. Kranzhoff,<sup>36,37</sup> V. Kringel,<sup>8,9</sup> N. V. Krishnendu,<sup>118</sup> S. Kroker,<sup>252</sup> A. Królak,<sup>253,186</sup> K. Kruska,<sup>8,9</sup> J. Kubisz,<sup>254</sup> G. Kuehn,<sup>8,9</sup> S. Kulkarni,<sup>215</sup> A. Kulur Ramamohan,<sup>34</sup> Achal Kumar,<sup>46</sup> Anil Kumar,<sup>232</sup> Praveen Kumar,<sup>177</sup> Prayush Kumar,<sup>24</sup> Rahul Kumar,<sup>2</sup> Rakesh Kumar,<sup>93</sup> J. Kume,<sup>255,256,42</sup> K. Kuns,<sup>35</sup> N. Kuntimaddi,<sup>33</sup> S. Kuroyanagi,<sup>207,257</sup> S. Kuwahara,<sup>42</sup> K. Kwak,<sup>238</sup> K. Kwan,<sup>34</sup> S. Kwon,<sup>42</sup> G. Lacaille,<sup>86</sup> D. Laghi,<sup>188,100</sup> A. H. Laity,<sup>163</sup> E. Lalande,<sup>258</sup> M. Lalleman,<sup>23</sup> P. C. Lalremruati,<sup>259</sup> M. Landry,<sup>2</sup> B. B. Lane,<sup>35</sup> R. N. Lang,<sup>35</sup> J. Lange,<sup>147</sup> R. Langgin,<sup>212</sup> B. Lantz,<sup>89</sup> I. La Rosa,<sup>98</sup> J. Larsen,<sup>199</sup> A. Lartaux-Vollard,<sup>41</sup> P. D. Lasky,<sup>6</sup> J. Lawrence,<sup>164</sup> M. Laxen,<sup>63</sup> C. Lazarte,<sup>137</sup> A. Lazzarini,<sup>11</sup> C. Lazzaro,<sup>156,155</sup> P. Leaci,<sup>39,38</sup> L. Leali,<sup>18</sup> Y. K. Lecoeuche,<sup>114</sup> H. M. Lee,<sup>260</sup> H. W. Lee,<sup>261</sup> J. Lee,<sup>78</sup> K. Lee,<sup>237</sup> R.-K. Lee,<sup>141</sup> R. Lee,<sup>35</sup> Sungho Lee,<sup>245</sup> Sunjae Lee,<sup>237</sup> Y. Lee,<sup>140</sup> I. N. Legred,<sup>11</sup> J. Lehmann,<sup>8,9</sup> L. Lehner,<sup>182</sup> M. Le Jean,<sup>175,116</sup> A. Lemaitre,<sup>262</sup> M. Lenti,<sup>61,176</sup> M. Leonardi,<sup>74,75,263</sup> M. Lequime,<sup>40</sup> N. Leroy,<sup>41</sup> M. Lesovsky,<sup>11</sup> N. Letendre,<sup>31</sup> M. Lethuillier,<sup>56</sup> Y. Levin,<sup>6</sup> K. Leyde,<sup>73</sup> A. K. Y. Li,<sup>11</sup> K. L. Li,<sup>264</sup> T. G. F. Li,<sup>109</sup> X. Li,<sup>148</sup> Y. Li,<sup>96</sup> Z. Li,<sup>86</sup> A. Lihos,<sup>122</sup> E. T. Lin,<sup>141</sup> F. Lin,<sup>140</sup> L. C.-C. Lin,<sup>264</sup> Y.-C. Lin,<sup>141</sup> C. Lindsay,<sup>200</sup> S. D. Linker,<sup>180</sup> A. Liu,<sup>218</sup> G. C. Liu,<sup>227</sup> Jian Liu,<sup>72</sup> F. Llamas Villarreal,<sup>164</sup> J. Llobera-Querol,<sup>98</sup> R. K. L. Lo,<sup>139</sup> J.-P. Locquet,<sup>109</sup> S. C. G. Loggins,<sup>265</sup> M. R. Loizou,<sup>132</sup> L. T. London,<sup>67</sup> A. Longo,<sup>60,61</sup> D. Lopez,<sup>165</sup> M. Lopez Portilla,<sup>71</sup> A. Lorenzo-Medina,<sup>177</sup> V. Lorette,<sup>41</sup> M. Lormand,<sup>63</sup> G. Losurdo,<sup>266,80</sup> E. Lotti,<sup>132</sup> T. P. Lott IV,<sup>57</sup> J. D. Lough,<sup>8,9</sup> H. A. Loughlin,<sup>35</sup> C. O. Lousto,<sup>110</sup> N. Low,<sup>123</sup> N. Lu,<sup>34</sup> L. Lucchesi,<sup>80</sup> H. Lück,<sup>9,8,9</sup> D. Lumaca,<sup>22</sup> A. P. Lundgren,<sup>267,268</sup> A. W. Lussier,<sup>258</sup> R. Macas,<sup>73</sup> M. MacInnis,<sup>35</sup> D. M. Macleod,<sup>33</sup> I. A. O. MacMillan,<sup>11</sup> A. Macquet,<sup>41</sup> K. Maeda,<sup>151</sup> S. Maenaut,<sup>109</sup> S. S. Magare,<sup>79</sup> R. M. Magee,<sup>11</sup> E. Maggio,<sup>1</sup> R. Maggiore,<sup>37,107</sup> M. Magnozzi,<sup>29,30</sup> M. Mahesh,<sup>97</sup> M. Maini,<sup>163</sup> S. Majhi,<sup>79</sup> E. Majorana,<sup>39,38</sup> C. N. Makarem,<sup>11</sup> D. Malakar,<sup>105</sup> J. A. Malaquias-Reis,<sup>19</sup> U. Mali,<sup>189</sup> S. Maliakal,<sup>11</sup> A. Malik,<sup>103</sup> L. Mallick,<sup>168,189</sup> A.-K. Malz,<sup>58</sup> N. Man,<sup>113</sup> M. Mancarella,<sup>99</sup> V. Mandic,<sup>18</sup> V. Mangano,<sup>170,155</sup> B. Mannix,<sup>77</sup> G. L. Mansell,<sup>78</sup> M. Manske,<sup>10</sup> M. Mantovani,<sup>62</sup> M. Mapelli,<sup>91,92,269</sup> C. Marinelli,<sup>101</sup> F. Marion,<sup>31</sup> A. S. Markosyan,<sup>89</sup> A. Markowitz,<sup>11</sup> E. Maros,<sup>11</sup> S. Marsat,<sup>100</sup> F. Martelli,<sup>60,61</sup> I. W. Martin,<sup>86</sup> R. M. Martin,<sup>192</sup> B. B. Martinez,<sup>130</sup> D. A. Martinez,<sup>54</sup> M. Martinez,<sup>43,270</sup> V. Martinez,<sup>128</sup> A. Martini,<sup>74,75</sup> J. C. Martins,<sup>19</sup> D. V. Martynov,<sup>118</sup> E. J. Marx,<sup>35</sup> L. Massaro,<sup>36,37</sup> A. Masserot,<sup>31</sup> M. Masso-Reid,<sup>86</sup> S. Mastrogiovanni,<sup>38</sup> T. Matcovich,<sup>51</sup> M. Matushechkina,<sup>8,9</sup> L. Maurin,<sup>208</sup> N. Mavalvala,<sup>35</sup> N. Maxwell,<sup>2</sup> G. McCarrol,<sup>63</sup> R. McCarthy,<sup>2</sup> D. E. McClelland,<sup>34</sup> S. McCormick,<sup>63</sup> L. McCuller,<sup>11</sup> S. McEachin,<sup>122</sup> C. McElhenny,<sup>122</sup> G. I. McGhee,<sup>86</sup> J. McGinn,<sup>86</sup> K. B. M. McGowan,<sup>143</sup> J. McIver,<sup>114</sup> A. McLeod,<sup>72</sup> I. McMahon,<sup>188</sup> T. McRae,<sup>34</sup> R. McTeague,<sup>86</sup> D. Meacher,<sup>10</sup> B. N. Meagher,<sup>78</sup> R. Mechum,<sup>110</sup> Q. Meijer,<sup>71</sup> A. Melatos,<sup>123</sup> C. S. Menoni,<sup>136</sup> F. Mera,<sup>2</sup> R. A. Mercer,<sup>10</sup> L. Mereni,<sup>175</sup>

- K. Merfeld,<sup>162</sup> E. L. Merilh,<sup>63</sup> J. R. Mérou,<sup>98</sup> J. D. Merritt,<sup>77</sup> M. Merzougui,<sup>113</sup> C. Messick,<sup>10</sup> B. Mestichelli,<sup>44</sup>  
M. Meyer-Conde,<sup>271</sup> F. Meylahn,<sup>8,9</sup> A. Mhaske,<sup>79</sup> A. Miani,<sup>74,75</sup> H. Miao,<sup>272</sup> C. Michel,<sup>175</sup>  
Y. Michimura,<sup>42</sup> H. Middleton,<sup>118</sup> D. P. Mihaylov,<sup>104</sup> S. J. Miller,<sup>11</sup> M. Millhouse,<sup>57</sup> E. Milotti,<sup>184,48</sup>  
V. Milotti,<sup>91</sup> Y. Minenkov,<sup>22</sup> E. M. Minihan,<sup>65</sup> Ll. M. Mir,<sup>43</sup> L. Mirasola,<sup>155,156</sup> M. Miravet-Tenés,<sup>137</sup>  
C.-A. Miritescu,<sup>43</sup> A. Mishra,<sup>24</sup> C. Mishra,<sup>106</sup> T. Mishra,<sup>46</sup> A. L. Mitchell,<sup>37,107</sup> J. G. Mitchell,<sup>65</sup> S. Mitra,<sup>79</sup>  
V. P. Mitrofanov,<sup>108</sup> K. Mitsuhashi,<sup>25</sup> R. Mittleman,<sup>35</sup> O. Miyakawa,<sup>50</sup> S. Miyoki,<sup>50</sup> A. Miyoko,<sup>65</sup> G. Mo,<sup>35</sup>  
L. Mobilia,<sup>60,61</sup> S. R. P. Mohapatra,<sup>11</sup> S. R. Mohite,<sup>7</sup> M. Molina-Ruiz,<sup>206</sup> M. Mondin,<sup>180</sup> M. Montani,<sup>60,61</sup>  
C. J. Moore,<sup>223</sup> D. Moraru,<sup>2</sup> A. More,<sup>79</sup> S. More,<sup>79</sup> C. Moreno,<sup>134</sup> E. A. Moreno,<sup>35</sup> G. Moreno,<sup>2</sup>  
A. Moreso Serra,<sup>82</sup> S. Morisaki,<sup>42,203</sup> Y. Moriwaki,<sup>151</sup> G. Morras,<sup>207</sup> A. Moscatello,<sup>91</sup> M. Mould,<sup>35</sup>  
B. Mours,<sup>64</sup> C. M. Mow-Lowry,<sup>37,107</sup> L. Muccillo,<sup>176,61</sup> F. Muciaccia,<sup>39,38</sup> D. Mukherjee,<sup>118</sup>  
Samanwaya Mukherjee,<sup>24</sup> Soma Mukherjee,<sup>164</sup> Subroto Mukherjee,<sup>93</sup> Suvodip Mukherjee,<sup>13</sup> N. Mukund,<sup>35</sup>  
A. Mullavey,<sup>63</sup> H. Mullock,<sup>114</sup> J. Mundi,<sup>219</sup> C. L. Mungoli,<sup>72</sup> M. Murakoshi,<sup>229</sup> P. G. Murray,<sup>86</sup> D. Nabari,<sup>74,75</sup>  
S. L. Nadji,<sup>8,9</sup> A. Nagar,<sup>28,273</sup> N. Nagarajan,<sup>86</sup> K. Nakagaki,<sup>50</sup> K. Nakamura,<sup>25</sup> H. Nakano,<sup>274</sup> M. Nakano,<sup>11</sup>  
D. Nanadoungar-Lacroze,<sup>43</sup> D. Nandi,<sup>12</sup> V. Napolano,<sup>62</sup> P. Narayan,<sup>215</sup> I. Nardecchia,<sup>22</sup> T. Narikawa,<sup>203</sup>  
H. Narola,<sup>71</sup> L. Naticchioni,<sup>38</sup> R. K. Nayak,<sup>259</sup> L. Negri,<sup>71</sup> A. Nela,<sup>86</sup> C. Nelle,<sup>77</sup> A. Nelson,<sup>130</sup>  
T. J. N. Nelson,<sup>63</sup> M. Nery,<sup>8,9</sup> A. Neunzert,<sup>2</sup> S. Ng,<sup>54</sup> L. Nguyen Quynh,<sup>275</sup> S. A. Nichols,<sup>12</sup> A. B. Nielsen,<sup>276</sup>  
Y. Nishino,<sup>25,42</sup> A. Nishizawa,<sup>277</sup> S. Nissanke,<sup>278,37</sup> W. Niu,<sup>7</sup> F. Nocera,<sup>62</sup> J. Noller,<sup>279</sup> M. Norman,<sup>33</sup>  
C. North,<sup>33</sup> J. Novak,<sup>116,233,280</sup> R. Nowicki,<sup>143</sup> J. F. Nuño Siles,<sup>207</sup> L. K. Nuttall,<sup>73</sup> K. Obayashi,<sup>229</sup>  
J. Oberling,<sup>2</sup> J. O'Dell,<sup>228</sup> E. Oelker,<sup>35</sup> M. Oertel,<sup>233,116,281,280</sup> G. Oganesyan,<sup>44,45</sup> T. O'Hanlon,<sup>63</sup>  
M. Ohashi,<sup>50</sup> F. Ohme,<sup>8,9</sup> R. Oliveri,<sup>116,281,280</sup> R. Omer,<sup>18</sup> B. O'Neal,<sup>122</sup> M. Onishi,<sup>151</sup> K. Oohara,<sup>282</sup>  
B. O'Reilly,<sup>63</sup> M. Orselli,<sup>51,76</sup> R. O'Shaughnessy,<sup>110</sup> S. O'Shea,<sup>86</sup> S. Oshino,<sup>50</sup> C. Osthelder,<sup>11</sup>  
I. Ota,<sup>12</sup> D. J. Ottaway,<sup>115</sup> A. Ouzriat,<sup>56</sup> H. Overmier,<sup>63</sup> B. J. Owen,<sup>283</sup> R. Ozaki,<sup>229</sup> A. E. Pace,<sup>7</sup>  
R. Pagano,<sup>12</sup> M. A. Page,<sup>25</sup> A. Pai,<sup>194</sup> L. Paiella,<sup>44</sup> A. Pal,<sup>284</sup> S. Pal,<sup>259</sup> M. A. Palaia,<sup>80,81</sup>  
M. Pálfi,<sup>202</sup> P. P. Palma,<sup>39,21,22</sup> C. Palomba,<sup>38</sup> P. Palud,<sup>20</sup> H. Pan,<sup>141</sup> J. Pan,<sup>72</sup> K. C. Pan,<sup>141</sup>  
P. K. Panda,<sup>232</sup> Shiksha Pandey,<sup>7</sup> Swadha Pandey,<sup>35</sup> P. T. H. Pang,<sup>37,71</sup> F. Pannarale,<sup>39,38</sup> K. A. Pannone,<sup>54</sup>  
B. C. Pant,<sup>103</sup> F. H. Panther,<sup>72</sup> M. Panzeri,<sup>60,61</sup> F. Paoletti,<sup>80</sup> A. Paolone,<sup>38,285</sup> A. Papadopoulos,<sup>86</sup>  
E. E. Papalexakis,<sup>210</sup> L. Papalini,<sup>80,81</sup> G. Papigkiotis,<sup>250</sup> A. Paquis,<sup>41</sup> A. Parisi,<sup>76,51</sup> B.-J. Park,<sup>245</sup>  
J. Park,<sup>286</sup> W. Parker,<sup>63</sup> G. Pascale,<sup>8,9</sup> D. Pascucci,<sup>94</sup> A. Pasqualetti,<sup>62</sup> R. Passaquieti,<sup>81,80</sup>  
L. Passenger,<sup>6</sup> D. Passuello,<sup>80</sup> O. Patane,<sup>2</sup> A. V. Patel,<sup>140</sup> D. Pathak,<sup>79</sup> A. Patra,<sup>33</sup> B. Patricelli,<sup>81,80</sup>  
B. G. Patterson,<sup>33</sup> K. Paul,<sup>106</sup> S. Paul,<sup>77</sup> E. Payne,<sup>11</sup> T. Pearce,<sup>33</sup> M. Pedraza,<sup>11</sup> A. Pele,<sup>11</sup> F. E. Peña  
Arellano,<sup>287</sup> X. Peng,<sup>118</sup> Y. Peng,<sup>57</sup> S. Penn,<sup>288</sup> M. D. Penuliar,<sup>54</sup> A. Perego,<sup>74,75</sup> Z. Pereira,<sup>132</sup>  
C. Périgois,<sup>289,92,91</sup> G. Perna,<sup>91</sup> A. Perreca,<sup>74,75,44</sup> J. Perret,<sup>20</sup> S. Perriès,<sup>56</sup> J. W. Perry,<sup>37,107</sup>  
D. Pesios,<sup>250</sup> S. Peters,<sup>165</sup> S. Petracca,<sup>205</sup> C. Petrillo,<sup>76</sup> H. P. Pfeiffer,<sup>1</sup> H. Pham,<sup>63</sup> K. A. Pham,<sup>18</sup>  
K. S. Phukon,<sup>118</sup> H. Phurailatpam,<sup>218</sup> M. Piarulli,<sup>100</sup> L. Piccari,<sup>39,38</sup> O. J. Piccinni,<sup>34</sup> M. Pichot,<sup>113</sup>  
M. Piendibene,<sup>81,80</sup> F. Piergiovanni,<sup>60,61</sup> L. Pierini,<sup>38</sup> G. Pierra,<sup>38</sup> V. Pierro,<sup>290,131</sup> M. Pietrzak,<sup>95</sup>  
M. Pillas,<sup>165</sup> F. Pilo,<sup>80</sup> L. Pinard,<sup>175</sup> I. M. Pinto,<sup>290,131,291,32</sup> M. Pinto,<sup>62</sup> B. J. Piotrkowski,<sup>10</sup>  
M. Pirello,<sup>2</sup> M. D. Pitkin,<sup>223,86</sup> A. Placidi,<sup>51</sup> E. Placidi,<sup>39,38</sup> M. L. Planas,<sup>98</sup> W. Plastino,<sup>211,22</sup>  
C. Plunkett,<sup>35</sup> R. Poggiani,<sup>81,80</sup> E. Polini,<sup>35</sup> J. Pomper,<sup>80,81</sup> L. Pompili,<sup>1</sup> J. Poon,<sup>218</sup> E. Porcelli,<sup>37</sup>  
E. K. Porter,<sup>20</sup> C. Posnansky,<sup>7</sup> R. Poulton,<sup>62</sup> J. Powell,<sup>154</sup> G. S. Prabhu,<sup>79</sup> M. Pracchia,<sup>165</sup>  
B. K. Pradhan,<sup>79</sup> T. Pradier,<sup>64</sup> A. K. Prajapati,<sup>93</sup> K. Prasai,<sup>292</sup> R. Prasanna,<sup>232</sup> P. Prasia,<sup>79</sup> G. Pratten,<sup>118</sup>  
G. Principe,<sup>184,48</sup> G. A. Prodi,<sup>74,75</sup> P. Prospero,<sup>80</sup> P. Proposito,<sup>21,22</sup> A. C. Providence,<sup>65</sup> A. Puecher,<sup>1</sup>  
J. Pullin,<sup>12</sup> P. Puppo,<sup>38</sup> M. Pürner,<sup>163</sup> H. Qi,<sup>16</sup> J. Qin,<sup>34</sup> G. Quémener,<sup>173,116</sup> V. Quetschke,<sup>164</sup>  
P. J. Quinonez,<sup>65</sup> N. Qutob,<sup>57</sup> R. Rading,<sup>230</sup> I. Rainho,<sup>137</sup> S. Raja,<sup>103</sup> C. Rajan,<sup>103</sup> B. Rajbhandari,<sup>110</sup>  
K. E. Ramirez,<sup>63</sup> F. A. Ramis Vidal,<sup>98</sup> M. Ramos Arevalo,<sup>164</sup> A. Ramos-Buades,<sup>98,37</sup> S. Ranjan,<sup>57</sup>  
K. Ransom,<sup>63</sup> P. Rapagnani,<sup>39,38</sup> B. Ratto,<sup>65</sup> A. Ravichandran,<sup>132</sup> A. Ray,<sup>96</sup> V. Raymond,<sup>33</sup>  
M. Razzano,<sup>81,80</sup> J. Read,<sup>54</sup> T. Regimbau,<sup>31</sup> S. Reid,<sup>55</sup> C. Reissel,<sup>35</sup> D. H. Reitze,<sup>11</sup> A. I. Renzini,<sup>126,11</sup>  
B. Revenu,<sup>293,41</sup> A. Revilla Peña,<sup>82</sup> R. Reyes,<sup>180</sup> L. Ricca,<sup>15</sup> F. Ricci,<sup>39,38</sup> M. Ricci,<sup>38,39</sup>  
A. Ricciardone,<sup>81,80</sup> J. Rice,<sup>78</sup> J. W. Richardson,<sup>210</sup> M. L. Richardson,<sup>115</sup> A. Rijal,<sup>65</sup> K. Riles,<sup>90</sup> H. K. Riley,<sup>33</sup>  
S. Rinaldi,<sup>269</sup> J. Rittmeyer,<sup>97</sup> C. Robertson,<sup>228</sup> F. Robinet,<sup>41</sup> M. Robinson,<sup>2</sup> A. Rocchi,<sup>22</sup> L. Rolland,<sup>31</sup>  
J. G. Rollins,<sup>11</sup> A. E. Romano,<sup>294</sup> R. Romano,<sup>3,4</sup> A. Romero,<sup>31</sup> I. M. Romero-Shaw,<sup>223</sup> J. H. Romie,<sup>63</sup>  
S. Ronchini,<sup>7</sup> T. J. Rooke,<sup>115</sup> L. Rosa,<sup>4,32</sup> T. J. Rosauer,<sup>210</sup> C. A. Rose,<sup>57</sup> D. Rosińska,<sup>124</sup> M. P. Ross,<sup>53</sup>  
M. Rossello-Sastre,<sup>98</sup> S. Rowan,<sup>86</sup> S. K. Roy,<sup>190,191</sup> S. Roy,<sup>15</sup> D. Rozza,<sup>126,127</sup> P. Ruggi,<sup>62</sup> N. Ruhama,<sup>238</sup>  
E. Ruiz Morales,<sup>295,207</sup> K. Ruiz-Rocha,<sup>143</sup> S. Sachdev,<sup>57</sup> T. Sadecki,<sup>2</sup> P. Saffarieh,<sup>37,107</sup> S. Safi-Harb,<sup>168</sup>

- M. R. Sah <sup>13</sup> S. Saha <sup>141</sup> T. Sainrat <sup>64</sup> S. Sajith Menon <sup>214, 39, 38</sup> K. Sakai <sup>296</sup> Y. Sakai <sup>271</sup>  
M. Sakellariadou <sup>67</sup> S. Sakon <sup>7</sup> O. S. Salafia <sup>158, 127, 126</sup> F. Salces-Carcoba <sup>11</sup> L. Salconi <sup>62</sup> M. Saleem <sup>147</sup>  
F. Salemi <sup>39, 38</sup> M. Sallé <sup>37</sup> S. U. Salunkhe <sup>79</sup> S. Salvador <sup>173, 172</sup> A. Salvarese <sup>147</sup> A. Samajdar <sup>71, 37</sup>  
A. Sanchez <sup>2</sup> E. J. Sanchez <sup>11</sup> L. E. Sanchez <sup>11</sup> N. Sanchis-Gual <sup>137</sup> J. R. Sanders <sup>181</sup> E. M. Sängler <sup>1</sup>  
F. Santoliquido <sup>44, 45</sup> F. Sarandrea <sup>28</sup> T. R. Saravanan <sup>79</sup> N. Sarin <sup>6</sup> P. Sarkar <sup>8, 9</sup> A. Sasli <sup>250</sup> P. Sassi <sup>51, 76</sup>  
B. Sassolas <sup>175</sup> B. S. Sathyaprakash <sup>7, 33</sup> R. Sato <sup>226</sup> S. Sato <sup>151</sup> Yukino Sato <sup>151</sup> Yu Sato <sup>151</sup> O. Sauter <sup>46</sup>  
R. L. Savage <sup>2</sup> T. Sawada <sup>50</sup> H. L. Sawant <sup>79</sup> S. Sayah <sup>175</sup> V. Scacco <sup>21, 22</sup> D. Schaetzel <sup>11</sup> M. Scheel <sup>148</sup>  
A. Schiebelbein <sup>189</sup> M. G. Schiworski <sup>78</sup> P. Schmidt <sup>118</sup> S. Schmidt <sup>71</sup> R. Schnabel <sup>97</sup> M. Schneewind <sup>8, 9</sup>  
R. M. S. Schofield <sup>77</sup> K. Schouteden <sup>109</sup> B. W. Schulte <sup>8, 9</sup> B. F. Schutz <sup>33, 8, 9</sup> E. Schwartz <sup>297</sup> M. Scialpi <sup>298</sup>  
J. Scott <sup>86</sup> S. M. Scott <sup>34</sup> R. M. Sedas <sup>63</sup> T. C. Seetharamu <sup>86</sup> M. Seglar-Arroyo <sup>43</sup> Y. Sekiguchi <sup>299</sup>  
D. Sellers <sup>63</sup> N. Sembo <sup>204</sup> A. S. Sengupta <sup>300</sup> E. G. Seo <sup>86</sup> J. W. Seo <sup>109</sup> V. Sequino <sup>32, 4</sup> M. Serra <sup>38</sup>  
A. Sevrin <sup>187</sup> T. Shaffer <sup>2</sup> U. S. Shah <sup>57</sup> M. A. Shaikh <sup>260</sup> L. Shao <sup>301</sup> A. K. Sharma <sup>98</sup> Preeti Sharma <sup>12</sup>  
Prianka Sharma <sup>103</sup> Ritwik Sharma <sup>18</sup> S. Sharma Chaudhary <sup>105</sup> P. Shawhan <sup>125</sup> N. S. Shcheblanov <sup>302, 262</sup>  
E. Sheridan <sup>143</sup> Z.-H. Shi <sup>141</sup> M. Shikauchi <sup>42</sup> R. Shimomura <sup>303</sup> H. Shinkai <sup>303</sup> S. Shirke <sup>79</sup> D. H. Shoemaker <sup>35</sup>  
D. M. Shoemaker <sup>147</sup> R. W. Short <sup>2</sup> S. ShyamSundar <sup>103</sup> A. Sider <sup>157</sup> H. Siegel <sup>190, 191</sup> D. Sigg <sup>2</sup>  
L. Silenzi <sup>36, 37</sup> L. Silvestri <sup>39, 169</sup> M. Simmonds <sup>115</sup> L. P. Singer <sup>304</sup> Amitesh Singh <sup>215</sup> Anika Singh <sup>11</sup>  
D. Singh <sup>206</sup> N. Singh <sup>98</sup> S. Singh <sup>216, 59</sup> A. M. Sintès <sup>98</sup> V. Sipala <sup>170, 155</sup> V. Skliris <sup>33</sup> B. J. J. Slagmolen <sup>34</sup>  
D. A. Slater <sup>199</sup> T. J. Slaven-Blair <sup>72</sup> J. Smetana <sup>118</sup> J. R. Smith <sup>54</sup> L. Smith <sup>86, 184, 48</sup> R. J. E. Smith <sup>6</sup>  
W. J. Smith <sup>143</sup> S. Soares de Albuquerque Filho <sup>60</sup> M. Soares-Santos <sup>188</sup> K. Somiya <sup>216</sup> I. Song <sup>141</sup> S. Soni <sup>35</sup>  
V. Sordini <sup>56</sup> F. Sorrentino <sup>29</sup> H. Sotani <sup>305</sup> F. Spada <sup>80</sup> V. Spagnuolo <sup>37</sup> A. P. Spencer <sup>86</sup> P. Spinicelli <sup>62</sup>  
A. K. Srivastava <sup>93</sup> F. Stachurski <sup>86</sup> C. J. Stark <sup>122</sup> D. A. Steer <sup>306</sup> N. Steinle <sup>168</sup> J. Steinlechner <sup>36, 37</sup>  
S. Steinlechner <sup>36, 37</sup> N. Stergioulas <sup>250</sup> P. Stevens <sup>41</sup> M. StPierre <sup>163</sup> M. D. Strong <sup>12</sup> A. Strunk <sup>2</sup>  
A. L. Stuver <sup>102, \*</sup> M. Suchenek <sup>95</sup> S. Sudhagar <sup>95</sup> Y. Sudo <sup>229</sup> N. Sueltmann <sup>97</sup> L. Suleiman <sup>54</sup> K. D. Sullivan <sup>12</sup>  
J. Sun <sup>240</sup> L. Sun <sup>34</sup> S. Sunil <sup>93</sup> J. Suresh <sup>113</sup> B. J. Sutton <sup>67</sup> P. J. Sutton <sup>33</sup> K. Suzuki <sup>216</sup> M. Suzuki <sup>203</sup>  
B. L. Swinkels <sup>37</sup> A. Syx <sup>116</sup> M. J. Szczepańczyk <sup>307</sup> P. Szewczyk <sup>124</sup> M. Tacca <sup>37</sup> H. Tagoshi <sup>203</sup>  
K. Takada <sup>203</sup> H. Takahashi <sup>271</sup> R. Takahashi <sup>25</sup> A. Takamori <sup>42</sup> S. Takano <sup>308</sup> H. Takeda <sup>309, 310</sup>  
K. Takeshita <sup>216</sup> I. Takimoto Schmiegelow <sup>44, 45</sup> M. Takou-Ayaoh <sup>78</sup> C. Talbot <sup>129</sup> M. Tamaki <sup>203</sup> N. Tamanini <sup>100</sup>  
D. Tanabe <sup>140</sup> K. Tanaka <sup>50</sup> S. J. Tanaka <sup>229</sup> S. Tanioka <sup>33</sup> D. B. Tanner <sup>46</sup> W. Tanner <sup>8, 9</sup> L. Tao <sup>210</sup>  
R. D. Tapia <sup>7</sup> E. N. Tapia San Martín <sup>37</sup> C. Taranto <sup>21, 22</sup> A. Taruya <sup>311</sup> J. D. Tasson <sup>152</sup> J. G. Tau <sup>110</sup>  
D. Tellez <sup>54</sup> R. Tenorio <sup>98</sup> H. Themann <sup>180</sup> A. Theodoropoulos <sup>137</sup> M. P. Thirugnanasambandam <sup>79</sup>  
L. M. Thomas <sup>11</sup> M. Thomas <sup>63</sup> P. Thomas <sup>2</sup> J. E. Thompson <sup>209</sup> S. R. Thondapu <sup>103</sup> K. A. Thorne <sup>63</sup>  
E. Thrane <sup>6</sup> J. Tissino <sup>44, 45</sup> A. Tiwari <sup>79</sup> Pawan Tiwari <sup>44</sup> Praveer Tiwari <sup>194</sup> S. Tiwari <sup>188</sup> V. Tiwari <sup>118</sup>  
M. R. Todd <sup>78</sup> M. Toffano <sup>91</sup> A. M. Toivonen <sup>18</sup> K. Toland <sup>86</sup> A. E. Tolley <sup>73</sup> T. Tomaru <sup>25</sup> V. Tommasini <sup>11</sup>  
T. Tomura <sup>50</sup> H. Tong <sup>6</sup> C. Tong-Yu <sup>140</sup> A. Torres-Forné <sup>137, 138</sup> C. I. Torrie <sup>11</sup> I. Tosta e Melo <sup>312</sup>  
E. Tourniefier <sup>31</sup> M. Trad Nery <sup>113</sup> K. Tran <sup>122</sup> A. Trapananti <sup>52, 51</sup> R. Travaglini <sup>167</sup> F. Travasso <sup>52, 51</sup>  
G. Traylor <sup>63</sup> M. Trevor <sup>125</sup> M. C. Tringali <sup>62</sup> A. Tripathee <sup>90</sup> G. Troian <sup>184, 48</sup> A. Trovato <sup>184, 48</sup> L. Trozzo <sup>4</sup>  
R. J. Trudeau <sup>11</sup> T. Tsang <sup>33</sup> S. Tsuchida <sup>313</sup> L. Tsukada <sup>212</sup> K. Turbang <sup>187, 23</sup> M. Turconi <sup>113</sup> C. Turski <sup>94</sup>  
H. Ubach <sup>82, 83</sup> N. Uchikata <sup>203</sup> T. Uchiyama <sup>50</sup> R. P. Udall <sup>11</sup> T. Uehara <sup>314</sup> K. Ueno <sup>42</sup> V. Undheim <sup>276</sup>  
L. E. Uronen <sup>218</sup> T. Ushiba <sup>50</sup> M. Vacatello <sup>80, 81</sup> H. Vahlbruch <sup>8, 9</sup> N. Vaidya <sup>11</sup> G. Vajente <sup>11</sup> A. Vajpeyi <sup>6</sup>  
J. Valencia <sup>98</sup> M. Valentini <sup>107, 37</sup> S. A. Vallejo-Peña <sup>294</sup> S. Vallerio <sup>28</sup> V. Valsan <sup>10</sup> M. van Dael <sup>37, 315</sup>  
E. Van den Bossche <sup>187</sup> J. F. J. van den Brand <sup>36, 107, 37</sup> C. Van Den Broeck <sup>71, 37</sup> M. van der Sluys <sup>37, 71</sup>  
A. Van de Walle <sup>41</sup> J. van Dongen <sup>37, 107</sup> K. Vandra <sup>102</sup> M. VanDyke <sup>119</sup> H. van Haevermaet <sup>23</sup>  
J. V. van Heijningen <sup>37, 107</sup> P. Van Hove <sup>64</sup> J. Vanier <sup>258</sup> M. VanKeuren <sup>104</sup> J. Vanosky <sup>2</sup> N. van Remortel <sup>23</sup>  
M. Vardaro <sup>36, 37</sup> A. F. Vargas <sup>123</sup> V. Varma <sup>132</sup> A. N. Vazquez <sup>89</sup> A. Vecchio <sup>118</sup> G. Vedovato <sup>92</sup> J. Veitch <sup>86</sup>  
P. J. Veitch <sup>115</sup> S. Venikoudis <sup>15</sup> R. C. Venterea <sup>18</sup> P. Verdier <sup>56</sup> M. Vereecken <sup>15</sup> D. Verkindt <sup>31</sup> B. Verma <sup>132</sup>  
Y. Verma <sup>103</sup> S. M. Vermeulen <sup>11</sup> F. Vetrano <sup>60</sup> A. Veutro <sup>38, 39</sup> A. Viceré <sup>60, 61</sup> S. Vidyant <sup>78</sup>  
A. D. Viets <sup>88</sup> A. Vijaykumar <sup>189</sup> A. Vilkhina <sup>110</sup> N. Villanueva Espinosa <sup>137</sup> V. Villa-Ortega <sup>177</sup>  
E. T. Vincent <sup>57</sup> J.-Y. Vinet

A. T. Wilkin,<sup>210</sup> B. M. Williams,<sup>119</sup> D. Williams<sup>Ⓢ</sup>,<sup>86</sup> M. J. Williams<sup>Ⓢ</sup>,<sup>73</sup> N. S. Williams<sup>Ⓢ</sup>,<sup>1</sup> J. L. Willis<sup>Ⓢ</sup>,<sup>11</sup> B. Willke<sup>Ⓢ</sup>,<sup>9, 8, 9</sup> M. Wils<sup>Ⓢ</sup>,<sup>109</sup> L. Wilson,<sup>104</sup> C. W. Winborn,<sup>105</sup> J. Winterflood,<sup>72</sup> C. C. Wipf,<sup>11</sup> G. Woan<sup>Ⓢ</sup>,<sup>86</sup> J. Woehler,<sup>36, 37</sup> N. E. Wolfe,<sup>35</sup> H. T. Wong<sup>Ⓢ</sup>,<sup>140</sup> I. C. F. Wong<sup>Ⓢ</sup>,<sup>218, 109</sup> K. Wong,<sup>189</sup> T. Wouters,<sup>71, 37</sup> J. L. Wright,<sup>2</sup> M. Wright<sup>Ⓢ</sup>,<sup>86, 71</sup> B. Wu,<sup>78</sup> C. Wu<sup>Ⓢ</sup>,<sup>141</sup> D. S. Wu<sup>Ⓢ</sup>,<sup>8, 9</sup> H. Wu<sup>Ⓢ</sup>,<sup>141</sup> K. Wu,<sup>119</sup> Q. Wu,<sup>53</sup> Y. Wu,<sup>96</sup> Z. Wu<sup>Ⓢ</sup>,<sup>100</sup> E. Wuchner,<sup>54</sup> D. M. Wysocki<sup>Ⓢ</sup>,<sup>10</sup> V. A. Xu<sup>Ⓢ</sup>,<sup>206</sup> Y. Xu<sup>Ⓢ</sup>,<sup>98</sup> N. Yadav<sup>Ⓢ</sup>,<sup>28</sup> H. Yamamoto<sup>Ⓢ</sup>,<sup>11</sup> K. Yamamoto<sup>Ⓢ</sup>,<sup>151</sup> T. S. Yamamoto<sup>Ⓢ</sup>,<sup>42</sup> T. Yamamoto<sup>Ⓢ</sup>,<sup>50</sup> R. Yamazaki<sup>Ⓢ</sup>,<sup>229</sup> T. Yan,<sup>118</sup> K. Z. Yang<sup>Ⓢ</sup>,<sup>18</sup> Y. Yang<sup>Ⓢ</sup>,<sup>145</sup> Z. Yarbrough<sup>Ⓢ</sup>,<sup>12</sup> J. Yebana,<sup>98</sup> S.-W. Yeh,<sup>141</sup> A. B. Yelikar<sup>Ⓢ</sup>,<sup>143</sup> X. Yin,<sup>35</sup> J. Yokoyama<sup>Ⓢ</sup>,<sup>316, 42</sup> T. Yokozawa,<sup>50</sup> S. Yuan,<sup>72</sup> H. Yuzurihara<sup>Ⓢ</sup>,<sup>50</sup> M. Zanolin,<sup>65</sup> M. Zeeshan<sup>Ⓢ</sup>,<sup>110</sup> T. Zelenova,<sup>62</sup> J.-P. Zendri,<sup>92</sup> M. Zeoli<sup>Ⓢ</sup>,<sup>15</sup> M. Zerrad,<sup>40</sup> M. Zevin<sup>Ⓢ</sup>,<sup>96</sup> L. Zhang,<sup>11</sup> N. Zhang,<sup>57</sup> R. Zhang<sup>Ⓢ</sup>,<sup>149</sup> T. Zhang,<sup>118</sup> C. Zhao<sup>Ⓢ</sup>,<sup>72</sup> Yue Zhao,<sup>161</sup> Yuhang Zhao,<sup>20</sup> Z.-C. Zhao<sup>Ⓢ</sup>,<sup>317</sup> Y. Zheng<sup>Ⓢ</sup>,<sup>105</sup> H. Zhong<sup>Ⓢ</sup>,<sup>18</sup> H. Zhou,<sup>78</sup> H. O. Zhu,<sup>72</sup> Z.-H. Zhu<sup>Ⓢ</sup>,<sup>317, 318</sup> A. B. Zimmerman<sup>Ⓢ</sup>,<sup>147</sup> L. Zimmermann,<sup>56</sup> M. E. Zucker<sup>Ⓢ</sup>,<sup>35, 11</sup> and J. Zweizig<sup>Ⓢ</sup><sup>11</sup>

<sup>1</sup>Max Planck Institute for Gravitational Physics (Albert Einstein Institute), D-14476 Potsdam, Germany

<sup>2</sup>LIGO Hanford Observatory, Richland, WA 99352, USA

<sup>3</sup>Dipartimento di Farmacia, Università di Salerno, I-84084 Fisciano, Salerno, Italy

<sup>4</sup>INFN, Sezione di Napoli, I-80126 Napoli, Italy

<sup>5</sup>University of Warwick, Coventry CV4 7AL, United Kingdom

<sup>6</sup>OzGrav, School of Physics & Astronomy, Monash University, Clayton 3800, Victoria, Australia

<sup>7</sup>The Pennsylvania State University, University Park, PA 16802, USA

<sup>8</sup>Max Planck Institute for Gravitational Physics (Albert Einstein Institute), D-30167 Hannover, Germany

<sup>9</sup>Leibniz Universität Hannover, D-30167 Hannover, Germany

<sup>10</sup>University of Wisconsin-Milwaukee, Milwaukee, WI 53201, USA

<sup>11</sup>LIGO Laboratory, California Institute of Technology, Pasadena, CA 91125, USA

<sup>12</sup>Louisiana State University, Baton Rouge, LA 70803, USA

<sup>13</sup>Tata Institute of Fundamental Research, Mumbai 400005, India

<sup>14</sup>Centre de Physique Théorique, Aix-Marseille Université, Campus de Luminy, 163 Av. de Luminy, 13009 Marseille, France

<sup>15</sup>Université catholique de Louvain, B-1348 Louvain-la-Neuve, Belgium

<sup>16</sup>Queen Mary University of London, London E1 4NS, United Kingdom

<sup>17</sup>University of California, Davis, Davis, CA 95616, USA

<sup>18</sup>University of Minnesota, Minneapolis, MN 55455, USA

<sup>19</sup>Instituto Nacional de Pesquisas Espaciais, 12227-010 São José dos Campos, São Paulo, Brazil

<sup>20</sup>Université Paris Cité, CNRS, Astroparticule et Cosmologie, F-75013 Paris, France

<sup>21</sup>Università di Roma Tor Vergata, I-00133 Roma, Italy

<sup>22</sup>INFN, Sezione di Roma Tor Vergata, I-00133 Roma, Italy

<sup>23</sup>Universiteit Antwerpen, 2000 Antwerpen, Belgium

<sup>24</sup>International Centre for Theoretical Sciences, Tata Institute of Fundamental Research, Bengaluru 560089, India

<sup>25</sup>Gravitational Wave Science Project, National Astronomical Observatory of Japan, 2-21-1 Osawa, Mitaka City, Tokyo 181-8588, Japan

<sup>26</sup>Advanced Technology Center, National Astronomical Observatory of Japan, 2-21-1 Osawa, Mitaka City, Tokyo 181-8588, Japan

<sup>27</sup>Theoretisch-Physikalisches Institut, Friedrich-Schiller-Universität Jena, D-07743 Jena, Germany

<sup>28</sup>INFN Sezione di Torino, I-10125 Torino, Italy

<sup>29</sup>INFN, Sezione di Genova, I-16146 Genova, Italy

<sup>30</sup>Dipartimento di Fisica, Università degli Studi di Genova, I-16146 Genova, Italy

<sup>31</sup>Univ. Savoie Mont Blanc, CNRS, Laboratoire d'Annecy de Physique des Particules - IN2P3, F-74000 Annecy, France

<sup>32</sup>Università di Napoli "Federico II", I-80126 Napoli, Italy

<sup>33</sup>Cardiff University, Cardiff CF24 3AA, United Kingdom

<sup>34</sup>OzGrav, Australian National University, Canberra, Australian Capital Territory 0200, Australia

<sup>35</sup>LIGO Laboratory, Massachusetts Institute of Technology, Cambridge, MA 02139, USA

<sup>36</sup>Maastricht University, 6200 MD Maastricht, Netherlands

<sup>37</sup>Nikhef, 1098 XG Amsterdam, Netherlands

<sup>38</sup>INFN, Sezione di Roma, I-00185 Roma, Italy

<sup>39</sup>Università di Roma "La Sapienza", I-00185 Roma, Italy

<sup>40</sup>Aix Marseille Univ, CNRS, Centrale Med, Institut Fresnel, F-13013 Marseille, France

<sup>41</sup>Université Paris-Saclay, CNRS/IN2P3, IJCLab, 91405 Orsay, France

<sup>42</sup>University of Tokyo, Tokyo, 113-0033, Japan

<sup>43</sup>Institut de Física d'Altes Energies (IFAE), The Barcelona Institute of Science and Technology, Campus UAB, E-08193 Bellaterra (Barcelona), Spain

<sup>44</sup>Gran Sasso Science Institute (GSSI), I-67100 L'Aquila, Italy

<sup>45</sup>INFN, Laboratori Nazionali del Gran Sasso, I-67100 Assergi, Italy

<sup>46</sup>University of Florida, Gainesville, FL 32611, USA

- <sup>47</sup> *Dipartimento di Scienze Matematiche, Informatiche e Fisiche, Università di Udine, I-33100 Udine, Italy*
- <sup>48</sup> *INFN, Sezione di Trieste, I-34127 Trieste, Italy*
- <sup>49</sup> *Tecnologico de Monterrey, Escuela de Ingeniería y Ciencias, 64849 Monterrey, Nuevo León, Mexico*
- <sup>50</sup> *Institute for Cosmic Ray Research, KAGRA Observatory, The University of Tokyo, 238 Higashi-Mozumi, Kamioka-cho, Hida City, Gifu 506-1205, Japan*
- <sup>51</sup> *INFN, Sezione di Perugia, I-06123 Perugia, Italy*
- <sup>52</sup> *Università di Camerino, I-62032 Camerino, Italy*
- <sup>53</sup> *University of Washington, Seattle, WA 98195, USA*
- <sup>54</sup> *California State University Fullerton, Fullerton, CA 92831, USA*
- <sup>55</sup> *SUPA, University of Strathclyde, Glasgow G1 1XQ, United Kingdom*
- <sup>56</sup> *Université Claude Bernard Lyon 1, CNRS, IP2I Lyon / IN2P3, UMR 5822, F-69622 Villeurbanne, France*
- <sup>57</sup> *Georgia Institute of Technology, Atlanta, GA 30332, USA*
- <sup>58</sup> *Royal Holloway, University of London, London TW20 0EX, United Kingdom*
- <sup>59</sup> *Astronomical course, The Graduate University for Advanced Studies (SOKENDAI), 2-21-1 Osawa, Mitaka City, Tokyo 181-8588, Japan*
- <sup>60</sup> *Università degli Studi di Urbino “Carlo Bo”, I-61029 Urbino, Italy*
- <sup>61</sup> *INFN, Sezione di Firenze, I-50019 Sesto Fiorentino, Firenze, Italy*
- <sup>62</sup> *European Gravitational Observatory (EGO), I-56021 Cascina, Pisa, Italy*
- <sup>63</sup> *LIGO Livingston Observatory, Livingston, LA 70754, USA*
- <sup>64</sup> *Université de Strasbourg, CNRS, IPHC UMR 7178, F-67000 Strasbourg, France*
- <sup>65</sup> *Embry-Riddle Aeronautical University, Prescott, AZ 86301, USA*
- <sup>66</sup> *Dipartimento di Fisica “E.R. Caianiello”, Università di Salerno, I-84084 Fisciano, Salerno, Italy*
- <sup>67</sup> *King’s College London, University of London, London WC2R 2LS, United Kingdom*
- <sup>68</sup> *Korea Institute of Science and Technology Information, Daejeon 34141, Republic of Korea*
- <sup>69</sup> *International College, Osaka University, 1-1 Machikaneyama-cho, Toyonaka City, Osaka 560-0043, Japan*
- <sup>70</sup> *Accelerator Laboratory, High Energy Accelerator Research Organization (KEK), 1-1 Oho, Tsukuba City, Ibaraki 305-0801, Japan*
- <sup>71</sup> *Institute for Gravitational and Subatomic Physics (GRASP), Utrecht University, 3584 CC Utrecht, Netherlands*
- <sup>72</sup> *OzGrav, University of Western Australia, Crawley, Western Australia 6009, Australia*
- <sup>73</sup> *University of Portsmouth, Portsmouth, PO1 3FX, United Kingdom*
- <sup>74</sup> *Università di Trento, Dipartimento di Fisica, I-38123 Povo, Trento, Italy*
- <sup>75</sup> *INFN, Trento Institute for Fundamental Physics and Applications, I-38123 Povo, Trento, Italy*
- <sup>76</sup> *Università di Perugia, I-06123 Perugia, Italy*
- <sup>77</sup> *University of Oregon, Eugene, OR 97403, USA*
- <sup>78</sup> *Syracuse University, Syracuse, NY 13244, USA*
- <sup>79</sup> *Inter-University Centre for Astronomy and Astrophysics, Pune 411007, India*
- <sup>80</sup> *INFN, Sezione di Pisa, I-56127 Pisa, Italy*
- <sup>81</sup> *Università di Pisa, I-56127 Pisa, Italy*
- <sup>82</sup> *Institut de Ciències del Cosmos (ICCUB), Universitat de Barcelona (UB), c. Martí i Franquès, 1, 08028 Barcelona, Spain*
- <sup>83</sup> *Departament de Física Quàntica i Astrofísica (FQA), Universitat de Barcelona (UB), c. Martí i Franquès, 1, 08028 Barcelona, Spain*
- <sup>84</sup> *Institut d’Estudis Espacials de Catalunya, c. Gran Capità, 2-4, 08034 Barcelona, Spain*
- <sup>85</sup> *Dipartimento di Medicina, Chirurgia e Odontoiatria “Scuola Medica Salernitana”, Università di Salerno, I-84081 Baronissi, Salerno, Italy*
- <sup>86</sup> *IGR, University of Glasgow, Glasgow G12 8QQ, United Kingdom*
- <sup>87</sup> *HUN-REN Wigner Research Centre for Physics, H-1121 Budapest, Hungary*
- <sup>88</sup> *Concordia University Wisconsin, Mequon, WI 53097, USA*
- <sup>89</sup> *Stanford University, Stanford, CA 94305, USA*
- <sup>90</sup> *University of Michigan, Ann Arbor, MI 48109, USA*
- <sup>91</sup> *Università di Padova, Dipartimento di Fisica e Astronomia, I-35131 Padova, Italy*
- <sup>92</sup> *INFN, Sezione di Padova, I-35131 Padova, Italy*
- <sup>93</sup> *Institute for Plasma Research, Bhat, Gandhinagar 382428, India*
- <sup>94</sup> *Universiteit Gent, B-9000 Gent, Belgium*
- <sup>95</sup> *Nicolaus Copernicus Astronomical Center, Polish Academy of Sciences, 00-716, Warsaw, Poland*
- <sup>96</sup> *Northwestern University, Evanston, IL 60208, USA*
- <sup>97</sup> *Universität Hamburg, D-22761 Hamburg, Germany*
- <sup>98</sup> *IAC3–IEEC, Universitat de les Illes Balears, E-07122 Palma de Mallorca, Spain*
- <sup>99</sup> *Aix-Marseille Université, Université de Toulon, CNRS, CPT, Marseille, France*
- <sup>100</sup> *Laboratoire des 2 Infinis - Toulouse (L2IT-IN2P3), F-31062 Toulouse Cedex 9, France*
- <sup>101</sup> *Università di Siena, Dipartimento di Scienze Fisiche, della Terra e dell’Ambiente, I-53100 Siena, Italy*
- <sup>102</sup> *Villanova University, Villanova, PA 19085, USA*

- <sup>103</sup>RRCAT, Indore, Madhya Pradesh 452013, India  
<sup>104</sup>Kenyon College, Gambier, OH 43022, USA  
<sup>105</sup>Missouri University of Science and Technology, Rolla, MO 65409, USA  
<sup>106</sup>Indian Institute of Technology Madras, Chennai 600036, India  
<sup>107</sup>Department of Physics and Astronomy, Vrije Universiteit Amsterdam, 1081 HV Amsterdam, Netherlands  
<sup>108</sup>Lomonosov Moscow State University, Moscow 119991, Russia  
<sup>109</sup>Katholieke Universiteit Leuven, Oude Markt 13, 3000 Leuven, Belgium  
<sup>110</sup>Rochester Institute of Technology, Rochester, NY 14623, USA  
<sup>111</sup>Université libre de Bruxelles, 1050 Bruxelles, Belgium  
<sup>112</sup>Bar-Ilan University, Ramat Gan, 5290002, Israel  
<sup>113</sup>Université Côte d'Azur, Observatoire de la Côte d'Azur, CNRS, Artemis, F-06304 Nice, France  
<sup>114</sup>University of British Columbia, Vancouver, BC V6T 1Z4, Canada  
<sup>115</sup>OzGrav, University of Adelaide, Adelaide, South Australia 5005, Australia  
<sup>116</sup>Centre national de la recherche scientifique, 75016 Paris, France  
<sup>117</sup>Univ Rennes, CNRS, Institut FOTON - UMR 6082, F-35000 Rennes, France  
<sup>118</sup>University of Birmingham, Birmingham B15 2TT, United Kingdom  
<sup>119</sup>Washington State University, Pullman, WA 99164, USA  
<sup>120</sup>Cornell University, Ithaca, NY 14850, USA  
<sup>121</sup>Laboratoire Kastler Brossel, Sorbonne Université, CNRS, ENS-Université PSL, Collège de France, F-75005 Paris, France  
<sup>122</sup>Christopher Newport University, Newport News, VA 23606, USA  
<sup>123</sup>OzGrav, University of Melbourne, Parkville, Victoria 3010, Australia  
<sup>124</sup>Astronomical Observatory Warsaw University, 00-478 Warsaw, Poland  
<sup>125</sup>University of Maryland, College Park, MD 20742, USA  
<sup>126</sup>Università degli Studi di Milano-Bicocca, I-20126 Milano, Italy  
<sup>127</sup>INFN, Sezione di Milano-Bicocca, I-20126 Milano, Italy  
<sup>128</sup>Université de Lyon, Université Claude Bernard Lyon 1, CNRS, Institut Lumière Matière, F-69622 Villeurbanne, France  
<sup>129</sup>University of Chicago, Chicago, IL 60637, USA  
<sup>130</sup>University of Arizona, Tucson, AZ 85721, USA  
<sup>131</sup>INFN, Sezione di Napoli, Gruppo Collegato di Salerno, I-80126 Napoli, Italy  
<sup>132</sup>University of Massachusetts Dartmouth, North Dartmouth, MA 02747, USA  
<sup>133</sup>Niels Bohr Institute, Copenhagen University, 2100 København, Denmark  
<sup>134</sup>Universidad de Guadalajara, 44430 Guadalajara, Jalisco, Mexico  
<sup>135</sup>Istituto di Astrofisica e Planetologia Spaziali di Roma, 00133 Roma, Italy  
<sup>136</sup>Colorado State University, Fort Collins, CO 80523, USA  
<sup>137</sup>Departamento de Astronomía y Astrofísica, Universitat de València, E-46100 Burjassot, València, Spain  
<sup>138</sup>Observatori Astronòmic, Universitat de València, E-46980 Paterna, València, Spain  
<sup>139</sup>Niels Bohr Institute, University of Copenhagen, 2100 København, Denmark  
<sup>140</sup>National Central University, Taoyuan City 320317, Taiwan  
<sup>141</sup>National Tsing Hua University, Hsinchu City 30013, Taiwan  
<sup>142</sup>OzGrav, Charles Sturt University, Wagga Wagga, New South Wales 2678, Australia  
<sup>143</sup>Vanderbilt University, Nashville, TN 37235, USA  
<sup>144</sup>University of the Chinese Academy of Sciences / International Centre for Theoretical Physics Asia-Pacific, Beijing 100049, China  
<sup>145</sup>Department of Electrophysics, National Yang Ming Chiao Tung University, 101 Univ. Street, Hsinchu, Taiwan  
<sup>146</sup>Kamioka Branch, National Astronomical Observatory of Japan, 238 Higashi-Mozumi, Kamioka-cho, Hida City, Gifu 506-1205, Japan  
<sup>147</sup>University of Texas, Austin, TX 78712, USA  
<sup>148</sup>CaRT, California Institute of Technology, Pasadena, CA 91125, USA  
<sup>149</sup>Northeastern University, Boston, MA 02115, USA  
<sup>150</sup>Dipartimento di Ingegneria Industriale (DIIN), Università di Salerno, I-84084 Fisciano, Salerno, Italy  
<sup>151</sup>Faculty of Science, University of Toyama, 3190 Gofuku, Toyama City, Toyama 930-8555, Japan  
<sup>152</sup>Carleton College, Northfield, MN 55057, USA  
<sup>153</sup>University of Szeged, Dóm tér 9, Szeged 6720, Hungary  
<sup>154</sup>OzGrav, Swinburne University of Technology, Hawthorn VIC 3122, Australia  
<sup>155</sup>INFN Cagliari, Physics Department, Università degli Studi di Cagliari, Cagliari 09042, Italy  
<sup>156</sup>Università degli Studi di Cagliari, Via Università 40, 09124 Cagliari, Italy  
<sup>157</sup>Université Libre de Bruxelles, Brussels 1050, Belgium  
<sup>158</sup>INAF, Osservatorio Astronomico di Brera sede di Merate, I-23807 Merate, Lecco, Italy  
<sup>159</sup>Departamento de Matemáticas, Universitat de València, E-46100 Burjassot, València, Spain  
<sup>160</sup>Montana State University, Bozeman, MT 59717, USA  
<sup>161</sup>The University of Utah, Salt Lake City, UT 84112, USA

- <sup>162</sup> Johns Hopkins University, Baltimore, MD 21218, USA
- <sup>163</sup> University of Rhode Island, Kingston, RI 02881, USA
- <sup>164</sup> The University of Texas Rio Grande Valley, Brownsville, TX 78520, USA
- <sup>165</sup> Université de Liège, B-4000 Liège, Belgium
- <sup>166</sup> DIFA- Alma Mater Studiorum Università di Bologna, Via Zamboni, 33 - 40126 Bologna, Italy
- <sup>167</sup> Istituto Nazionale Di Fisica Nucleare - Sezione di Bologna, viale Carlo Berti Pichat 6/2 - 40127 Bologna, Italy
- <sup>168</sup> University of Manitoba, Winnipeg, MB R3T 2N2, Canada
- <sup>169</sup> INFN-CNAF - Bologna, Viale Carlo Berti Pichat, 6/2, 40127 Bologna BO, Italy
- <sup>170</sup> Università degli Studi di Sassari, I-07100 Sassari, Italy
- <sup>171</sup> INFN, Laboratori Nazionali del Sud, I-95125 Catania, Italy
- <sup>172</sup> Université de Normandie, ENSICAEN, UNICAEN, CNRS/IN2P3, LPC Caen, F-14000 Caen, France
- <sup>173</sup> Laboratoire de Physique Corpusculaire Caen, 6 boulevard du maréchal Juin, F-14050 Caen, France
- <sup>174</sup> The University of Sheffield, Sheffield S10 2TN, United Kingdom
- <sup>175</sup> Université Claude Bernard Lyon 1, CNRS, Laboratoire des Matériaux Avancés (LMA), IP2I Lyon / IN2P3, UMR 5822, F-69622 Villeurbanne, France
- <sup>176</sup> Università di Firenze, Sesto Fiorentino I-50019, Italy
- <sup>177</sup> IGFAE, Universidad de Santiago de Compostela, E-15782 Santiago de Compostela, Spain
- <sup>178</sup> Dipartimento di Scienze Matematiche, Fisiche e Informatiche, Università di Parma, I-43124 Parma, Italy
- <sup>179</sup> INFN, Sezione di Milano Bicocca, Gruppo Collegato di Parma, I-43124 Parma, Italy
- <sup>180</sup> California State University, Los Angeles, Los Angeles, CA 90032, USA
- <sup>181</sup> Marquette University, Milwaukee, WI 53233, USA
- <sup>182</sup> Perimeter Institute, Waterloo, ON N2L 2Y5, Canada
- <sup>183</sup> Corps des Mines, Mines Paris, Université PSL, 60 Bd Saint-Michel, 75272 Paris, France
- <sup>184</sup> Dipartimento di Fisica, Università di Trieste, I-34127 Trieste, Italy
- <sup>185</sup> Université Côte d'Azur, Observatoire de la Côte d'Azur, CNRS, Lagrange, F-06304 Nice, France
- <sup>186</sup> National Center for Nuclear Research, 05-400 Świerk-Otwock, Poland
- <sup>187</sup> Vrije Universiteit Brussel, 1050 Brussel, Belgium
- <sup>188</sup> University of Zurich, Winterthurerstrasse 190, 8057 Zurich, Switzerland
- <sup>189</sup> Canadian Institute for Theoretical Astrophysics, University of Toronto, Toronto, ON M5S 3H8, Canada
- <sup>190</sup> Stony Brook University, Stony Brook, NY 11794, USA
- <sup>191</sup> Center for Computational Astrophysics, Flatiron Institute, New York, NY 10010, USA
- <sup>192</sup> Montclair State University, Montclair, NJ 07043, USA
- <sup>193</sup> HUN-REN Institute for Nuclear Research, H-4026 Debrecen, Hungary
- <sup>194</sup> Indian Institute of Technology Bombay, Powai, Mumbai 400 076, India
- <sup>195</sup> Centro de Física das Universidades do Minho e do Porto, Universidade do Minho, PT-4710-057 Braga, Portugal
- <sup>196</sup> Aix Marseille Univ, CNRS/IN2P3, CPPM, Marseille, France
- <sup>197</sup> CNR-SPIN, I-84084 Fisciano, Salerno, Italy
- <sup>198</sup> Scuola di Ingegneria, Università della Basilicata, I-85100 Potenza, Italy
- <sup>199</sup> Western Washington University, Bellingham, WA 98225, USA
- <sup>200</sup> SUPA, University of the West of Scotland, Paisley PA1 2BE, United Kingdom
- <sup>201</sup> Barry University, Miami Shores, FL 33168, USA
- <sup>202</sup> Eötvös University, Budapest 1117, Hungary
- <sup>203</sup> Institute for Cosmic Ray Research, KAGRA Observatory, The University of Tokyo, 5-1-5 Kashiwa-no-Ha, Kashiwa City, Chiba 277-8582, Japan
- <sup>204</sup> Department of Physics, Graduate School of Science, Osaka Metropolitan University, 3-3-138 Sugimoto-cho, Sumiyoshi-ku, Osaka City, Osaka 558-8585, Japan
- <sup>205</sup> University of Sannio at Benevento, I-82100 Benevento, Italy and INFN, Sezione di Napoli, I-80100 Napoli, Italy
- <sup>206</sup> University of California, Berkeley, CA 94720, USA
- <sup>207</sup> Instituto de Física Teórica UAM-CSIC, Universidad Autónoma de Madrid, 28049 Madrid, Spain
- <sup>208</sup> Laboratoire d'Acoustique de l'Université du Mans, UMR CNRS 6613, F-72085 Le Mans, France
- <sup>209</sup> University of Southampton, Southampton SO17 1BJ, United Kingdom
- <sup>210</sup> University of California, Riverside, Riverside, CA 92521, USA
- <sup>211</sup> Dipartimento di Ingegneria Industriale, Elettronica e Meccanica, Università degli Studi Roma Tre, I-00146 Roma, Italy
- <sup>212</sup> University of Nevada, Las Vegas, Las Vegas, NV 89154, USA
- <sup>213</sup> University of Nottingham NG7 2RD, UK
- <sup>214</sup> Ariel University, Ramat HaGolan St 65, Ari'el, Israel
- <sup>215</sup> The University of Mississippi, University, MS 38677, USA

- <sup>216</sup> Graduate School of Science, Institute of Science Tokyo,  
2-12-1 Ookayama, Meguro-ku, Tokyo 152-8551, Japan
- <sup>217</sup> Institute of Physics, Academia Sinica, 128 Sec. 2, Academia Rd., Nankang, Taipei 11529, Taiwan
- <sup>218</sup> The Chinese University of Hong Kong, Shatin, NT, Hong Kong
- <sup>219</sup> American University, Washington, DC 20016, USA
- <sup>220</sup> Dipartimento di Fisica, Università degli studi di Milano, Via Celoria 16, I-20133, Milano, Italy
- <sup>221</sup> INFN, sezione di Milano, Via Celoria 16, I-20133, Milano, Italy
- <sup>222</sup> Department of Applied Physics, Fukuoka University,  
8-19-1 Nanakuma, Jonan, Fukuoka City, Fukuoka 814-0180, Japan
- <sup>223</sup> University of Cambridge, Cambridge CB2 1TN, United Kingdom
- <sup>224</sup> University of Lancaster, Lancaster LA1 4YW, United Kingdom
- <sup>225</sup> College of Industrial Technology, Nihon University,  
1-2-1 Izumi, Narashino City, Chiba 275-8575, Japan
- <sup>226</sup> Faculty of Engineering, Niigata University, 8050 Ikarashi-2-no-cho, Nishi-ku, Niigata City, Niigata 950-2181, Japan
- <sup>227</sup> Department of Physics, Tamkang University, No. 151,  
Yingzhuan Rd., Danshui Dist., New Taipei City 25137, Taiwan
- <sup>228</sup> Rutherford Appleton Laboratory, Didcot OX11 0DE, United Kingdom
- <sup>229</sup> Department of Physical Sciences, Aoyama Gakuin University,  
5-10-1 Fuchinobe, Sagamihara City, Kanagawa 252-5258, Japan
- <sup>230</sup> Helmut Schmidt University, D-22043 Hamburg, Germany
- <sup>231</sup> Nambu Yoichiro Institute of Theoretical and Experimental Physics (NITEP),  
Osaka Metropolitan University, 3-3-138 Sugimoto-cho,  
Sumiyoshi-ku, Osaka City, Osaka 558-8585, Japan
- <sup>232</sup> Directorate of Construction, Services & Estate Management, Mumbai 400094, India
- <sup>233</sup> Observatoire Astronomique de Strasbourg, 11 Rue de l'Université, 67000 Strasbourg, France
- <sup>234</sup> Faculty of Physics, University of Białystok, 15-245 Białystok, Poland
- <sup>235</sup> National Astronomical Observatories, Chinese Academic of Sciences,  
20A Datun Road, Chaoyang District, Beijing, China
- <sup>236</sup> School of Astronomy and Space Science, University of Chinese Academy of Sciences,  
20A Datun Road, Chaoyang District, Beijing, China
- <sup>237</sup> Sungkyunkwan University, Seoul 03063, Republic of Korea
- <sup>238</sup> Department of Physics, Ulsan National Institute of Science and Technology (UNIST),  
50 UNIST-gil, Ulju-gun, Ulsan 44919, Republic of Korea
- <sup>239</sup> Institute for Cosmic Ray Research, The University of Tokyo,  
5-1-5 Kashiwa-no-Ha, Kashiwa City, Chiba 277-8582, Japan
- <sup>240</sup> Chung-Ang University, Seoul 06974, Republic of Korea
- <sup>241</sup> University of Washington Bothell, Bothell, WA 98011, USA
- <sup>242</sup> Laboratoire de Physique et de Chimie de l'Environnement,  
Université Joseph KI-ZERBO, 9GH2+3V5, Ouagadougou, Burkina Faso
- <sup>243</sup> Ewha Womans University, Seoul 03760, Republic of Korea
- <sup>244</sup> National Institute for Mathematical Sciences, Daejeon 34047, Republic of Korea
- <sup>245</sup> Korea Astronomy and Space Science Institute, Daejeon 34055, Republic of Korea
- <sup>246</sup> Department of Astronomy and Space Science, Chungnam National University,  
9 Daehak-ro, Yuseong-gu, Daejeon 34134, Republic of Korea
- <sup>247</sup> Institute of Particle and Nuclear Studies (IPNS),  
High Energy Accelerator Research Organization (KEK),  
1-1 Oho, Tsukuba City, Ibaraki 305-0801, Japan
- <sup>248</sup> Division of Science, National Astronomical Observatory of Japan,  
2-21-1 Osawa, Mitaka City, Tokyo 181-8588, Japan
- <sup>249</sup> Nagoya University, Nagoya, 464-8601, Japan
- <sup>250</sup> Department of Physics, Aristotle University of Thessaloniki, 54124 Thessaloniki, Greece
- <sup>251</sup> Bard College, Annandale-On-Hudson, NY 12504, USA
- <sup>252</sup> Technical University of Braunschweig, D-38106 Braunschweig, Germany
- <sup>253</sup> Institute of Mathematics, Polish Academy of Sciences, 00656 Warsaw, Poland
- <sup>254</sup> Astronomical Observatory, Jagiellonian University, 31-007 Cracow, Poland
- <sup>255</sup> Department of Physics and Astronomy, University of Padova, Via Marzolo, 8-35151 Padova, Italy
- <sup>256</sup> Sezione di Padova, Istituto Nazionale di Fisica Nucleare (INFN), Via Marzolo, 8-35131 Padova, Italy
- <sup>257</sup> Department of Physics, Nagoya University, ES building,  
Furocho, Chikusa-ku, Nagoya, Aichi 464-8602, Japan
- <sup>258</sup> Université de Montréal/Polytechnique, Montreal, Quebec H3T 1J4, Canada
- <sup>259</sup> Indian Institute of Science Education and Research, Kolkata, Mohampur, West Bengal 741252, India
- <sup>260</sup> Seoul National University, Seoul 08826, Republic of Korea
- <sup>261</sup> Department of Computer Simulation, Inje University,  
197 Inje-ro, Gimhae, Gyeongsangnam-do 50834, Republic of Korea

- <sup>262</sup> NAVIER, *École des Ponts, Univ Gustave Eiffel, CNRS, Marne-la-Vallée, France*
- <sup>263</sup> *Gravitational Wave Science Project, National Astronomical Observatory of Japan (NAOJ), Mitaka City, Tokyo 181-8588, Japan*
- <sup>264</sup> *Department of Physics, National Cheng Kung University, No.1, University Road, Tainan City 701, Taiwan*
- <sup>265</sup> *St. Thomas University, Miami Gardens, FL 33054, USA*
- <sup>266</sup> *Scuola Normale Superiore, I-56126 Pisa, Italy*
- <sup>267</sup> *Institució Catalana de Recerca i Estudis Avançats, E-08010 Barcelona, Spain*
- <sup>268</sup> *Institut de Física d'Altes Energies, E-08193 Barcelona, Spain*
- <sup>269</sup> *Institut fuer Theoretische Astrophysik, Zentrum fuer Astronomie Heidelberg, Universitaet Heidelberg, Albert Ueberle Str. 2, 69120 Heidelberg, Germany*
- <sup>270</sup> *Institucio Catalana de Recerca i Estudis Avançats (ICREA), Passeig de Lluís Companys, 23, 08010 Barcelona, Spain*
- <sup>271</sup> *Research Center for Space Science, Advanced Research Laboratories, Tokyo City University, 3-3-1 Ushikubo-Nishi, Tsuzuki-Ku, Yokohama, Kanagawa 224-8551, Japan*
- <sup>272</sup> *Tsinghua University, Beijing 100084, China*
- <sup>273</sup> *Institut des Hautes Etudes Scientifiques, F-91440 Bures-sur-Yvette, France*
- <sup>274</sup> *Faculty of Law, Ryukoku University, 67 Fukakusa Tsukamoto-cho, Fushimi-ku, Kyoto City, Kyoto 612-8577, Japan*
- <sup>275</sup> *Phenikaa Institute for Advanced Study (PIAS), Phenikaa University, Yen Nghia, Ha Dong, Hanoi, Vietnam*
- <sup>276</sup> *University of Stavanger, 4021 Stavanger, Norway*
- <sup>277</sup> *Physics Program, Graduate School of Advanced Science and Engineering, Hiroshima University, 1-3-1 Kagamiyama, Higashihiroshima City, Hiroshima 739-8526, Japan*
- <sup>278</sup> *GRAPPA, Anton Pannekoek Institute for Astronomy and Institute for High-Energy Physics, University of Amsterdam, 1098 XH Amsterdam, Netherlands*
- <sup>279</sup> *University College London, London WC1E 6BT, United Kingdom*
- <sup>280</sup> *Observatoire de Paris, 75014 Paris, France*
- <sup>281</sup> *Laboratoire Univers et Théories, Observatoire de Paris, 92190 Meudon, France*
- <sup>282</sup> *Graduate School of Science and Technology, Niigata University, 8050 Ikarashi-2-no-cho, Nishi-ku, Niigata City, Niigata 950-2181, Japan*
- <sup>283</sup> *University of Maryland, Baltimore County, Baltimore, MD 21250, USA*
- <sup>284</sup> *CSIR-Central Glass and Ceramic Research Institute, Kolkata, West Bengal 700032, India*
- <sup>285</sup> *Consiglio Nazionale delle Ricerche - Istituto dei Sistemi Complessi, I-00185 Roma, Italy*
- <sup>286</sup> *Department of Astronomy, Yonsei University, 50 Yonsei-Ro, Seodaemun-Gu, Seoul 03722, Republic of Korea*
- <sup>287</sup> *Department of Physics, University of Guadalajara, Av. Revolucion 1500, Colonia Olimpica C.P. 44430, Guadalajara, Jalisco, Mexico*
- <sup>288</sup> *Hobart and William Smith Colleges, Geneva, NY 14456, USA*
- <sup>289</sup> *INAF, Osservatorio Astronomico di Padova, I-35122 Padova, Italy*
- <sup>290</sup> *Dipartimento di Ingegneria, Università del Sannio, I-82100 Benevento, Italy*
- <sup>291</sup> *Museo Storico della Fisica e Centro Studi e Ricerche "Enrico Fermi", I-00184 Roma, Italy*
- <sup>292</sup> *Kennesaw State University, Kennesaw, GA 30144, USA*
- <sup>293</sup> *Subatech, CNRS/IN2P3 - IMT Atlantique - Nantes Université, 4 rue Alfred Kastler BP 20722 44307 Nantes CÉDEX 03, France*
- <sup>294</sup> *Universidad de Antioquia, Medellín, Colombia*
- <sup>295</sup> *Departamento de Física - ETSIDI, Universidad Politécnica de Madrid, 28012 Madrid, Spain*
- <sup>296</sup> *Department of Electronic Control Engineering, National Institute of Technology, Nagaoka College, 888 Nishikatakai, Nagaoka City, Niigata 940-8532, Japan*
- <sup>297</sup> *Trinity College, Hartford, CT 06106, USA*
- <sup>298</sup> *Dipartimento di Fisica e Scienze della Terra, Università Degli Studi di Ferrara, Via Saragat, 1, 44121 Ferrara FE, Italy*
- <sup>299</sup> *Faculty of Science, Toho University, 2-2-1 Miyama, Funabashi City, Chiba 274-8510, Japan*
- <sup>300</sup> *Indian Institute of Technology, Palaj, Gandhinagar, Gujarat 382355, India*
- <sup>301</sup> *Kavli Institute for Astronomy and Astrophysics, Peking University, Yiheyuan Road 5, Haidian District, Beijing 100871, China*
- <sup>302</sup> *Laboratoire MSME, Cité Descartes, 5 Boulevard Descartes, Champs-sur-Marne, 77454 Marne-la-Vallée Cedex 2, France*
- <sup>303</sup> *Faculty of Information Science and Technology, Osaka Institute of Technology, 1-79-1 Kitayama, Hirakata City, Osaka 573-0196, Japan*
- <sup>304</sup> *NASA Goddard Space Flight Center, Greenbelt, MD 20771, USA*
- <sup>305</sup> *Faculty of Science and Technology, Kochi University, 2-5-1 Akebono-cho, Kochi-shi, Kochi 780-8520, Japan*

<sup>306</sup>*Laboratoire de Physique de l'École Normale Supérieure, ENS, (CNRS,*

*Université PSL, Sorbonne Université, Université Paris Cité), F-75005 Paris, France*

<sup>307</sup>*Faculty of Physics, University of Warsaw, Ludwika Pasteura 5, 02-093 Warszawa, Poland*

<sup>308</sup>*Laser Interferometry and Gravitational Wave Astronomy,*

*Max Planck Institute for Gravitational Physics, Callinstrasse 38, 30167 Hannover, Germany*

<sup>309</sup>*The Hakubi Center for Advanced Research, Kyoto University,*

*Yoshida-honmachi, Sakyou-ku, Kyoto City, Kyoto 606-8501, Japan*

<sup>310</sup>*Department of Physics, Kyoto University, Kita-Shirakawa Oiwake-cho, Sakyou-ku, Kyoto City, Kyoto 606-8502, Japan*

<sup>311</sup>*Yukawa Institute for Theoretical Physics (YITP), Kyoto University,*

*Kita-Shirakawa Oiwake-cho, Sakyou-ku, Kyoto City, Kyoto 606-8502, Japan*

<sup>312</sup>*University of Catania, Department of Physics and Astronomy, Via S. Sofia, 64, 95123 Catania CT, Italy*

<sup>313</sup>*National Institute of Technology, Fukui College, Geshi-cho, Sabae-shi, Fukui 916-8507, Japan*

<sup>314</sup>*Department of Communications Engineering, National Defense Academy of Japan,*

*1-10-20 Hashirimizu, Yokosuka City, Kanagawa 239-8686, Japan*

<sup>315</sup>*Eindhoven University of Technology, 5600 MB Eindhoven, Netherlands*

<sup>316</sup>*Kavli Institute for the Physics and Mathematics of the Universe (Kavli IPMU), WPI,*

*The University of Tokyo, 5-1-5 Kashiwa-no-Ha, Kashiwa City, Chiba 277-8583, Japan*

<sup>317</sup>*Department of Astronomy, Beijing Normal University,*

*Xinjiekwai Street 19, Haidian District, Beijing 100875, China*

<sup>318</sup>*School of Physics and Technology, Wuhan University,*

*Bayi Road 299, Wuchang District, Wuhan, Hubei, 430072, China*

The angular distribution of gravitational-wave power from persistent sources may exhibit anisotropies arising from the large-scale structure of the Universe. This motivates directional searches for astrophysical and cosmological gravitational-wave backgrounds, as well as continuous-wave emitters. We present results of such a search using data from the first observing run through the first portion of the fourth observing run of the LIGO-Virgo-KAGRA Collaborations. We apply gravitational-wave radiometer techniques to generate skymaps and search for both narrowband and broadband persistent gravitational-wave sources. Additionally, we use spherical harmonic decomposition to probe spatially extended sources. No evidence of persistent gravitational-wave signals is found, and we set the most stringent constraints to date on such emissions. For narrowband point sources, our sensitivity estimate to effective strain amplitude lies in the range  $(0.03 - 8.4) \times 10^{-24}$  across all sky and frequency range (20 – 160) Hz. For targeted sources—Scorpius X-1, SN 1987A, the Galactic Center, Terzan 5, and NGC 6397—we constrain the strain amplitude with best limits ranging from  $\sim 1.1 \times 10^{-25}$  to  $6.5 \times 10^{-24}$ . For persistent broadband sources, we constrain the gravitational-wave flux  $F_{\alpha, \hat{n}}^{95\%, \text{UL}}(25 \text{ Hz}) < (0.008 - 5.5) \times 10^{-8} \text{ erg cm}^{-2} \text{ s}^{-1} \text{ Hz}^{-1}$ , depending on the sky direction  $\hat{n}$  and spectral index  $\alpha = 0, 2/3, 3$ . Finally, for extended sources, we place upper limits on the strain angular power spectrum  $C_\ell^{1/2} < (0.63 - 17) \times 10^{-10} \text{ sr}^{-1}$ .

## I. INTRODUCTION

A gravitational-wave background (GWB) is a diffuse signal resulting from the incoherent superposition of numerous unresolved gravitational wave (GW) sources. Its stochastic nature may stem from either the formation mechanisms of the sources or the limited sensitivity of current detectors. A wide range of sources is expected to contribute to the GWB, each with distinct characteristics and frequency signatures. The GWB is typically categorized into two main types: the astrophysical GWB [1], arising from unresolved sources such as compact binary coalescences [2–6] and rotating neutron stars [7–15], and the cosmological GWB [16], potentially generated by early-universe phenomena such as inflation [17–19], cosmic strings [20–23], or phase transitions [24, 25].

While to first order the GWB is expected to be homogeneous and isotropic across the sky, it may exhibit

two kinds of anisotropy: large-scale and local. Large-scale anisotropies may arise from the uneven distribution of sources on cosmological scales [26–34], propagation effects due to large-scale structures along the line of sight [35], and kinematic anisotropies caused by the motion of the observer relative to the GWB rest frame [36–40]. In contrast, local anisotropies can be caused by nearby, spatially clustered sources, for example a concentration of millisecond pulsars in regions such as the Galactic plane and Virgo cluster, leading to prominent hotspots in the sky [36, 41–45].

The LIGO-Virgo-KAGRA Collaboration (LVK) has set progressively improved upper limits (ULs) on the GWB energy density of both isotropic and anisotropic components [46–54]. To look for GWB anisotropies, the LVK performs directional searches using a GW-radiometer algorithm to generate skymaps and a spherical harmonics (SPH) decomposition to compute angular power spectra [55–57]. These tools can be used to identify cosmological, astrophysical, or local anisotropies. In addition, the GW radiometer algorithm designed to search for GWB is also well suited to look for other types

---

\* Deceased, September 2024.

of persistent GW sources, including continuous gravitational wave (CGW) sources.

Until the third observing run (O3), the pixel-based anisotropic searches [51–53] performed by LVK, targeting point-like persistent sources, typically followed two approaches: narrowband radiometer (NBR) searches, which focused on specific directions (Scorpius X-1, the Galactic Center, SN 1987A, etc.) across multiple narrow frequency bins, and broadband radiometer (BBR) searches, which scanned the entire sky but averaged over a wide frequency range. As a result, the prospects of detecting unknown anisotropies were limited, since neither approach could simultaneously explore the full angular and spectral properties of the signal. In addition, matched-filtering-based searches for persistent signals from galactic or extragalactic sources, such as neutron stars [58–60] or boson clouds around black holes [61–63], are computationally expensive and inherently limited by signal modeling assumptions. To address this limitation, we introduced a new strategy in O3: performing directional searches in narrow frequency bins across the whole sky. This approach, formalized as the all-sky-all-frequency radiometer (ASAF) search [54], enables a more comprehensive exploration of potential anisotropic signals without prior assumptions on their location or frequency content.

All of the above searches are performed in pixel basis, which is well-suited for probing localized sources. However, as mentioned above, GWB anisotropies can also be expanded in the SPH basis, which is more appropriate for studying extended or diffuse sources. The LVK has also conducted searches using the SPH basis and reported ULs on the angular power spectra using data up to O3 [51–53].

In this paper, we present results from all four analyses: ASAF, targeted NBR, BBR, and SPH, performed on the LVK observational data from the first observing run (O1), second observing run (O2), O3, and the first portion of the fourth observing run (O4a). These analyses benefit from data collected by an increasingly sensitive global network of GW detectors, whose improved sensitivity over the years has significantly enhanced our ability to probe anisotropic sources of persistent GWs. Despite this progress, we do not find evidence for such sources in any of the four analyses and therefore set ULs on the GW emission depending on specific sky directions or angular scales.

We note that this paper has two companions, one focusing on new results of the isotropic GWB search [64] and the other discussing cosmological implications of the new isotropic search results [65].

The paper is organized as follows. In Sec. II, we introduce the GW radiometer algorithm and search methodologies. In Sec. III, we present results from ASAF ra-

diometer search, targeted NBR search, BBR search, and SPH search for extended sources. Finally, in Sec. IV, we summarize our findings and outline prospects for future searches. Comprehensive descriptions of the individual analyses can be found in the Appendices.

## II. MOTIVATION AND METHODS

### A. Gravitational Wave Radiometer

The dimensionless GW energy density parameter,  $\Omega_{\text{GW}}(f, \hat{n})$ , characterizes the energy content of the GWB per unit logarithmic frequency  $f$  and unit solid angle in the direction  $\hat{n}$ . It is given by

$$\Omega_{\text{GW}}(f, \hat{n}) = \frac{2\pi^2}{3H_0^2} f^3 \mathcal{P}(f, \hat{n}), \quad (1)$$

where  $\mathcal{P}(f, \hat{n})$  denotes the one-sided power spectral density (PSD) of the GW strain field. This quantity corresponds to the second moment of a stationary, Gaussian, and unpolarized stochastic GW signal [66].  $H_0 = 67.9 \text{ km s}^{-1} \text{ Mpc}^{-1}$  in the above equation denotes the Hubble constant [67].

We aim to measure the angular distribution of the GWB, i.e.,  $\mathcal{P}(f, \hat{n})$ , by performing a cross-correlation<sup>1</sup> between data from a pair of detectors (usually referred to as baseline, denoted by  $I$ , with the subscripts  $i = 1, 2$  labeling the two detectors) that are geographically separated. We construct the cross spectral density (CSD) estimator:

$$C^I(t; f) \equiv \frac{2}{T \overline{w_1 w_2}} \tilde{s}_1^*(t; f) \tilde{s}_2(t; f), \quad (2)$$

where  $\tilde{s}_i(t; f)$  represents the short Fourier transform (SFT) computed from a time segment centered around time  $t$ , using a 50% overlapping Hann window with a segment duration of  $T = 192$  s. The factor  $\overline{w_1 w_2}$  accounts for the effect of windowing on the estimator [68, 69].

In the presence of Gaussian, additive, and stationary noise—assumed to be uncorrelated between detectors at different sites—the noise- and source-averaged correlation, denoted by  $\langle \cdot \rangle_{\hat{h}, N}$ , is given by

$$\langle C^I(t; f) \rangle_{\hat{h}, N} = \int d^2 \hat{n} \gamma^I(t; f, \hat{n}) \mathcal{P}(f, \hat{n}), \quad (3)$$

which encodes information about the source anisotropy. The overlap reduction function (ORF) [70–72],  $\gamma^I(t; f, \hat{n})$ , acts as a transfer function by mapping the spatial distribution of GW power onto the measured cross-correlation. It depends on the signal frequency, the observation time, the source sky location, the individual detector response functions, and the distance between the detectors.

<sup>1</sup> We note that the estimator constructed via cross-correlation is nearly optimal, given that the auto-correlation is not utilized to

detect the GWB signal [50].

To probe specific types of angular distributions, we discretize the sky  $\mathcal{P}(f, \hat{n})$  using an appropriate basis  $e_\mu(\hat{n})$ , i.e.,

$$\mathcal{P}(f, \hat{n}) \equiv \sum_{\mu} \mathcal{P}_{\mu}(f) e_{\mu}(\hat{n}). \quad (4)$$

The explicit expression for the ORF in an appropriate basis is given by

$$\gamma_{\mu}^I(t; f) \equiv \sum_{A=+, \times} \int d^2 \hat{n} F_1^A(t, \hat{n}) F_2^A(t, \hat{n}) e_{\mu}(\hat{n}) e^{-2\pi i f \frac{\Delta \vec{x}^I(t) \cdot \hat{n}}{c}}, \quad (5)$$

where  $F_i^A$  denotes the individual detector response functions, and  $\Delta \vec{x}^I$  is the separation vector between the detectors.

In this article, we utilize two types of bases: (i) the pixel basis  $e_{\mu}(\hat{n}) = \delta^2(\hat{n} - \hat{n}_{\mu})$  under the assumption the source is localized in the direction  $\hat{n}_{\mu}$ ; and (ii) the SPH basis  $e_{\mu}(\hat{n}) = Y_{\ell m}(\hat{n})$ , with  $\mu = (\ell, m)$ , under the assumption the source is spatially extended. We note that the esti-

mators can be transformed between pixel and SPH basis via forward and inverse SPH transforms [73]. Additionally, it is important to note that  $e_{\mu}(\hat{n}) = Y_{00}(\hat{n})$  corresponds to the isotropic component of the GWB angular distribution.

Assuming that the CSD for each time segment is a Gaussian random variable, the maximum likelihood estimator for GWB anisotropy,  $\mathcal{P}_{\mu}(f)$ , (for positive frequency) is obtained by maximizing the joint likelihood across different times and baselines as in Ref. [54], and it reads

$$\hat{\mathcal{P}}_f = \mathbf{\Gamma}_f^{-1} \cdot \mathbf{X}_f, \quad \hat{\mathcal{P}}_{\mu}(f) = \sum_{\mu'} (\mathbf{\Gamma}^{-1})_{\mu\mu'}(f) X_{\mu'}(f). \quad (6)$$

Here,  $\mathbf{X}_f$  is the narrowband *dirty map* and  $\mathbf{\Gamma}_f$  is the narrowband *Fisher information matrix*, defined as follows [54, 74]:

$$\begin{aligned} \mathbf{X}_f &\equiv \gamma_f^{\dagger} \cdot \mathbf{N}_f^{-1} \cdot \mathbf{C}_f, & X_{\mu}(f) &\propto \sum_{I; 1, 2 \in I} \frac{\gamma_{\mu}^{I*}(t; f) C^I(t; f)}{P_1(t; f) P_2(t; f)}, \\ \mathbf{\Gamma}_f &\equiv \gamma_f^{\dagger} \cdot \mathbf{N}_f^{-1} \cdot \gamma_f, & \Gamma_{\mu\mu'}(f) &\propto \sum_{I; 1, 2 \in I} \frac{\gamma_{\mu}^{I*}(t; f) \gamma_{\mu'}^I(t; f)}{P_1(t; f) P_2(t; f)}, \end{aligned} \quad (7)$$

where  $\mathbf{N}_f$  denotes the covariance matrix for the CSD and  $P_{1,2}(t; f)$  are the noise one-sided PSDs. The narrowband skymaps in the above equations are the foundation of all the anisotropic analyses in this paper.

## B. All-sky All-frequency radiometer search

The ASAF radiometer search targets point-like, persistent, narrowband GW sources by scanning the frequency band and the sky using a HEALPix grid ( $N_{\text{side}} = 16$ )<sup>2</sup> [75] and a frequency bin of 1/32 Hz. Such sources can exhibit two types of waveforms in the time domain: (i) CGW signal from a single GW source, and (ii) a narrowband GWB arising from multiple unresolved sources along a given line of sight, resulting in an incoherent signal. Being an unmodeled search, the radiometer search is robust against the signal model and serves as an alternative for detecting GW signatures from poorly known sources,

e.g., neutron stars having frequent glitches and/or accretion from a binary companion [76] or unknown CGW sources [60].

We compute the point estimate, which serves as an estimator for the signal power and its associated uncertainty due to random noise. This is achieved by utilizing narrowband dirty maps and the Fisher information matrix shown in Eq. (7), both constructed in the pixel basis, as described by the equations below

$$\begin{aligned} \hat{\mathcal{P}}_{\hat{n}}(f) &= [\mathbf{\Gamma}_{\hat{n}\hat{n}}(f)]^{-1} X_{\hat{n}}(f), \\ \sigma_{\hat{n}}^2(f) &= [\mathbf{\Gamma}_{\hat{n}\hat{n}}(f)]^{-1}, \end{aligned} \quad (8)$$

where there is no summation over  $\hat{n}$ . Owing to the baseline's blind spots, the Fisher information matrix in the pixel basis is highly ill-conditioned [56, 77–81]. To avoid introducing numerical noise due to inversion of insensitive modes and their dependence on regularization,

<sup>2</sup> This results in a sky grid with  $12 N_{\text{side}}^2 = 3072$  pixels, each covering  $13.4 \text{ deg}^2$ .

we proceed without incorporating pixel correlations. As shown in Ref. [80], this approximation is justified given the current detector sensitivity when constructing clean map estimators.

### C. Targeted-narrowband radiometer search

The radiometer algorithm can be used in a pixel-based approach to target specific sky locations. For this analysis, five astrophysically motivated locations have been selected: three of them—Scorpius X-1, the Galactic Center, and the supernova remnant SN 1987A—were also analyzed in previous directional stochastic searches [51–53], while two globular clusters, Terzan 5 and NGC 6397, are introduced as new targets. These sources span a range of astrophysical scenarios, including accreting neutron stars, dense stellar environments, and young supernova remnants, and are all plausible hosts of CGW emission [60]. A brief overview of each source and its relevance to GW searches is provided in Appendix C 1.

Unlike the ASAF search, targeting specific locations allows us to account for the specific signal spread caused by Earth’s Doppler modulation or the intrinsic characteristics of the source. To do so, we combine the information from nearby frequency bins by performing a running average throughout the entire search frequency range. The characteristic window of the average is defined as the  $N$  neighboring bins around a fixed frequency bin required to recover all the power spread by the phase evolution of the source. The output of the bin combination is a new power spectrum with the same original frequency resolution  $\delta f$ , but now accounting for the frequency variations of the signal throughout the observation time. The details regarding how the values of  $N$  can be determined are given in Appendix C 2.

### D. Broadband radiometer search

The BBR search is designed to measure the GWB energy density from point-like sources across the sky and serves as a crucial tool for identifying persistent sources when there is stochasticity in the phase evolution of the signal due to a large number of sources. This search still relies on the same methods as in the ASAF analysis, while further assuming the point-like GWB sources are broadband in frequency with an angular power spectral density  $\mathcal{P}(f, \hat{n})$ . Throughout this work, we search for GWBs whose  $\mathcal{P}(f, \hat{n})$  can be factorized in one frequency-dependent and one angular-dependent factor [36, 53, 66], namely:

$$\mathcal{P}(f, \hat{n}) = \mathcal{P}_{\hat{n}_0}(f) \delta^2(\hat{n} - \hat{n}_0) = \bar{H}(f) \mathcal{P}(\hat{n}), \quad (9)$$

where  $\bar{H}(f)$  is the spectral shape of the GWB, normalized such that  $\bar{H}(f_{\text{ref}}) = 1$ , with  $f_{\text{ref}} = 25$  Hz [50, 53]. We model  $\bar{H}(f)$  as a simple power law, characterized by

a spectral index  $\alpha$  that is fixed throughout the search, such that [66]

$$\bar{H}(f) \equiv \bar{H}(f; \alpha, f_{\text{ref}}) = \left( \frac{f}{f_{\text{ref}}} \right)^{\alpha-3}, \quad (10)$$

$$\mathcal{P}(\hat{n}) \equiv \mathcal{P}(\hat{n}; \alpha, f_{\text{ref}}) = \mathcal{P}_{\alpha, \hat{n}_0}(f_{\text{ref}}) \delta^2(\hat{n} - \hat{n}_0). \quad (11)$$

We consider three different GWB power-law models:  $\alpha = 0$ , consistent with a cosmological GWB from slow-roll inflation or cosmic strings [16];  $\alpha = 2/3$ , compatible with an astrophysical GWB from compact binary coalescence (CBC)s [1]; and  $\alpha = 3$ , corresponding to a flat strain power spectrum [82].

By following the same maximum-likelihood approach presented in Sec. II A, one can derive the expressions for the broadband dirty maps and Fisher matrix:

$$X_{\hat{n}} = \sum_f \bar{H}(f) X_{\hat{n}}(f), \quad (12)$$

$$\Gamma_{\hat{n}\hat{n}'} = \sum_f \bar{H}^2(f) \Gamma_{\hat{n}\hat{n}'}(f), \quad (13)$$

with  $X_{\hat{n}}(f)$  and  $\Gamma_{\hat{n}\hat{n}'}(f)$  from Eq. (7), and the maximum-likelihood estimator for  $\mathcal{P}(\hat{n})$

$$\hat{\mathcal{P}}_{\hat{n}} = \frac{\sum_f \bar{H}(f) \sigma_{\hat{n}}^{-2}(f) \hat{\mathcal{P}}_{\hat{n}}(f)}{\sum_{f'} \bar{H}^2(f') \sigma_{\hat{n}}^{-2}(f')}. \quad (14)$$

We rescale this estimator to express it in units of the GW energy flux spectrum at the reference frequency  $f_{\text{ref}}$ , where  $\mathcal{P}(f_{\text{ref}}, \hat{n}) = \mathcal{P}_{\alpha, \hat{n}}$  given  $\bar{H}(f_{\text{ref}}) = 1$ , as

$$\hat{\mathcal{F}}_{\alpha, \hat{n}}(f_{\text{ref}}) = \frac{\pi c^3}{4G} f_{\text{ref}}^2 \hat{\mathcal{P}}_{\alpha, \hat{n}}. \quad (15)$$

### E. Spherical harmonics search

This analysis is intended to search for an anisotropic distribution of spatially extended sources with a broadband spectrum, as opposed to the point sources targeted by the radiometer analyses discussed above. While we follow the same factorization as given by Eq. (9) of the BBR search, we adopt the SPH functions as a basis to characterize the anisotropies of extended sources [57]

$$\mathcal{P}(f, \hat{n}) = \bar{H}(f) \sum_{\ell=0}^{\ell_{\text{max}}} \sum_{m=-\ell}^{\ell} \mathcal{P}_{\ell m} Y_{\ell m}(\hat{n}), \quad (16)$$

where  $Y_{\ell m}(\hat{n})$  is an SPH function of the mode  $(\ell, m)$  evaluated at the sky position  $\hat{n}$ . Since now we search for a GWB signal with a broadband spectrum, we construct a *broadband* version of the  $\hat{\mathcal{P}}$  estimator from its narrowband counterpart, following the derivation in Eq. (14) but adapted to the SPH basis. The  $\hat{\mathcal{P}}$  estimator is referred to as the *clean map*, and the inversion of the Fisher matrix physically represents the deconvolution of the antenna pattern and detector noise.

To interpret the anisotropies of GWBs under the assumption of statistical isotropy, we are more interested in the angular power of estimated  $\hat{\mathcal{P}}_{\ell m}$ , rather than their specific realization on the sky. Therefore, we introduce the estimator of the angular power spectrum in the unit of  $\text{sr}^{-2}$

$$\hat{C}_\ell = \left( \frac{2\pi^2 f_{\text{ref}}^3}{3H_0^2} \right)^2 \frac{1}{2\ell + 1} \sum_m \left[ |\hat{\mathcal{P}}_{\ell m}|^2 - (\Sigma_{\text{R}})_{\ell m, \ell m} \right], \quad (17)$$

with its variance (under the weak-signal limit) given by:

$$\text{Var}[\hat{C}_\ell] \approx \left( \frac{2\pi^2 f_{\text{ref}}^3}{3H_0^2} \right)^4 \frac{2}{(2\ell + 1)^2} \sum_{m, m'} |(\Sigma_{\text{R}})_{\ell m, \ell m'}|^2, \quad (18)$$

$\Sigma_{\text{R}}$  is the covariance matrix of the *regularized* clean-map estimator, defined as:

$$\Sigma_{\text{R}} = \mathbf{\Gamma}_{\text{R}}^{-1} \cdot \mathbf{\Gamma} \cdot \mathbf{\Gamma}_{\text{R}}^{-1}, \quad (19)$$

where  $\mathbf{\Gamma}$  is the Fisher matrix of the dirty map on the SPH basis and  $\mathbf{\Gamma}_{\text{R}}$  is its regularized version, whose details can be found in Appendix E 2.

Also, due to the angular resolution limit, we perform the analysis for SPH modes only up to the angular scale given by  $\ell_{\text{max}} = 3, 4, 16$  for  $\alpha = 0, 2/3, 3$ , respectively [51–53]. Technical details concerning the Fisher-matrix regularization as well as the angular resolution are discussed in Appendices E 1 and E 2. We eventually compare this  $\hat{C}_\ell$  estimator to its theoretical predictions to characterize a potential signal or to place constraints on relevant theoretical models.

The estimator described above, which we refer to as the *auto- $\hat{C}_\ell$*  estimator, has been used in previous LVK analyses [51–53]. However, Ref. [83] showed that in the presence of an astrophysical GWB, it is significantly biased by the shot-noise-dominated nature of the signal, which arises from the discrete spatial or temporal realization of individual events. This consideration motivates us to also adopt the *cross- $\hat{C}_\ell$*  estimator, defined as

$$\hat{C}_\ell^{(\text{cross})} = \left( \frac{2\pi^2 f_{\text{ref}}^3}{3H_0^2} \right)^2 \frac{1}{2\ell + 1} \frac{1}{n(n-1)} \sum_m \sum_{i \neq j} \hat{\mathcal{P}}_{\ell m}^{(i)} \hat{\mathcal{P}}_{\ell m}^{(j)*}, \quad (20)$$

with its variance (under the weak-signal limit<sup>3</sup>)

$$\begin{aligned} \text{Var}[\hat{C}_\ell] \approx & \left( \frac{2\pi^2 f_{\text{ref}}^3}{3H_0^2} \right)^4 \frac{2}{(2\ell + 1)^2} \frac{1}{n^2(n-1)^2} \\ & \times \sum_{m, m'} \sum_{i \neq j} (\Sigma_{\text{R}}^{(i)})_{\ell m, \ell m'} (\Sigma_{\text{R}}^{(j)})_{\ell m', \ell m}, \end{aligned} \quad (21)$$

<sup>3</sup> While the weak-signal limit mentioned in Sec. II A assumes the detector noise to dominate over the GWB signal and astrophysical shot noise in the *individual* time-frequency components, Eqs. (18) and (21) involve the whole dataset and subsets, respectively, after marginalizing across times and frequencies.

where  $n$  distinct clean maps are involved and  $\Sigma_{\text{R}}^{(i)}$  represents a covariance matrix of regularized clean maps derived from  $i$ -th dataset. See Appendix E 3 for how we divide the whole dataset into subsets in the optimal way.

To either claim a detection of an anisotropic GWB or place ULs on the angular power spectrum, given the observed  $\hat{\mathcal{P}}_{\ell m}$  estimator, we evaluate its statistical significance. Specifically, we compute  $p$ -values for the real and imaginary parts of the  $\hat{\mathcal{P}}$  estimator, respectively, in each SPH mode using its expected probability density function (PDF) based on Monte Carlo samples with the detailed procedure discussed in Appendix E 4. We generate 50,000 such  $\hat{\mathcal{P}}^{\text{sim}}$  samples for the whole dataset and compute a  $p$ -value for each real and imaginary part of each SPH mode. As a significance indicator, we adopt a 5%  $p$ -value threshold, which we refer to as a *local* threshold. Additionally, due to the presence of multiple observations across all the SPH modes, we account for the trials factor in a conservative way by dividing each local threshold by the number of SPH modes,  $(\ell_{\text{max}} + 1)^2$ , to obtain the *global*  $p$ -value threshold.

### III. RESULTS

To perform all the four analyses described above, we analyze data from O1 and O2 of the LIGO detectors [84–90] located in Hanford (H) and Livingston (L); from O3 of LIGO [91–94] and Virgo [95–98] (V); and from O4a of LIGO [99–102].

These datasets are preprocessed following the procedure described in [64]. Time-domain cuts are applied by removing segments affected by non-Gaussian features, hardware injections, and known instrumental artifacts; applying non-stationarity cuts; and gating loud glitches. These cuts are identical to those used in [64]. In addition, frequency-domain cuts are applied to remove bins identified through coherence studies as contaminated by instrumental artifacts. Details of the observing run, including the time- and frequency-domain cuts and the effective dataset, are provided in Tab. IV of Appendix A.

We compute the CSD by combining the SFTs of 192-second segments from all detector pairs, using a coarse-grained frequency resolution of  $\Delta f = 1/32$  Hz and including the corresponding variances.

To reduce computational and storage costs in GWB searches, we fold the 192-second segments across a sidereal day (23h 56m 4s), leveraging the temporal symmetry of the ORF due to Earth’s rotation [69, 103]. This preserves all necessary information while enabling efficient maximum-likelihood analysis over the full run.

We generate folded datasets for all observing runs [104] up to and including O4a, and perform all analyses using the `PyStoch` package [73, 74], which now provides a unified framework supporting both pixel- and SPH-based analyses from O4a onward.

### A. All-sky All-frequency radiometer search

To identify a potential GW signature in the data and set constraints on source parameters in the absence of a detection, we use the estimators constructed in Sec. II B following the method outlined in Ref. [54] and detailed in Appendix B.

We use a detection statistic, the signal-to-noise ratio (SNR), defined as

$$\hat{\rho}_{\hat{n}}(f) \equiv \frac{\hat{\mathcal{P}}_{\hat{n}}(f)}{\sigma_{\hat{n}}(f)}, \quad (22)$$

to evaluate the significance of the data. The distribution of this statistic, obtained from O4a data using both the random (unphysical) timeshift method [54] and the zero-lag data (i.e., data without timeshift), is shown in Appendix B 1. The zero-lag data is mostly consistent with the random-timeshifted data within 2-sigma Poisson errors. With a global  $p$ -value threshold of 5%, no evidence is found for a persistent narrowband GW source. A total of 505 sub-threshold candidates identified for follow-up, and details are provided in Appendix B 1.

Next, assuming that the GW signal remains in the same frequency bin and sky direction, we combine data from the O1–O4a observing runs (including multiple baselines for O3). This assumption sets an upper bound on the frequency drift of a CGW signal:

$$\frac{0.03125 \text{ Hz}}{8.3 \text{ years}} = 1.2 \times 10^{-10} \text{ Hz s}^{-1}. \quad (23)$$

We note that incorporating data from multiple datasets reduced the notch fraction from 11.4% in O4a to 7.9% in O1–O4a. The zero-lag data remains consistent with the null hypothesis. Additionally, we investigate the top three SNR candidates in zero-lag with  $\text{SNR} > 5.5$ . We find that these candidates are associated with data quality issues at these frequencies, including hardware injections and calibration lines [99]. Finally, a total of 562 sub-threshold follow-up candidates have been identified for the follow-up with methods tuned for searching for a CGW (see Appendix B 1 for the details).

Having found the data to be consistent with Gaussian noise, we set Bayesian ULs on the effective strain amplitude, defined as

$$h_{\text{eff}, \hat{n}}(f) \equiv [\mathcal{P}_{\hat{n}}(f) \Delta f]^{1/2}, \quad (24)$$

with 95% confidence. We note that the effective strain amplitude defined above is equal to the intrinsic strain amplitude  $h_0$  for a circularly polarized CGW, provided the signal remains confined within a single frequency bin [105, 106]. In practice, this assumption is violated due to factors such as arbitrary polarization, Doppler shifts from the Earth’s orbital motion, and intrinsic source motion (e.g., proper motion or binary orbital motion), which introduce biases in the estimator. The Doppler shift from the Earth’s motion around the Sun

can be approximated as  $f_0 \times 2 \times 10^{-4} \cos \delta$ , where  $f_0$  is GW frequency in the Solar System Barycentre frame and  $\delta$  is the source declination. Consequently, above  $\sim 160$  Hz, the signal drifts beyond a single frequency bin. We therefore restrict our UL estimates to the 20–160 Hz range, which we refer to as sensitivity estimates in further discussion.

As shown in Tab. I, the sensitivity estimate with O4a and O1–O3 data across sky and frequencies lie in the ranges  $(3.46 - 223.12) \times 10^{-26}$  and  $(3.39 - 963.23) \times 10^{-26}$  [54], respectively. After combining all available data (i.e., O1–O4a), the sensitivity lies in range  $(2.94 - 845.68) \times 10^{-26}$ .

To assess the improvement in the sensitivity estimate with the addition of the latest data, comparing only the minimum or maximum sensitivity across datasets is not a robust approach. This is primarily due to two reasons. First, specific frequency bins may be notched in one dataset but present in another, preventing a uniform comparison. For example, the notch fraction decreases from 7.6% in O4a to 0.4% in the combined O1–O4a dataset (below 160 Hz). Second, the reported sensitivity incorporates both a point estimate and its associated uncertainty, both of which can fluctuate across the sky, introducing intrinsic statistical variability. We therefore compute the sensitivity improvement using the ratio of median sensitivity across these shared frequency bins. As shown in Tab. I, the median sensitivity ratios for O4a to O1–O3 and O1–O4a to O1–O3 are 0.89 and 0.79 respectively, indicating an overall improvement by a factor of 1.12 (1.26).

To understand the variation of sensitivity across sky directions and frequencies, we consider a simplified model in which the sensitivity for each frequency-pixel pair is approximated as a combination of the point estimate and its associated uncertainty. Given that the observed SNR for frequency-pixel pairs is consistent with Gaussian noise with zero mean, the point-estimate  $\hat{\mathcal{P}}_{\hat{n}}(f)$  can be assumed to be centered near zero. Consequently, the sky-averaged sensitivity can be approximated as (using Eqs. 7 and 8)

$$\text{Sensitivity}(f) \equiv \langle \sigma_{\hat{n}}(f) \rangle_{\hat{n}}^{1/2} \propto (P_1(f)P_2(f))^{1/4}, \quad (25)$$

where  $P_1(f)$  and  $P_2(f)$  are noise PSD for detector 1 and 2 in baseline  $I$ . The sky-averaged sensitivity as a function of frequency is shown in the left panel of Fig. 1 for O1–O4a (blue) and O1–O3 (yellow). The trend follows the shape of the typical noise curve, i.e.,  $(P_1(f)P_2(f))^{1/4}$ , with the shaded region indicating 1-sigma sky fluctuations. Similarly, the frequency-averaged sensitivity for a given sky direction  $\hat{n}$  is given by (using Eqs. 7 and 8)

$$\text{Sensitivity}_{\hat{n}} \equiv \langle \sigma_{\hat{n}}(f) \rangle_f^{1/2} \propto \left( \sum_t \Gamma_{\hat{n}}(t) \right)^{1/4}, \quad (26)$$

where  $\Gamma_{\hat{n}}(t) = \sum_A F_1^A(t, \hat{n}) F_2^A(t, \hat{n})$  is the combined antenna response [56], and the summation is over observing

Run	Vetoed-Frequency Fraction (%)	Range ( $\times 10^{-26}$ )	Median ( $\times 10^{-26}$ )	Median Common $f$ ( $\times 10^{-26}$ )	Median (Mean) Ratio $\frac{\text{Run}}{\text{O1-O3}}$
O4a	7.6	3.46 - 223.12	9.00	9.29	0.89 (0.72)
O1-O3	1.2	3.39 - 963.23	10.04	10.39	1 (1)
O1-O4a	0.4	2.94 - 845.68	8.41	8.24	0.79 (0.67)

TABLE I. We present Bayesian sensitivity estimate on the effective strain amplitude  $h_{\text{eff}}$  for three datasets: O4a, O1-O3, and the combined O1-O4a. When comparing the median sensitivity of O4a to O1-O4a, an improvement is observed. To account for differences in the vetoed frequency bins across observing runs, we also compare median sensitivity over the common frequency range.

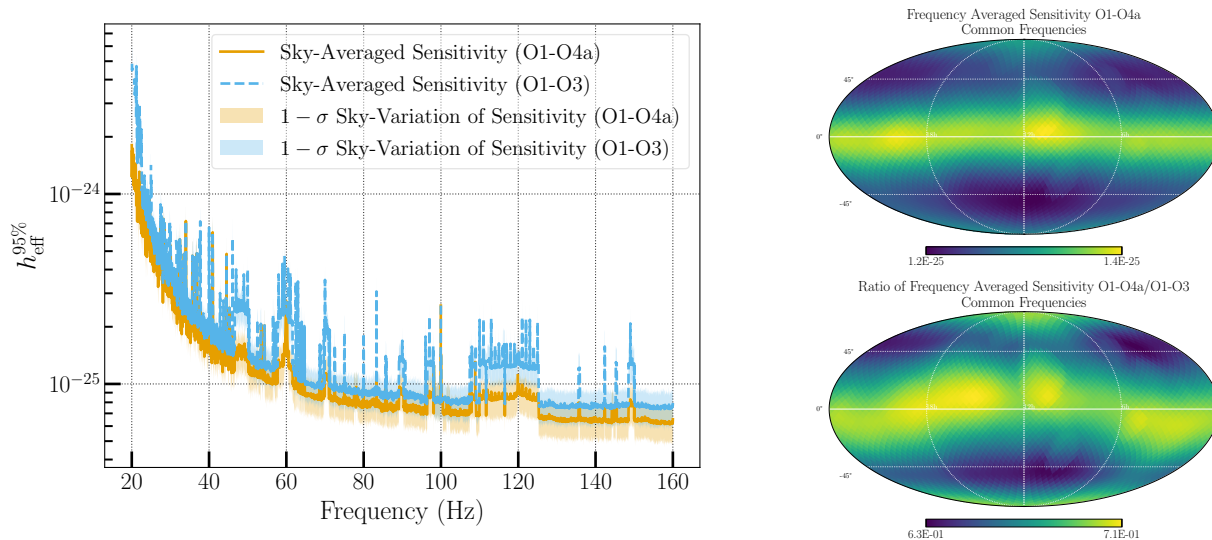


FIG. 1. Bayesian sensitivity estimate to Effective Strain Amplitude  $h_{\text{eff}}$ : Left panel: Sky-averaged sensitivity from the O1-O3 and O1-O4a datasets are shown as blue and yellow solid lines, respectively. The shaded regions represent 1-sigma variations in the estimates across the sky. The overall shape of the curves reflects the detectors' sensitivity profiles. Gaps indicate vetoed frequency bins, while narrow vertical peaks correspond to instrumental spectral lines that were not vetoed, as their impact on the analysis was minimal. Top Right Panel: Skymap of frequency-averaged sensitivity using O1-O4a data. The observed pattern reflects the typical sky sensitivity of an HL-dominated network. As expected, the sensitivity is worse near the poles and equator, with improved sensitivity in the mid-declination regions. Bottom Right Panel: Skymap showing the ratio of frequency-averaged sensitivity from O1-O4a to that from O1-O3.

time. This captures the directional variation in detector response over the full observing run. The corresponding skymap of frequency-averaged sensitivity for O1-O4a is shown in the top right panel of Fig. 1. For the HL baseline-dominated data, the most sensitive sky regions lie between declinations of approximately  $20^\circ$ – $60^\circ$ , with reduced sensitivity near the celestial poles and equator.

The bottom right panel of Fig. 1 presents the ratio of frequency-averaged sensitivity between O1-O4a and O1-O3 across the sky, which varies between 0.63 and 0.71.

### 1. Marginal Outlier at 92.8125 Hz

Signs of non-Gaussianity are observed in the negative SNR tails of the zero-lag data, with the samples originating from the same frequency bin at 92.8125 Hz. While an actual astrophysical source is not expected to produce

negative SNR in our analysis, this candidate lies close to the SNR threshold for a two-sided  $p$ -value. Therefore, a follow-up analysis was conducted, with details provided below.

In the O4a data, we identified a frequency bin at 92.8125 Hz with extreme SNR values: a minimum of  $-6.12$  and a maximum of  $5.2$  in the zero-lag dataset. The minimum SNR lies in the negative tail and is just above the two-sided threshold of  $-6.18$  corresponding to a 5%  $p$ -value (see O4a SNR histogram in Appendix B). While the positive SNR is not significant enough to be classified as an outlier, the frequency-pixel pair was selected as a sub-threshold follow-up candidate. The associated SNR skymap is given in Appendix B. In the random-timeshifted dataset, the SNR range narrows to  $-2$  to  $2$ , and the skymap structure disappears—consistent with behaviour expected in the case of a persistent signal. We investigate both tails to determine whether the excess power arises from detector noise or a GW signal.

We note that, while most hardware injections were too weak to be confidently detected with our search method, the injection near 52.8 Hz was identified as a sub-threshold follow-up candidate, with an SNR of 4.25—lower than that of the observed “outlier”. As shown in Appendix B, the SNR in the outlier frequency bin steadily builds up in the zero-lag run and stands out compared to both neighbouring frequency bins and the random time-shifted dataset.

We also performed a simulation by injecting a GW signal with  $\text{SNR} \sim 4.9$  at the sky location corresponding to the observed maximum SNR, convolved with the detector response, and added to numerous noise realizations. We find that, in approximately 4 out of  $10^4$  trials, the negative SNR exceeds the positive by a magnitude of 0.9, with the maximum SNR exceeding 5.1, and the observed sky map is found to be a good match with the simulated map (see Appendix B).

When combining O4a data with previous observing runs (O1–O4a), the SNR decreases from  $-6.12$  to  $-4.3$  and from  $5.2$  to  $3.6$ . For a persistent astrophysical source lasting  $\sim 8$  years, we would expect the SNR—particularly in the positive direction—to increase if earlier data were sensitive and the signal remained in the same frequency bin. Otherwise, a decrease in SNR upon combining runs may instead indicate a detector noise artifact that was absent in previous runs. We note that O3 HL data have sensitivity comparable to O4a HL data, while other datasets were insufficiently sensitive.

We do not see any excess auto-power localized in these frequency bins in the individual detectors; the nearest unknown excess power is observed in the L detector at around 92.7 Hz (3 bins away). We have not identified any coherent instrumental witness channel that could account for the elevated SNR. While some periods of elevated detector noise are present, there is no evidence of persistent or long-term non-stationary noise. Removing these periods from the analysed data does reduce the SNR, but the pattern in the sky persists. The results remain inconclusive, and this frequency bin will be monitored in future observing runs to gather additional data.

## B. Targeted-narrowband radiometer search

For all five directions, we computed the SNR by combining the appropriately sized frequency bins across the detectors. The best SNRs after bin combination are shown in Tab. II, together with their  $p$ -values. The  $p$ -values are calculated from the maximum SNR distribution obtained by simulating many realizations of strain power (details are shown in Appendix C 3).

Since we do not find any evidence for narrowband GWs, we place 95% confidence ULs on the GW strain spectrum from the five selected targets, shown in Fig. 2 together with the  $1\sigma$  sensitivity. The results indicate a median improvement by a factor of 1.6–1.7 compared to previous results from O1 to O3, with strain amplitudes

ranging from  $\sim 1.1 \times 10^{-25}$  to  $6.5 \times 10^{-24}$  depending on the target.

Since the O4a data have the best sensitivity so far, it is worth comparing the contribution that the O4a dataset is giving to improve the reach of our searches. At higher frequencies, O4a alone can provide better sensitivity than the combined O1 to O3 data. It also helps to improve the previous ULs in all the frequency ranges for all selected targets. The combination with future stages of the run promises to significantly increase the reach of our searches.

It is also useful to compare the results obtained with CGW searches. CGW searches use techniques that, for sources with at least a partial knowledge of the parameters, grant a much longer coherence time and hence better sensitivity than the targeted radiometer (for example, Ref. [107] for the previous run and [108] for O4a).

Taking into account the several semi-coherent methods used for the O3 all-sky search for isolated pulsars [109], the sensitivity estimation over the whole sky is comparable to the ULs shown in this section. However, more precise UL estimation, like the one shown in the first half of the third observing run (O3a) all-sky isolated CGW search [110], can lead to significantly lower limits than the best ones obtained with SN 1987A of  $h_0 \simeq 10^{-25}$ . As a reference for the most recent SN 1987A dedicated search, see also the 90% confidence UL on O3 data in [111].

A directed search to the Galactic Center in O3, using a CW semi-coherent method, generally showed better sensitivity estimations than the targeted NBR search [112].

Regarding Sco X-1, to assess the astrophysical significance of the signal strength probed in this search, a commonly used benchmark is the torque-balance level. In most CGW searches of this target (see, for example, [113, 114], and the studies with updated ephemeris in [115, 116]), an order-of-magnitude estimate of the torque-balance level is adopted as a reference point to evaluate whether the explored parameter space is astrophysically relevant. Given the absence of a detection in our search, we compare our ULs with this benchmark and find that they remain above the torque-balance level.

These upper limits assume a generic polarization and marginalize over inclination and polarization angle (see Appendix C 4). However, if we instead consider the circular polarization case—typically not quoted in our fully unmodeled analyses—our results indicate that the search has surpassed the torque-balance threshold under the hypothesis of circular polarization (more details are shown in Appendix C 5).

## C. Broadband radiometer search

We present the results of the BBR analysis for the O4a dataset only and after combining them with the previously existing results from O1 to O3, which we also summarize in Tab. III. We have performed such an analysis

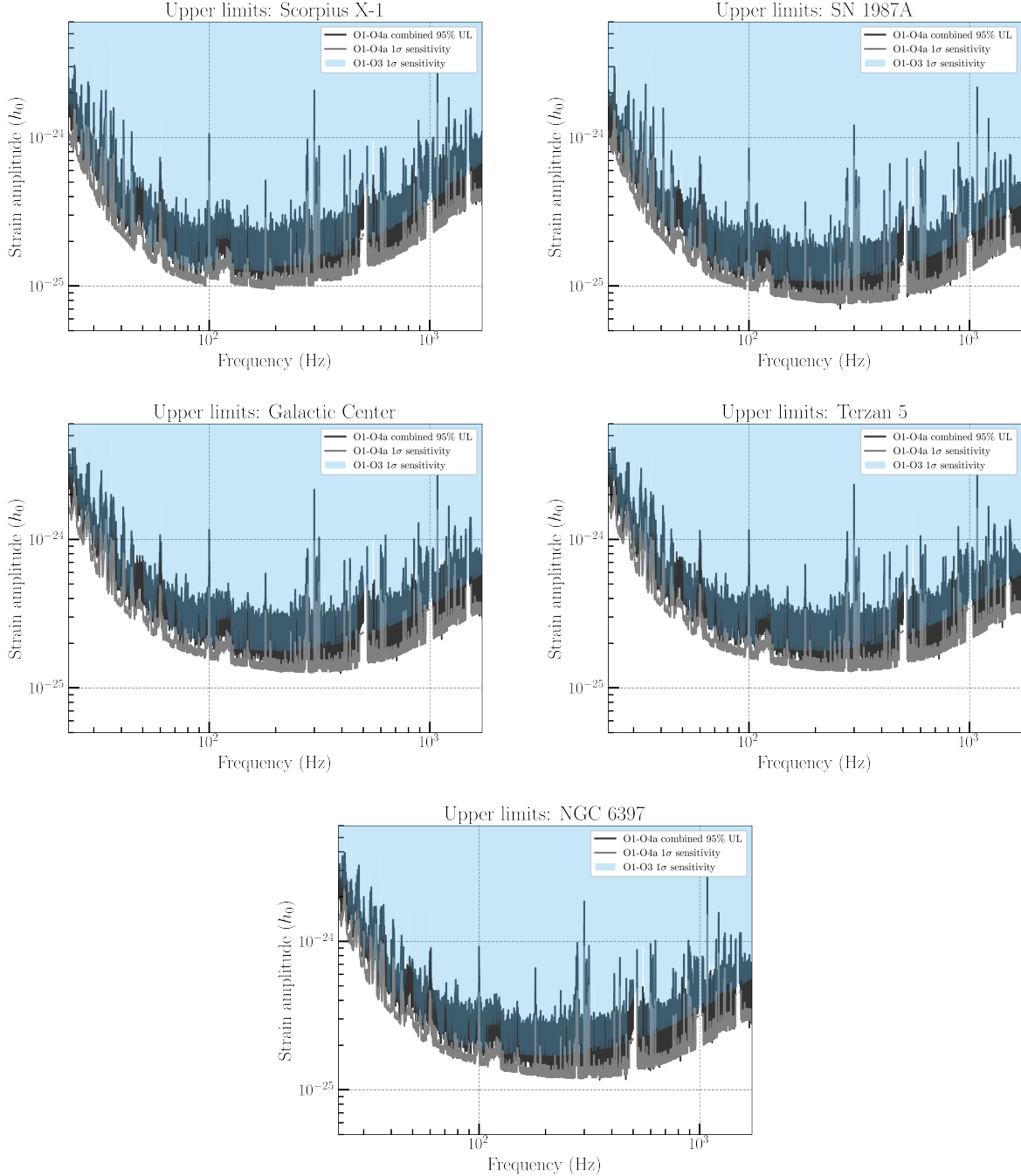


FIG. 2. Plots showing the ULs for the five targets of the O1-O4a NBR search. In each plot, the black solid line shows the Bayesian ULs set at 95% confidence level, while the gray line is the  $1\sigma$  sensitivity estimation in the hypothesis of no signal. The shaded blue area shows the  $1\sigma$  sensitivity estimation with data up to the O3 run, highlighting the sensitivity improvement granted by adding the O4a run to the analyses.

for three spectral indices, namely  $\alpha = \{0, 2/3, 3\}$ , whose final results are the skymaps shown in Fig. 3. As in Ref. [53] we pixelate the sky by employing the HEALPix scheme [75], but instead of using  $N_{\text{side}} = 32$  as in [53], here we use  $N_{\text{side}} = 16$ . We have opted for this choice as a compromise among the different angular resolutions of

the baselines at the lower and upper ends of their most sensitive frequency bands, for different spectral indices  $\alpha$  [56, 117]. We recall that we apply the same data quality prescriptions as detailed in Sec. III and Appendix A.

Following the methods from Appendix D, we have first evaluated the SNR maps for  $\alpha = 0, 2/3$ , and 3, and then

Direction	Max SNR	Frequency band (Hz)	$p$ -value (%)	Best UL ( $\times 10^{-25}$ )	Frequency band (Hz)
Scorpius X-1	4.2	1706.09375 – 1707.21875	53.7	1.5	192.9375 – 193.0625
SN 1987A	4.1	1672.6875 – 1672.75	59.0	1.1	246.75 – 246.8125
Galactic Center	4.4	372.28125 – 372.90625	22.5	1.9	227.4062 – 228.03125
Terzan5	4.5	821.46875 – 822.09375	16.3	1.9	260.71875 – 261.34375
NGC6397	4.5	264.84375 – 265.40625	18.2	1.7	251.40625 – 251.96875

TABLE II. Results of the targeted-narrowband radiometer search on the O1-O4a combined datasets. We show the maximum SNR with its estimated  $p$ -value and frequency bin for each search direction. We also give the best 95% confidence-level GW strain ULs, with the corresponding frequency band, taken as the median of the most sensitive 1-Hz band.

$\alpha$	$\Omega_{\text{gw}}(f)$	$\bar{H}(f)$	Max SNR (% $p$ -value)		UL ranges ( $10^{-8}$ ) [erg cm $^{-2}$ s $^{-1}$ Hz $^{-1}$ ]	
			HL(O4a)	O1+O2+O3+O4a	O1+O2+O3+O4a	O1+O2+O3 (HLV)
0	constant	$\propto f^{-3}$	1.7 (93)	2.2 (72)	1.2 – 5.5	1.7 – 7.6
2/3	$\propto f^{2/3}$	$\propto f^{-7/3}$	1.8 (97)	2.4 (76)	0.6 – 3.0	0.85 – 4.1
3	$\propto f^3$	constant	3.8 (20)	3.8 (19)	0.008 – 0.092	0.013 – 0.11

TABLE III. The maximum SNR across all sky positions, its estimated  $p$ -value, and the range of the 95% ULs on GW energy flux  $F_{\alpha, \hat{n}}^{95\%, \text{UL}}(25 \text{ Hz})$  [erg cm $^{-2}$  s $^{-1}$  Hz $^{-1}$ ] set by the BBR search by combining the LIGO data from O1 to O4a and the Virgo O3 data. The median improvement across the sky compared to limits from the O3 analysis is a factor of 1.4-1.7, depending on  $\alpha$ . O1+O2+O3 (HLV) ULs reported in the last column differ from the ULs in [53] due to the different  $N_{\text{side}}$  parameter we are employing here.

we have assessed the statistical significance of the maximum SNR for each spectral index. We find that these SNR values are consistent with the noise-only hypothesis, and we therefore proceed with the UL calculation. There is no evidence of outliers in the BBR results, in contrast to the ASAF outlier in the 92.8125 Hz skymap. This is not inconsistent with the ASAF outlier, which is a narrowband feature and does not contribute significantly when integrating over the whole frequency band in the BBR analysis [118].

Fig. 3 illustrates the skymaps showing the 95% Bayesian ULs on the GW energy flux  $F_{\alpha, \hat{n}}(25 \text{ Hz})$  in CGS units for  $\alpha = 0, 2/3$  and 3, obtained by combining the data from O1 to O4a. When comparing Fig. 3 to the results from the first three observing runs, we find that the median improvement in ULs across the sky is a factor of 1.4 for  $\alpha = 0$ , 1.4 for  $\alpha = 2/3$ , and 1.7 for  $\alpha = 3$ , respectively.

#### D. Spherical harmonics search

Following the procedure for significance assessment described in Sec. II E, we compute the  $p$ -value for each real and imaginary part of the clean map estimator for the combined dataset across O1-O4a, and compare them to the local and global  $p$ -value thresholds, respectively. We find that all SPH modes lie within the global  $p$ -value threshold across the three power-law spectrum models, indicating consistency with a Gaussian distribution. See Appendix E 4 for more details. Given the absence of a detected GWB signal, we compute ULs on  $C_\ell^{1/2}$  at each angular scale characterized by the  $\ell$  value, for different

power-law frequency spectrum models. Fig. 4 shows the  $C_\ell$  ULs derived from the two estimators for each power-law spectrum model. Also, the uncertainties of  $\hat{C}_\ell$  measurement are improved by factors of 1.4-2.2 compared to the previous search, as discussed with more details in Appendix E 4.

Note that the variance of the  $\hat{C}_\ell$  estimator and its ULs depend on the definition of the  $\hat{C}_\ell$  estimator or even the specific regularization we apply to the Fisher matrix. Therefore, one should not quantitatively compare the ULs reported here to those in Ref. [53], where the regularization was performed differently as compared to what is presented in this paper. The improvement factors mentioned above are based on the ULs recomputed for O1+O2+O3 data using the consistent regularization method, described in Appendix E 2 for either definition of the  $C_\ell$  estimators. For the same reason, these ULs cannot be compared between the two different estimators. Even though we apply the same regularization to both cases, the variance of the cross- $\hat{C}_\ell$  estimator also depends on how the entire dataset is split into subsets since the inversion of a Fisher matrix is not a linear operation. Therefore, we treat these estimators as two different ways to present our search results.

Below, we consider the implications of our results for different astrophysical models. For  $\alpha = 2/3$ , the UL found here for the corresponding  $\ell$  modes is  $C_\ell^{1/2} < 1.2 \times 10^{-9} \text{ sr}^{-1}$ , whereas several theoretical studies in the literature [119–121] predict a range of  $C_\ell^{1/2} \sim (0.2 - 5) \times 10^{-11} \text{ sr}^{-1}$  for  $1 \leq \ell \leq 4$ , assuming the normalized GW energy density due to an isotropic GWB of compact binaries is  $\Omega_{\text{GW}} \lesssim (2.2 - 6.7) \times 10^{-9}$  [64]. Also, note that the shot noise term is expected to be

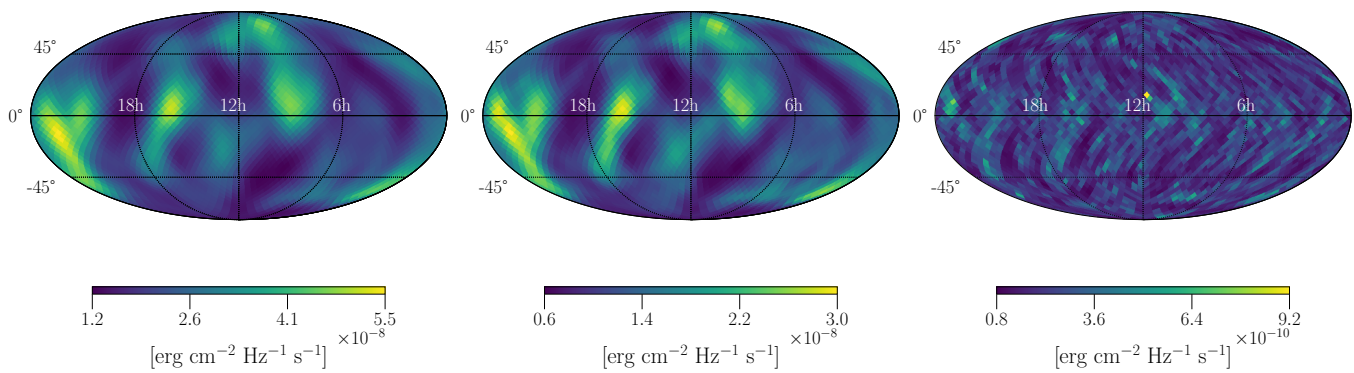


FIG. 3. 95% confidence Bayesian UL skymaps from a BBR search for point-like sources. The maps are presented in the equatorial coordinate system and show UL skymaps of the GW energy flux from the combination of all the data from O1 to O4a LIGO observing runs and the Virgo O3 data.  $\alpha = 0, 2/3, \text{ and } 3$  are represented from left to right.

$(C_\ell^{\text{shot}})^{1/2} \sim 10^{-10} \text{ sr}^{-1}$ , dominating the anticipated true astrophysical power spectrum [122], and is still below the obtained ULs by an order of magnitude. This is consistent with the fact that the point estimates for the two types of the  $\hat{C}_\ell$  estimators are not significantly different.

For  $\alpha = 0$ , we find the UL to be  $C_\ell^{1/2} \leq (0.7 - 1.7) \times 10^{-9} \text{ sr}^{-1}$  for  $1 \leq \ell \leq 3$ , whereas the theoretical study on Nambu-Goto strings based on the model 3 in Ref. [123], combined with the most up-to-date constraints on  $G\mu$  using the isotropic component of the GWB [65],  $G\mu \lesssim (2.7 \sim 4.2) \times 10^{-15}$ , sets  $C_1^{1/2} \lesssim 10^{-12} \text{ sr}^{-1}$ . For both choices of the power spectra ( $\alpha = 0$  and  $\alpha = 2/3$ ), we conclude that the predictions of the theoretical models are consistent with the search results presented here.

#### IV. CONCLUSIONS

We do not find evidence for GW signals in any of the four analyses using data from the first three observing runs of LIGO, Virgo, and O4a. Hence, each analysis yielded the most stringent constraints to date from the directional search for persistent GWs. For the all-sky all-frequency analysis, we observe a median (mean) improvement factor of 1.12 (1.38) in Bayesian sensitivity estimate to the effective strain amplitude when comparing O4a to O1–O3 in Tab. I. Combining data from O1–O4a enhances this improvement by a factor of 1.13 relative to O4a alone, and the fraction of notched frequency bins is reduced from 11.4% to 7.9%. For the targeted-narrowband radiometer analysis, O4a contributes significantly to improve the upper limits of the entire frequency range (see Fig. 2), in particular at higher frequencies. In the broadband radiometer analysis, when comparing with the first three observing runs in Tab. III, the median improvement across the sky in the upper limits on the GW energy flux is 1.4, 1.4, and 1.7 for  $\alpha = 0, 2/3, 3$ , respectively. Lastly, the spherical harmonic analysis has introduced a cross- $C_\ell$  estimator to remove the potential shot noise and GWB bias as opposed to the conventional auto- $C_\ell$  estimator.

The uncertainty on the angular power spectrum,  $C_\ell$ , derived from each estimator has improved by a factor of 1.4–2.2 compared to the first three observing runs. Also, the upper limits for each estimator shown in Fig. 4 are consistent with the predictions of the theoretical models, such as cosmic strings and kinematic dipole.

During O4a, the Virgo detector was not in science mode and is therefore not included in our analysis. However, as noted in previous studies [53], incorporating the Virgo detector into the network (even with its higher noise levels compared to the LIGO detectors) serves as a natural regularizer in extended source searches. This, in turn, enables us to resolve finer structures in the GW skymaps. As shown in [124], current directional analyses are not affected by correlated noise, such as magnetic correlations between detectors. While these contributions are currently negligible, they are expected to become increasingly important as detector sensitivities improve.

Improvements in detector sensitivity, longer observing runs, and larger network configuration will get us closer to the detection of potential local anisotropies or previously unknown point-like sources. It is also worth noting that the potential of all-sky all-frequency sources to uncover unknown narrowband signals represents an exciting direction for future investigations. A thorough investigation of the potential follow-up candidates from the all-sky all-frequency analyses, as presented in Ref. [125], could provide valuable insights into the nature and significance of the identified candidates.

Looking ahead, as the fourth observing run progresses, we will continue to incorporate additional data and update the findings reported in this paper.

#### ACKNOWLEDGEMENTS

This material is based upon work supported by NSF’s LIGO Laboratory, which is a major facility fully funded by the National Science Foundation. The authors also gratefully acknowledge the support of the Science and

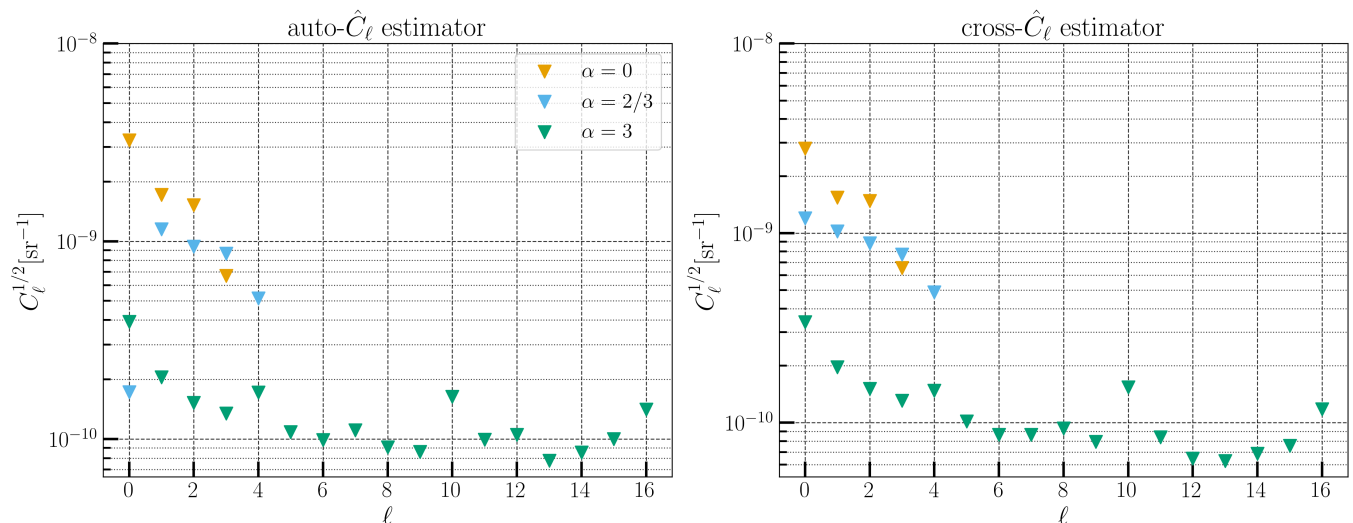


FIG. 4. 95% ULs on the two  $C_\ell$  estimators for different  $\alpha$  using combined O1+O2+O3+O4a data.

Technology Facilities Council (STFC) of the United Kingdom, the Max-Planck-Society (MPS), and the State of Niedersachsen/Germany for support of the construction of Advanced LIGO and construction and operation of the GEO 600 detector. Additional support for Advanced LIGO was provided by the Australian Research Council. The authors gratefully acknowledge the Italian Istituto Nazionale di Fisica Nucleare (INFN), the French Centre National de la Recherche Scientifique (CNRS) and the Netherlands Organization for Scientific Research (NWO) for the construction and operation of the Virgo detector and the creation and support of the EGO consortium. The authors also gratefully acknowledge research support from these agencies as well as by the Council of Scientific and Industrial Research of India, the Department of Science and Technology, India, the Science & Engineering Research Board (SERB), India, the Ministry of Human Resource Development, India, the Spanish Agencia Estatal de Investigación (AEI), the Spanish Ministerio de Ciencia, Innovación y Universidades, the European Union NextGenerationEU/PRTR (PRTR-C17.I1), the ICSC - Centro Nazionale di Ricerca in High Performance Computing, Big Data and Quantum Computing, funded by the European Union NextGenerationEU, the Comunitat Autònoma de les Illes Balears through the Conselleria d'Educació i Universitats, the Conselleria d'Innovació, Universitats, Ciència i Societat Digital de la Generalitat Valenciana and the CERCA Programme Generalitat de Catalunya, Spain, the Polish National Agency for Academic Exchange, the National Science Centre of Poland and the European Union - European Regional Development Fund; the Foundation for Polish Science (FNP), the Polish Ministry of Science and Higher Education, the Swiss National Science Foundation (SNSF), the Russian Science Foundation, the European Commission, the European Social Funds (ESF), the European Regional Development Funds (ERDF), the Royal Soci-

ety, the Scottish Funding Council, the Scottish Universities Physics Alliance, the Hungarian Scientific Research Fund (OTKA), the French Lyon Institute of Origins (LIO), the Belgian Fonds de la Recherche Scientifique (FRS-FNRS), Actions de Recherche Concertées (ARC) and Fonds Wetenschappelijk Onderzoek - Vlaanderen (FWO), Belgium, the Paris Ile-de-France Region, the National Research, Development and Innovation Office of Hungary (NKFIH), the National Research Foundation of Korea, the Natural Sciences and Engineering Research Council of Canada (NSERC), the Canadian Foundation for Innovation (CFI), the Brazilian Ministry of Science, Technology, and Innovations, the International Center for Theoretical Physics South American Institute for Fundamental Research (ICTP-SAIFR), the Research Grants Council of Hong Kong, the National Natural Science Foundation of China (NSFC), the Israel Science Foundation (ISF), the US-Israel Binational Science Fund (BSF), the Leverhulme Trust, the Research Corporation, the National Science and Technology Council (NSTC), Taiwan, the United States Department of Energy, and the Kavli Foundation. The authors gratefully acknowledge the support of the NSF, STFC, INFN and CNRS for provision of computational resources. This work was supported by MEXT, the JSPS Leading-edge Research Infrastructure Program, JSPS Grant-in-Aid for Specially Promoted Research 26000005, JSPS Grant-in-Aid for Scientific Research on Innovative Areas 2402: 24103006, 24103005, and 2905: JP17H06358, JP17H06361 and JP17H06364, JSPS Core-to-Core Program A. Advanced Research Networks, JSPS Grants-in-Aid for Scientific Research (S) 17H06133 and 20H05639, JSPS Grant-in-Aid for Transformative Research Areas (A) 20A203: JP20H05854, the joint research program of the Institute for Cosmic Ray Research, University of Tokyo, the National Research Foundation (NRF), the Computing Infrastructure Project of the Global Science experimental Data hub

Center (GSDC) at KISTI, the Korea Astronomy and Space Science Institute (KASI), the Ministry of Science and ICT (MSIT) in Korea, Academia Sinica (AS), the AS Grid Center (ASGC) and the National Science and Technology Council (NSTC) in Taiwan under grants including the Science Vanguard Research Program, the Advanced Technology Center (ATC) of NAOJ, and the Mechanical Engineering Center of KEK.

## Appendix A: Observing runs and dataset

Tab. IV details each individual observing run of the detectors from O1 to O4a, including their start and end times, the amount of data lost through time-domain cuts, and the effective data available for the GWB directional searches. As part of the time-domain cuts, we exclude data contaminated by instrumental artifacts, hardware injections used for signal validation, and segments containing known GW signals. We also apply a standard non-stationarity cut [64] to eliminate segments that do not behave as Gaussian noise. The table also shows the fraction of frequency bins removed from the analysis. These removals follow the same frequency-domain cuts described earlier, based on coherence studies identifying contamination from instrumental artifacts. The specific bins removed may vary across analyses depending on sensitivity to narrow spectral features.

## Appendix B: ASAF radiometer search

### 1. Significance

We summarize the statistical framework used here to identify the GW signal in the ASAF search.

The null hypothesis assumes that the data contain only Gaussian noise, while the alternative hypothesis is that a GW source is present in at least one frequency-pixel pair. The detection statistic is the SNR (Eq. (22)), which under the null ideally follows a zero-mean Gaussian distribution.

Because real detector data include non-Gaussian features such as narrowband artifacts and glitches, the null SNR distribution is obtained using the random time-shift (TS) method [54]. The procedure involves dividing the data from the entire observing run into multiple jobs (2493 in the case of O4a), each typically having a maximum duration of 5000 seconds. For each job, the data from one detector is held fixed while the data from the other detector is shifted by a random time delay, uniformly sampled between 1 and 2 seconds. This random time-shifting process effectively eliminates any coherent and persistent signals, ensuring that only the noise background remains in the data [54].

After ensuring the Gaussianity of the null distribution, we proceed to test the zero-lag (ZL) data (without an unphysical time-shift) against the null hypothesis. We

determine the observed highest SNR across frequency-pixel pairs and compute the local  $p$ -value,  $p_L$ , assuming a Gaussian distribution for noise. Since many simultaneous tests increase the chances of false positives (the look-elsewhere effect), we adjust to global  $p$ -value,  $p_G$ , using Sidak's correction [126, 127]:

$$p_G = 1 - (1 - p_L)^{N_{\text{trials}}} \approx N_{\text{trials}} p_L \quad \text{for } p_L \ll 1. \quad (\text{B1})$$

where  $N_{\text{trials}}$  is the number of frequency-pixel pairs. We reject the null hypothesis if  $p_G < 5\%$ .

### 2. Follow-up Candidates Identification

After assessing the significance of our data, we identify sub-threshold candidates for follow-up using more sensitive methods, such as matched-filtering-based searches [125]. We first determine the sky pixel with the maximum SNR,

$$\hat{\rho}_{\text{max}}(f) \equiv \max_{\hat{n}} \hat{\rho}_{\hat{n}}(f), \quad (\text{B2})$$

for each frequency bin in both zero-lag and time-shifted data. The full frequency range is divided into 10 Hz sub-bands for the time-shifted data. For each sub-band, we compute the histogram of  $\hat{\rho}_{\text{max}}(f)$  and determine the threshold below which 99% of the histogram area lies. This results in an array of sub-band-wise thresholds, which are then smoothed using a running average. Candidates in the zero-lag data with SNR exceeding this threshold are selected for further investigation. If the zero-lag data is consistent with random-timeshifted data (and Gaussian noise), this procedure is expected to yield at least  $\approx 513$  candidates. The following calculation shows why this number of candidates is expected:

$$\begin{aligned} \text{Sub-bands} &= \frac{(1726 - 20) \text{ Hz}}{10 \text{ Hz}} \\ &\approx 171, \end{aligned}$$

$$\text{Bins per sub-band} = \frac{10 \text{ Hz}}{\Delta f} = 320,$$

$$\text{Top-1\% candidates per sub-band} = 320 \times 0.01 \approx 3,$$

$$\text{Total Top-1\% candidates} = 171 \times 3 = 513. \quad (\text{B3})$$

### 3. Upper Limit Calculation

We adopt a hybrid frequentist-Bayesian approach for setting constraints [128]. Assuming the point estimate is a sufficient statistic for measuring GW source properties, we apply Bayes' theorem to construct the posterior distribution.

For clarity, the dependence of estimators  $[\hat{\mathcal{P}}_{\hat{n}}(f), \sigma_{\hat{n}}(f)]$  and strain parameter  $h_{\text{eff},\hat{n}}(f)$  on direction and frequency is assumed to be implicit in

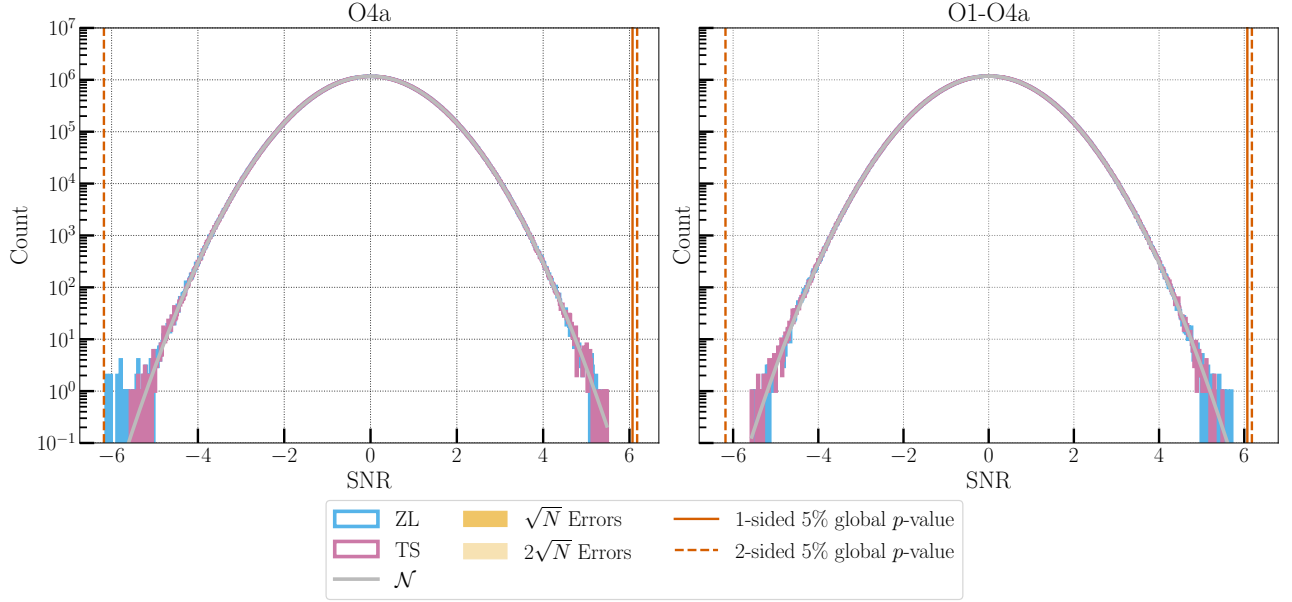


FIG. 5. ASAF search results — Significance: Left Panel: Distribution of SNR for the zero-lag (blue) and time-shifted (magenta) datasets with O4a observing run. The time-shifted (unphysical) distribution is consistent with a Gaussian (gray line) with mean  $-5 \times 10^{-4}$  and standard deviation 0.98. Poisson 1- and 2-sigma uncertainties for the time-shifted histogram are shown as a yellow-shaded region. The zero-lag histogram is largely consistent with the time-shifted data, except for non-Gaussian excess at negative SNR. Vertical brown lines (solid and dashed) indicate the 1- and 2-sided 5% global  $p$ -value SNR thresholds. Although an astrophysical signal is expected to yield a positive SNR, we investigate the origin of the observed negative SNR feature. Right Panel: Same as the figure in the right panel but with O1-O4a data.

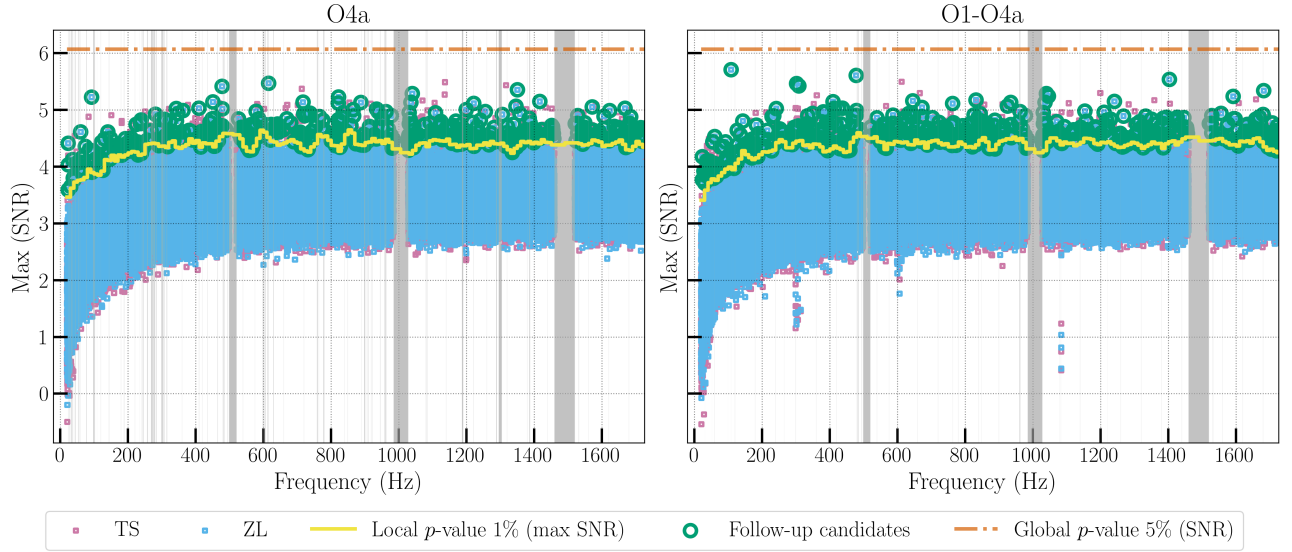


FIG. 6. Follow-up sub-threshold candidates: Left Panel: Distribution of the maximum SNR statistic (y-axis) as a function of frequency (x-axis) obtained with O4a observing run, where Max (SNR) denotes the maximum SNR across the sky within each frequency bin. Scatter points for the zero-lag and time-shifted datasets are shown in blue and magenta, respectively. Gray vertical lines indicate vetoed frequency bins excluded due to known instrumental artifacts. The brown horizontal line indicates the SNR threshold corresponding to a 5% 1-sided global  $p$ -value. The yellow curve shows the maxSNR threshold corresponding to a 99% local  $p$ -value in each 10-Hz band, smoothed over three neighboring bands. While the zero-lag data is consistent with Gaussian noise, we identify 505 sub-threshold follow-up candidates marked with teal circles, which may be further analysed using matched-filtering-based CGW search pipelines. Right Panel: Same as the left panel, but using data from O1-O4a observing runs.

Run [51–54]	Start time (UTC)	End time (UTC)	Detectors	Time domain cut (%)	Effective data (days)	Frequency notch fraction (%)	
						ASAF analysis	Other analyses
O1	2015-09-18 15:00	2016-01-12 16:00	H, L	35	29.85	25.5	21.1
O2	2016-11-30 16:00	2017-08-25 22:00	H, L	16	99	19.6	15.3
O3	2019-04-01 15:00	2020-03-27 17:00	H, L, V	10.7 (HL)	169 (HL)	21 (HL)	14.8 (HL)
				14.3 (HV)	146 (HV)	34.8 (HV)	25.2 (HV)
				14.7 (LV)	153 (LV)	28.15 (LV)	21.9 (LV)
O4a	2023-05-24 15:00	2024-01-16 16:00	H, L	8.3	108.65	11.4	11.4

TABLE IV. This table shows the individual observing runs, their start and end times, the detectors involved, the data quality cuts (both time and frequency domain) applied, and the effective data used in this analysis.

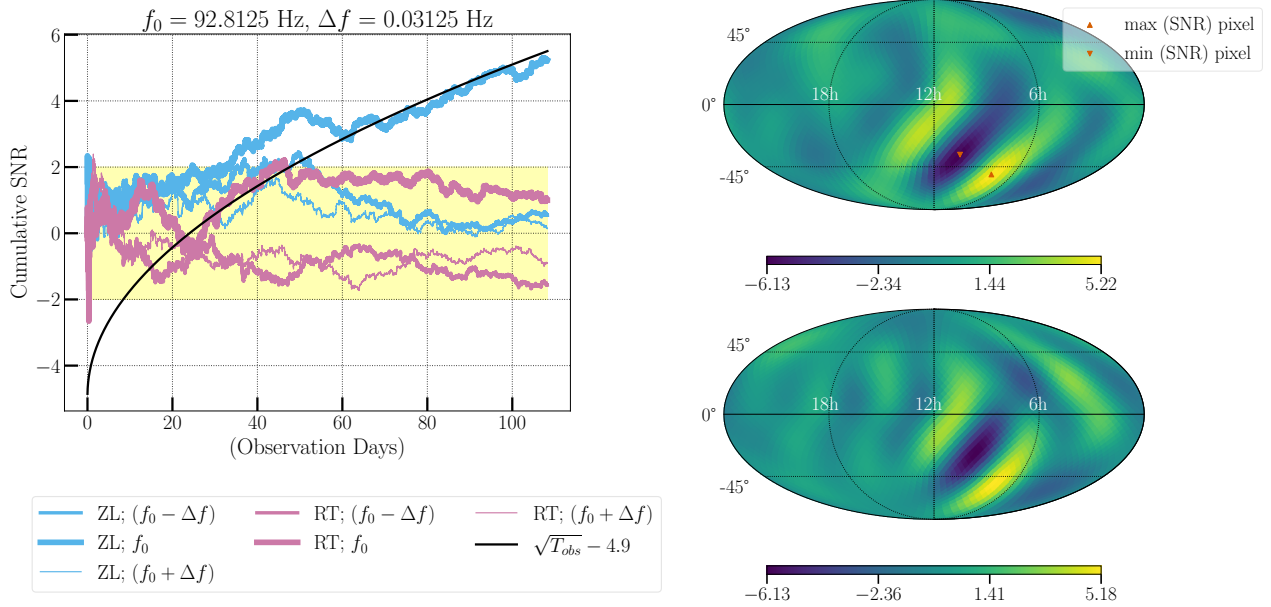


FIG. 7. Details of O4a marginal outlier towards negative SNR tail: The SNR skymap for 92.8125 Hz marginal outlier in O4a is shown in the top right panel. The positive and negative SNR blobs may be correlated through the point spread function: a GW source at the location of maximum SNR could produce a corresponding negative SNR feature next to it. To test this, we simulate skymap by injecting a source in the positive SNR direction and recover a map similar to the observed map, as shown in the bottom right panel. This motivates further investigation of both blobs. In the left panel, we show the evolution of cumulative SNR in the direction of maximum SNR (marked by an up triangle in the top right panel) as a function of observing days during O4a. The thick blue indicates the outlier frequency bin, while the two other thin blue curves represent the adjacent frequency bins immediately before and after the outlier. The magenta lines represent SNR evolution for random timeshifted data.

the following discussion. Each element in the matrices  $\left[\hat{\mathbf{P}}, \boldsymbol{\sigma}\right]$  here represents an observation from the individual dataset (e.g., baseline or observing run).

$$0.95 = \int_0^{(h_{\text{eff}})^{95\%}} dh_{\text{eff}} \frac{L(\hat{\mathbf{P}} \Delta f | \mathbf{E}, h_{\text{eff}}) p(h_{\text{eff}})}{\int dh_{\text{eff}} L(\hat{\mathbf{P}} \Delta f | \mathbf{E}, h_{\text{eff}}) p(h_{\text{eff}})}. \quad (\text{B4})$$

The integrand in the above equation represents the posterior distribution for  $h_{\text{eff}}$ , where  $L(\hat{\mathbf{P}} \Delta f | \mathbf{E}, h_{\text{eff}})$  is the likelihood and  $p(h_{\text{eff}})$  is the prior for  $h_{\text{eff}}$ . The likelihood  $L(\hat{\mathbf{P}} \Delta f | \mathbf{E}, h_{\text{eff}})$  is modelled as a multivariate Gaussian distribution for the random vector  $\hat{\mathbf{P}} \Delta f \sim \mathcal{N}[(h_{\text{eff}})^2 \mathbf{I}, \mathbf{E}]$  where  $\mathbf{I}$  is a column matrix with unit elements. The prior is assumed to follow a uniform distribution,  $h_{\text{eff}} \sim U[0, 10 \sqrt{\sigma} \Delta f]$  [54] where  $\sigma^2$  is squared sum of variance from individual dataset, i.e.,  $\sigma^2 = \sum_i \Sigma_{ii}$ . We note that the integration in the denominator spans the prior-defined range of  $h_{\text{eff}}$ .

Given that the strain data is obtained by calibrating the detector response to GW strain, our estimator is subject to calibration uncertainties (see [48–54, 129] for details). Marginalization over calibration uncertainty introduces an additional covariance term to the noise variance matrix of  $\hat{\mathbf{P}}$  [130]. The modified covariance matrix  $\mathbf{E}$  is given by

$$\mathbf{E} = \boldsymbol{\Sigma} + (h_{\text{eff}})^4 \mathbf{D}, \quad (\text{B5})$$

where  $\boldsymbol{\Sigma}$  is the noise covariance matrix, defined as  $\Sigma_{ij} = \sigma_i^2 \delta_{ij} \Delta f$ , and  $\mathbf{D}$  accounts for calibration errors. The indices  $i, j$  run over the number of analyzed datasets. As an example, for the baselines HL and LV, the  $\mathbf{D}$  matrix is

$$D = \begin{pmatrix} \epsilon_H^2 + \epsilon_L^2 + \epsilon_H^2 \epsilon_L^2 & \epsilon_L^2 \\ \epsilon_L^2 & \epsilon_L^2 + \epsilon_V^2 + \epsilon_L^2 \epsilon_V^2 \end{pmatrix}, \quad (\text{B6})$$

where  $\epsilon_H$ ,  $\epsilon_L$ , and  $\epsilon_V$  are the amplitude calibration uncertainties of the individual detectors [131].<sup>4</sup> The off-diagonal elements in the matrix are present only when the datasets analyzed from a given observing run share common detectors.

## Appendix C: Targeted narrowband radiometer

### 1. Source direction and its relevance

In this section, we list the sources chosen for the targeted search, explaining their relevance and selection criteria.

<sup>4</sup> The uncertainties adopted for different detectors and observing runs in this study are as follows:  $\epsilon_H^{O1} = 0.048$ ,  $\epsilon_L^{O1} = 0.054$ ,  $\epsilon_H^{O2} = 0.026$ ,  $\epsilon_L^{O2} = 0.0385$ ,  $\epsilon_H^{O3} = 0.0696$ ,  $\epsilon_L^{O3} = 0.0637$ ,  $\epsilon_V^{O3} = 0.05$ ,  $\epsilon_H^{O4a} = 0.0693$ , and  $\epsilon_L^{O4a} = 0.041$ .

**Scorpius X-1:** It is a neutron star in a low mass X-ray binary (LMXB) system, considered one of the most promising targets for CGW searches [58, 59]. In several searches [114, 116, 132], a torque balance is assumed between accretion spin-up from the companion star and angular momentum loss by gravitational emission (see also [133, 134]), and it has a known position and ephemeris. However, its rotational frequency remains unknown [135], and a spin wandering effect is expected, caused by stochastic fluctuations of the accretion rate [136]. The difficulty in characterizing its rotation makes it an optimal target for an unmodeled narrowband search, like the targeted NBR, across a large frequency range.

**Galactic Center:** Identified as the location of the supermassive black hole Sagittarius A\*, it has been addressed as the host of multiple potential GWs sources, making it a target for dedicated searches for persistent signals [54, 137, 138]. Being a potential host of many unresolved sources with unknown parameters, it is another natural target for our search.

**SN 1987A:** A young supernova (SN) remnant, SN 1987A has been identified as a promising target for GW searches due to its recent origin [139, 140]. However, until recently, it was not possible to confirm the existence of a neutron star at its center. This has now been established through electromagnetic emission detected by the James Webb Space Telescope [141]. Although the source parameters remain unknown, this confirmation underscores the relevance of SN 1987A as a target for GW searches.

**Terzan 5 and NGC 6397:** Globular clusters are known to contain many neutron stars and can be promising targets for GW searches. Among the possible selection criteria, we follow [142] and [143] that point to Terzan 5 and NGC 6397 as a possible host of a large number of unresolved sources, together with the fact that Terzan 5 alone hosts approximately 18% of the known millisecond pulsars [144]. However, other criteria exist (for example, see [145]).

### 2. Bin Combination

The value of the number  $N$  of bins to be combined, for the individual sources analyzed, is determined as follows: for Scorpius X-1, assuming torque balance and hence neglecting steady spin variation during the observing time, it is computed using the evolution predicted by its orbital parameters (see [146]). For the Galactic Center, Terzan 5, and NGC 6397 – which may host a large number of unknown sources – we compensate only the Earth’s Doppler modulation, fixing  $N = 10$  for all of them.

The high latitude of SN 1987A causes a negligible Doppler spread due to Earth’s motion with the default frequency resolution used ( $\Delta f = 1/32$  Hz); hence, in this case,  $N = 1$ .

However, SN 1987A is a young supernova remnant, and it is expected to have a strong spin-down effect due to

rotational energy loss. We did not consider the cumulative effect of different observing runs when establishing the bin combination, as this would require specific techniques to account for the several-month gaps between runs, under various assumptions about the source's spin derivatives (see, for example, the study carried out in [147]).

This leads to ULs that are less conservative than those obtained by combining additional bins, under the assumption that the entire signal is confined to a single frequency bin rather than distributed across several.

### 3. Significance

For a given target  $\hat{n}$ , to assess the significance of the SNR-frequency data results after the bin combination, a  $p$ -value is estimated with the following process: 1) a large number ( $n \sim 256$ ) noise-only distributions of  $\mathcal{P}_{\hat{n}}(f)$  are generated, drawing for each frequency bin a value from Gaussian distributions with mean 0 and the corresponding  $\sigma_f$  obtained from the data; 2) for each realization, the generated  $\mathcal{P}_{\hat{n}_{\text{sim}}}(f)$  and the measured  $\sigma(f)$  are combined according to the data from the given target, yielding a simulated SNR distribution with the same bin combination; 3) the maximum SNR from each of the simulated distributions is stored; 4) a range of  $p$ -values running from  $[0, 1]$  in  $n$  steps are generated and associated with the maximum SNRs obtained; 5) via a linear interpolation the data SNRs are matched to the SNR- $p$ -value distribution obtained by the simulations. A frequency bin whose SNR corresponds to a  $p$ -value of less than 5% is considered an outlier that needs to be analyzed more thoroughly.

### 4. Bayesian posterior and UL plots

In the following, the calculation of the upper limits via the integration of Bayesian posteriors will be broken down. The starting point is the definition of expectation value and variance of the cross-correlation statistics for persistent GW signals. They can be written respectively [105]:

$$\mu_{\mathcal{P}} = \frac{\sum_j (A^{+2} F_{1j}^+ F_{2j}^+ + A^{\times 2} F_{1j}^{\times} F_{2j}^{\times}) (F_{1j}^+ F_{2j}^+ + F_{1j}^{\times} F_{2j}^{\times})}{\sum_j (F_{1j}^+ F_{2j}^+ + F_{1j}^{\times} F_{2j}^{\times})^2}. \quad (\text{C1})$$

and

$$\sigma_{\mathcal{P}}^2 = \frac{2P_1 P_2}{T_{\text{coh}}^2 \sum_j (F_{1j}^+ F_{2j}^+ + F_{1j}^{\times} F_{2j}^{\times})^2}, \quad (\text{C2})$$

where the sum is over the  $M$  segments of the semicoherent search with coherence time  $T_{\text{coh}}$ ; the GW amplitudes for the two polarizations  $A^+$ ,  $A^\times$  depend on the source inclination angle  $\iota$  and the GW strain tensor amplitude

$h_0$ <sup>5</sup>; the antenna patterns for the two polarizations and the two detectors at the time segment  $j$ ,  $F_{\{1,2\}j}^{\{+, \times\}}$ , depend explicitly on the polarization angle  $\psi$ ; the single-sided power spectral density estimations for the two detectors are  $P_{1,2}$ . In the case of circularly polarised signal  $A^+ = A^\times = h_0$  and  $\mu_{\mathcal{P}} = h_0^2$ .

The ULs are computed by integrating the Bayesian posterior function up to the value  $h_0^{UL}$  that returns the chosen 95% confidence:

$$0.95 = \int_0^{h_0^{UL}} p(h_0 | \mathcal{P}, \sigma_{\mathcal{P}}). \quad (\text{C3})$$

For a given frequency bin, the posterior comes from the marginalization integral

$$p(h_0 | \mathcal{P}) \propto \int_{-1}^1 d(\cos \iota) p(\iota) \int_{-\pi/4}^{\pi/4} d\psi p(\psi) \int_{-1}^3 d\lambda p(\mathcal{P} | h_0, \iota, \psi, \lambda) p(\lambda) \quad (\text{C4})$$

over the inclination angle  $\iota$ , the polarization angle  $\psi$  [105] and the calibration factor  $\lambda$  [130].

The priors for the first two integrals—respectively  $p(\iota)$  and  $p(\psi)$ —will be uniform distributions within the integral range, and their values will be absorbed in the  $\propto$  symbol. The latter integral is over an unknown correction factor representing the uncertainty in the calibration. We assume for it a Gaussian prior distribution  $p(\lambda)$ , with  $\sigma_\lambda$  as standard deviation, a known parameter called *calibration error*.

The likelihood distribution is

$$L(\mathcal{P} | h_0, \iota, \psi, \lambda) = \exp \left[ -\frac{1}{2} \left( \frac{\lambda \mathcal{P} - \mu_{\mathcal{P}}}{\lambda \sigma_{\mathcal{P}}} \right)^2 \right], \quad (\text{C5})$$

where the dependence on  $h_0, \iota, \psi$  lies within  $\mu_{\mathcal{P}}$ .

The marginalized posterior for a generic polarization will be:

$$p(h_0 | \mathcal{P}) \propto \int_{-1}^1 d(\cos \iota) \int_{-\pi/4}^{\pi/4} d\psi \int_{-1}^3 d\lambda \exp \left[ -\frac{1}{2} \left( \frac{\lambda \mathcal{P} - \mu_{\mathcal{P}}}{\lambda \sigma_{\mathcal{P}}} \right)^2 - \frac{1}{2} \left( \frac{\lambda}{\sigma_\lambda} \right)^2 \right]. \quad (\text{C6})$$

In the case of a circularly polarized signal, the likelihood becomes independent of  $\iota$  and  $\psi$ , and the posterior integral will simply reduce to

$$L(h_0 | \mathcal{P}) \propto \int_{-1}^3 d\lambda \exp \left[ -\frac{1}{2} \left( \frac{\lambda \mathcal{P} - h_0}{\lambda \sigma_{\mathcal{P}}} \right)^2 - \frac{1}{2} \left( \frac{\lambda}{\sigma_\lambda} \right)^2 \right]. \quad (\text{C7})$$

<sup>5</sup>  $A^+ = \frac{1}{2} h_0 (1 + \cos^2 \iota)$  and  $A^\times = h_0 \cos \iota$ , where  $\iota$  is the source inclination angle.

It has been shown that there is a scale factor of  $\sim 2.5$  between ULs computed with a marginalization for a generic polarization with respect to the circular polarization ones, which depends only on the SNR of the search results [105]. Calculating the integrals in Eq. (C6) for each frequency bin can consume a large amount of computing resources, hence ULs for the two cases are simulated only for a small number of SNR values between -8 and 8. The ratio between the two simulated distributions will be called “upper limit ratios”.

The final UL values are computed under the computationally much simpler hypothesis of circular polarization. Assuming a Gaussian prior for the calibration factor, an analytical solution for the marginalized posterior exists [148, 149] in the form of:

$$p(h_0|\mathcal{P}) \propto \frac{1}{\sqrt{2\pi}E^2} \exp\left[-\frac{1}{2} \frac{(\mathcal{P} - h_0^2)^2}{E^2}\right], \quad (\text{C8})$$

where  $E \equiv \sigma_{\mathcal{P}} + h_0^4 \sigma_{\lambda}$ . By interpolation on the real SNR data, the UL ratios are applied to reproduce the ULs for a generic polarization.

For the combination of datasets, we have to treat the combined effect of the calibration error of the different runs, changing how the ULs are produced. It can be shown that the combined likelihood is the product of the single dataset likelihood [130]:

$$L(\mathcal{P}|h_0, \boldsymbol{\lambda}) = \prod_i L(\mathcal{P}_i|h_0, \lambda_i). \quad (\text{C9})$$

With  $\mathcal{P} = \{\mathcal{P}_1, \dots, \mathcal{P}_n\}$  we indicate the vector of the detection statistics for a fixed frequency bin and with  $\boldsymbol{\lambda} = \{\lambda_1, \dots, \lambda_n\}$  the vector of the unknown calibration factor we want to marginalize, across the  $n$  datasets. The marginalized posterior will, in turn, be

$$p(h_0|\mathcal{P}) \propto \int d\boldsymbol{\lambda} L(\mathcal{P}|h_0, \boldsymbol{\lambda}) p(\boldsymbol{\lambda}). \quad (\text{C10})$$

It is important to underline that the detector baseline calibration uncertainty affecting our results is the combination of the single detector calibration uncertainties. This, in general, will produce covariance matrices with off-diagonal elements like in the example in Eq. (B6) that have to be considered in the integration. If, in turn, we consider the same baseline across different runs, we can consider the single-run calibration uncertainties independently of each other and separate the integrals. In this case as well, the marginalized posterior will be the product of the single dataset posteriors:

$$p(h_0|\mathcal{P}) = \prod_i p(h_0|\mathcal{P}_i). \quad (\text{C11})$$

## 5. Comparison between UL and torque balance for Scorpius X-1

An order-of-magnitude estimate of the torque-balance level, often used in Sco X-1 CGW searches [113, 114] to

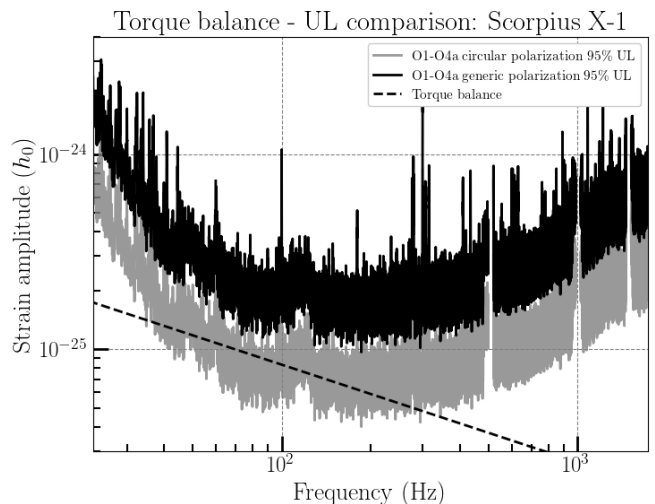


FIG. 8. Comparison of the UL for generic polarization (solid black line) and a circularly polarized signal (solid gray line) with the torque-balance level from Eq. (C12) (dashed black line). While the former does not reach the torque-balance threshold, the latter lies well below it.

gauge the astrophysical relevance of the explored parameter space, is given by

$$h_0 \approx 3.4 \times 10^{-26} \left( \frac{f_0}{600 \text{ Hz}} \right)^{-1/2}. \quad (\text{C12})$$

This curve is shown in Fig. 8 as a dashed black line. If we compare the 95% confidence level UL obtained by the NBR search to the torque-balance curve, it is evident that for a generic polarization, the search does not reach amplitudes below the torque balance hypothesis.

On the other hand, if we consider a circularly polarized signal, then the ULs are not marginalized over inclination and polarization angle, reaching lower effective strain amplitudes. In this scenario, and in agreement with the aforementioned searches, our results surpass the torque-balance limit.

## Appendix D: Broadband radiometer search - Statistical significance

To assess whether a signal is present or not in the BBR search data in Sec. III C, we consider the SNR map for each spectral index and evaluate the statistical significance of the maximum SNR under the hypothesis that only noise is present in the data. This is accomplished by simulating  $N_{\text{trials}}$  realizations of the SNR sky-maps and selecting the maximum SNR for each of them, hence constructing the probability distribution function of the maximum SNR. In practice, for each trial: 1) we simulate a skymap where each pixel contains Gaussian noise; 2) we color the noise in each pixel by using the singular values decomposition of the Fisher matrix to generate

the simulated dirty map in the absence of any signal; 3) we use the diagonal of the Fisher matrix to obtain  $\sigma_{\hat{n}} = (\text{diag}\{\Gamma_{\hat{n}\hat{n}'}\})^{-1/2}$  and the simulated estimator map  $\hat{\mathcal{P}}_{\hat{n}, \text{noise}}$  in the absence of a signal; 4) we obtain the SNR map as  $\hat{\mathcal{P}}_{\hat{n}, \text{noise}}/\sigma_{\hat{n}}$ ; 5) we select the maximum SNR and add it to the histogram of the maximum-SNR distribution. After  $N_{\text{trials}}$ , we evaluate the maximum-SNR statistical significance ( $p$ -value) as the ratio of the number of histogram entries that exceed the maximum value of the observed SNRs to the total number of the histogram entries (i.e.,  $N_{\text{trial}}$ ).

If the statistical significance of the maximum SNR is consistent with the noise-only hypothesis, we proceed with the evaluation of the ULs on the GWB angular power spectrum. The evaluation of the ULs follows the same Bayesian approach as that described in Appendix B by replacing  $h_0^{\text{eff}}$  with  $\mathcal{P}$  and  $\hat{\mathcal{P}} \Delta f$  with  $\hat{\mathcal{P}}$  in Eq. (B4), which we then rescale to GW energy flux units.

## Appendix E: Spherical harmonics analysis

### 1. Angular resolution

The number of SPH modes to evaluate scales as  $(\ell_{\text{max}} + 1)^2$ , and hence, in practice, one cannot search for arbitrary high-order modes due to substantial computational costs. More importantly, the interferometry in general imposes a minimum angular scale below which a given baseline becomes insensitive to real signals. For a monochromatic signal at the frequency  $f^*$ , the interferometry-limited angular scale is given by

$$\theta = \frac{c}{2d f^*}, \quad (\text{E1})$$

where  $d$  is the separation of two GW detectors, e.g.,  $d = 3000$  km for the LIGO detectors. Since SPH searches target broadband signals,  $f^*$  cannot be uniquely determined, but is approximated by the dominant frequency component of the signals. This dominant frequency can be estimated by the tangent point between a given power-law spectrum and the baseline's sensitivity curve, i.e., *power-law integrated curve* [150]. Therefore, the larger power-law index  $\alpha$  leads to a higher value of  $f^*$ , e.g.,  $f^* = 52.5, 256.5$  Hz for  $\alpha = 0, 3$ , respectively. Once  $\theta$  is known, the highest SPH mode  $\ell_{\text{max}}$ , which corresponds to the minimum angular scale, can be expressed as  $\ell_{\text{max}} = \pi/\theta$ . Following this argument, we have adopted  $\ell_{\text{max}} = 3, 4, 16$  for  $\alpha = 0, 2/3, 3$ , respectively [51–53].

### 2. Regularization of the Fisher matrix

Apart from the angular resolution mentioned above, another numerical issue arises from the fact that the Fisher matrix is often *ill-conditioned*—that is, some of

its eigenvalues are extremely small, which makes the inversion of the Fisher matrix numerically unstable and introduces additional numerical noise. This issue can be mitigated by regularizing the Fisher matrix; in previous analyses, we addressed this by discarding negligible eigenmodes. In O4a, we revisited the criterion for identifying such negligible eigenmodes, taking into account their residual sum of squares (RSS) to strike a balance between noise variance and signal recovery bias. Regularizing the Fisher matrix is a common mathematical problem, and hence, there are several regularization methods developed in the field of astronomy [77, 81, 151–153]. Our approach is to replace the singular values for a subset of the SPH modes (e.g.,  $M$  out of the total  $N$  modes) that have smaller eigenvalues than a given threshold ( $\lambda_M$ ) with infinities, i.e.,

$$\mathbf{U} \mathbf{\Gamma} \mathbf{V} = \text{diag}(\lambda_1, \dots, \lambda_M, \dots, \lambda_N) \quad (\text{E2})$$

$$\rightarrow \text{diag}(\infty, \dots, \infty, \lambda_{M+1}, \dots, \lambda_N), \quad (\text{E3})$$

where  $\mathbf{U}, \mathbf{V}$  are each a unitary matrix, which diagonalizes  $\mathbf{\Gamma}$ , and  $\lambda_i$  are the  $i$ -th singular values of  $\mathbf{\Gamma}$  sorted as  $\lambda_1 < \lambda_2 < \dots < \lambda_N$ . This would effectively remove the contribution from the regularized SPH modes after inverting the Fisher matrix [57]. Note that the clean map estimator would be affected by a potential bias in the presence of astrophysical anisotropies

$$\langle \hat{\mathcal{P}}_{\mu} \rangle = \mathbf{\Gamma}_{\text{R}}^{-1} \cdot \mathbf{\Gamma} \cdot \mathcal{P} \neq \mathcal{P}, \quad (\text{E4})$$

where  $\mathbf{\Gamma}_{\text{R}}$  is a regularized Fisher matrix. Although, technically speaking, the fractional number of singular modes to keep,  $f_{\text{keep}}$ , is still arbitrary, optimizing the regularization involves a trade-off relation between a lower variance, i.e., larger SNR, and the accuracy of the clean map estimator [117].

Since O1, LVK has adopted an empirical approach that keeps 2/3 of the total modes, i.e.,  $f_{\text{keep}} = (N - M)/N = 2/3$  across different  $\alpha$  values [51–53]. In O4a, we revisit this approach and introduce an alternative justification by computing RSS of the clean map estimator for a given simulated signal [77, 81]. This is defined as

$$\text{RSS} = |\hat{\mathcal{P}}_{(k)} - \mathcal{P}^{\text{inj}}|^2, \quad (\text{E5})$$

where  $\mathcal{P}^{\text{inj}}$  is an injected GWB signal and  $\hat{\mathcal{P}}_{(k)}$  is a clean map estimator with the noise realization using the Fisher matrix derived from the time-shifted O4a dataset, and the regularization keeping  $k$  singular modes. For each  $k$ , we repeat this computation with 10 different noise realizations and take their mean value. Since the mean of RSS follows

$$\langle \text{RSS} \rangle = \langle |\hat{\mathcal{P}}_{(k)}|^2 \rangle - 2 \text{Re} \left[ \langle \hat{\mathcal{P}}_{(k)} \rangle \cdot \mathcal{P}^{\text{inj}} \right] + |\mathcal{P}^{\text{inj}}|^2 \quad (\text{E6})$$

$$= \underbrace{\langle \sigma_{\mathcal{P}}^2 \rangle}_{\text{variance}} + \underbrace{\left| \langle \hat{\mathcal{P}}_{(k)} \rangle - \mathcal{P}^{\text{inj}} \right|^2}_{\text{bias}}, \quad (\text{E7})$$

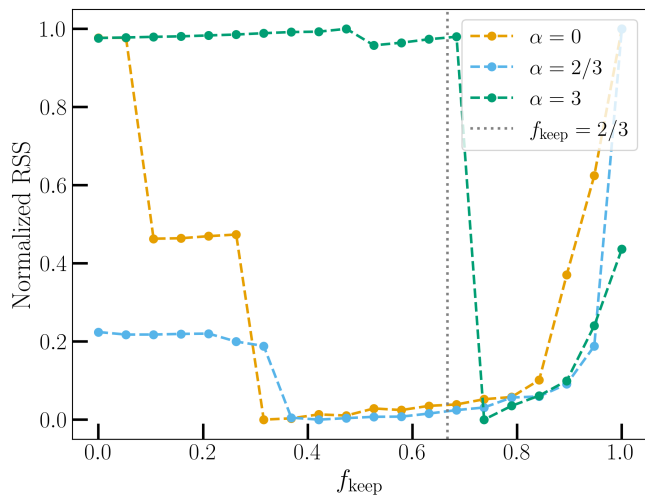


FIG. 9. Normalized RSS as a function of  $f_{\text{keep}}$  for each  $\alpha$  value.

the first and second terms in Eq. (E7) represent the variance and bias of the clean map, respectively. Therefore, minimizing (RSS) in terms of  $k$  identifies the optimal point that compromises the variance and bias. In principle, RSS values depend on the anisotropy model of the injected GWB, and here we consider only the monopole component, i.e.,  $\mathcal{P}_{\ell m} = 0$  ( $\ell \neq 0$  or  $m \neq 0$ ), as a plausible detection scenario.

Fig. 9 shows a *normalized* RSS as a function of  $f_{\text{keep}}$  for each  $\alpha$  value, which demonstrates the optimal  $f_{\text{keep}}$  of 0.3, 0.35 and 0.72 for  $\alpha = 0, 2/3, 3$ , respectively. We will adopt these values for the regularization applied to the main results of the SPH analysis.

Also, Fig. 10 shows the distribution of eigenvalues for the Fisher matrix with different  $\alpha$  values combining O1 to O4a data. The two dashed lines with each color compare the number of modes to keep between the conventional ( $f_{\text{keep}} = 2/3$ ) and the RSS regularization methods. Compared to the conventional  $f_{\text{keep}} = 2/3$ , the new regularization keeps fewer modes for  $\alpha = 0, 2/3$ , while keeping more modes for  $\alpha = 3$ . Although this change in  $f_{\text{keep}}$  alters the variance of the clean map estimator, we note that it does not indicate a physical change in the sensitivity, but rather a different way of presenting the results.

### 3. Cross $\hat{C}_\ell$ estimator

In the limiting case where the detector data contain only detector noise, the auto- $\hat{C}_\ell$  estimator given by Eq. (17) is unbiased. However, Ref. [83] showed that in the presence of an astrophysical GWB, it is significantly biased by the shot-noise-dominated nature of the signal, which arises from the discrete spatial or temporal realization of individual events. Also, this shot noise effect scales as  $\propto 1/T_{\text{obs}}$  in terms of  $C_\ell$ , where

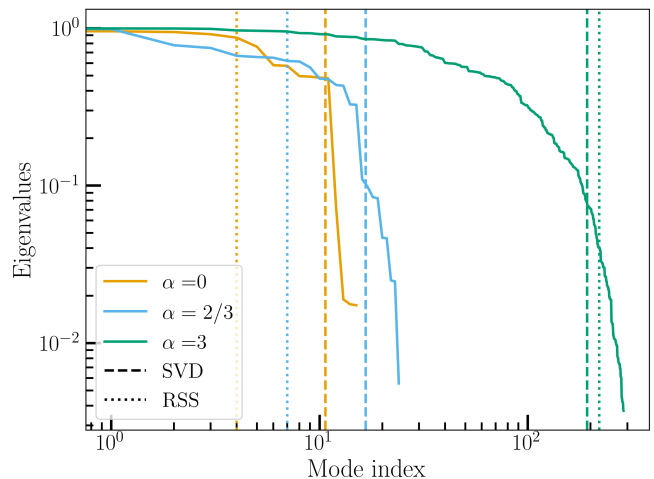


FIG. 10. Distribution of eigenvalues for the Fisher matrix with different  $\alpha$  values combining O1 to O4a data. The two dashed lines with each color compare the number of modes to keep between the conventional ( $f_{\text{keep}} = 2/3$ ) and new (RSS) regularization methods.

$T_{\text{obs}}$  is the observation time, which is the same scaling expected for the ULs set by the search. As a result, shot noise may become a limiting factor in future SPH searches—particularly if sensitivity improves faster than the  $1/T_{\text{obs}}$  scaling, whether due to enhanced detector sensitivity or the inclusion of additional detectors. In such a regime, the analysis could begin to detect GWB signals from plausible astrophysical populations, e.g., from CBCs. In addition, Ref. [83] found that the auto- $\hat{C}_\ell$  estimator is biased even in the absence of shot noise in the GWB signal.

Therefore, we introduced the cross- $\hat{C}_\ell$  estimator shown in Eq. (20), which involves multiple clean maps derived from subsets of the whole dataset. For each subset, we compute the corresponding dirty map  $\mathbf{X}^{(i)}$  and Fisher matrix  $\mathbf{\Gamma}^{(i)}$ , and follow the same deconvolution procedure as described earlier to obtain the individual clean maps. This cross- $\hat{C}_\ell$  estimator, obtained by summing over all pairs of distinct maps, is by construction unbiased, accounting for the fact that the bias arises from autocorrelation of each data segment. This concerns contributions to the bias not only due to the GWB signal and shot noise but also the detector noise, which is why  $\Sigma_{\text{R}}$  is no longer subtracted from the clean map product, unlike in Eq. (17). In practice, there are many ways to divide the total dataset into subsets, with no trivial choice. However, following Ref. [83], we aim for constructing subsets of the data with approximately equal sensitivity, leading to the best UL on the  $C_\ell$  measurement. Therefore, in our case, we combine data across different observing runs and baselines to yield data subsets with approximately equal sensitivity as follows: The data from the O1 and O2, as well as the HV and LV baselines of the O3, are combined into one subset. The total dirty map and Fisher matrix

of this subset are then given by

$$\begin{aligned}\mathbf{X}^{(1)} &= \mathbf{X}^{\text{O1}} + \mathbf{X}^{\text{O2}} + \mathbf{X}^{\text{O3(HV)}} + \mathbf{X}^{\text{O3(LV)}}, \\ \mathbf{\Gamma}^{(1)} &= \mathbf{\Gamma}^{\text{O1}} + \mathbf{\Gamma}^{\text{O2}} + \mathbf{\Gamma}^{\text{O3(HV)}} + \mathbf{\Gamma}^{\text{O3(LV)}},\end{aligned}\quad (\text{E8})$$

respectively, similar to Ref. [52]. We construct the first subset in this manner and divide the HL baseline dataset from O3 and O4a according to the sensitivity of this dataset, since O1, O2, and the HV and LV baselines of O3 are significantly less sensitive than the HL baselines of O3 and O4a. Specifically, the data from the HL baseline of O3 and O4a are divided equally into 6 and 11 subsets, respectively. For each subset, we compute the corresponding dirty map,  $\mathbf{X}^{(i)}$ , and Fisher matrix,  $\mathbf{\Gamma}^{(i)}$ , where the index  $i$  ranges from 2 to 7 for O3 and from 8 to 18 for O4a.

#### 4. UL and significance computation

Following the procedure for significance assessment described in Sec. II E, we compute the  $p$ -value for each real and imaginary part of the clean map estimator for the combined dataset across O1-O4a, and compare all these  $p$ -values to the local and global  $p$ -value thresholds, respectively. For better visualization, we convert each  $p$ -value to a  $z$ -score, which ranges between  $[-\infty, \infty]$ , through the inverse error function. Including the  $\alpha = 3$  case shown in Fig. 11, all SPH modes lie within the global  $p$ -value threshold (the dashed lines) across the three power-law spectrum models, indicating the consistency with a Gaussian distribution. Similarly, we investigate  $p$ -values for the 18 subsets of data used to compute the cross- $\hat{C}_\ell$  estimator and confirm that they remain within the global  $p$ -value threshold with very few exceptions<sup>6</sup>. Therefore, we confirm that no confident detection is made at a  $p$ -value below  $< 5\%$ . We then compute the  $C_\ell$  point estimates and their  $1\sigma$  uncertainty using Eqs. (18) and (21) for either of the two estimators, respectively. Although the auto- $\hat{C}_\ell$  estimator is potentially biased due to shot noise in an astrophysical GWB signal, Fig. 12 shows that the differences between the two estimators remain consistently within their  $1\sigma$  error bars across all  $\ell$  values. This suggests that such a bias is not noticeable, as expected in the absence of a detected signal, given the current search sensitivity.

Given the absence of a detected GWB signal, we compute ULs on  $C_\ell^{1/2}$  at each angular scale characterized by the  $\ell$  value, for different power-law frequency spectrum models, by constructing Bayesian posteriors from

the Monte Carlo samples using the same procedure described for computing  $p$ -values in Sec. II E. The  $\hat{\mathcal{P}}^{\text{sim}}$  samples generated for the whole dataset and each of the 18 subsets are converted into the auto- $\hat{C}_\ell$  and cross- $\hat{C}_\ell$  estimators based on Eq. (17) and Eq. (20), respectively. We add the observed  $C_\ell$  point estimates to each sample and construct the simulated PDF,  $p(C_\ell|\hat{C}_\ell)$ . Furthermore, we account for the calibration uncertainty by marginalizing this simulated PDF over the calibration factor  $\lambda$  such that

$$p(C_\ell|\hat{C}_\ell) = \int d\lambda p(C_\ell|\hat{C}_\ell, \lambda) p(\lambda), \quad (\text{E9})$$

where

$$p(C_\ell|\hat{C}_\ell, \lambda) = p(C_\ell/\lambda^2|\hat{C}_\ell, \lambda_0 = 1), \quad (\text{E10})$$

$$p(\lambda) \propto \exp\left\{-\left(\frac{\lambda - 1}{2\sigma_\lambda^2}\right)^2\right\}. \quad (\text{E11})$$

The variance of the calibration factor,  $\sigma_\lambda^2$ , is given by the sum of the individual calibration uncertainties measured in each baseline and observing run<sup>7</sup>, i.e.,  $\sigma_\lambda^2 = \sum_i \epsilon_i^2$ . Eventually, we identify 95th percentiles of  $p(C_\ell|\hat{C}_\ell)$  and define it as the UL at the 95% confidence level.

When we generate the  $\hat{\mathcal{P}}^{\text{sim}}$  samples, we need to account for a complication due to the requirement that the clean maps be real quantities on the pixel basis; each sample needs to conserve the following symmetry

$$\Gamma_{\ell-m, \ell'-m'} = (-1)^{m+m'} \Gamma_{\ell m, \ell' m'}^*. \quad (\text{E12})$$

The clean map estimator  $\hat{\mathcal{P}}_{\ell m}$  follows a multi-variate *complex* Gaussian distribution with zero mean and the covariance matrix  $\mathbf{\Sigma}$  given by Eq. (19). To satisfy this condition, we draw each real and imaginary part of a sample separately by constructing a *real* covariance matrix

$$\begin{pmatrix} \text{Re}\hat{\mathcal{P}}^{\text{sim}} \\ \text{Im}\hat{\mathcal{P}}^{\text{sim}} \end{pmatrix} \sim \mathcal{N}\left(\begin{bmatrix} 0 \\ 0 \end{bmatrix}, \begin{bmatrix} \mathbf{\Sigma}_{\text{RR}} & \mathbf{\Sigma}_{\text{RI}} \\ \mathbf{\Sigma}_{\text{IR}} & \mathbf{\Sigma}_{\text{II}} \end{bmatrix}\right), \quad (\text{E13})$$

where each block matrix in the real covariance matrix is

<sup>6</sup> Considering all individual data subsets and for  $\alpha \in \{2/3, 3\}$ , the global  $p$ -value threshold was exceeded for a negligible number of SPH modes. For  $\alpha = 0$ , however, this occurred for approximately 4% of all SPH modes. Due to this notable deviation from Gaussianity in the latter case, the results of the cross- $\hat{C}_\ell$  estimator for  $\alpha = 0$  should be interpreted with caution.

<sup>7</sup> Technically, for the cross- $\hat{C}_\ell$  estimator, the propagation of the calibration error differs from the auto- $\hat{C}_\ell$  estimator because it computes the cross-power of the clean map across the subsets rather than its auto-power, and hence this calibration factor should be derived differently. We leave this modification as future work.

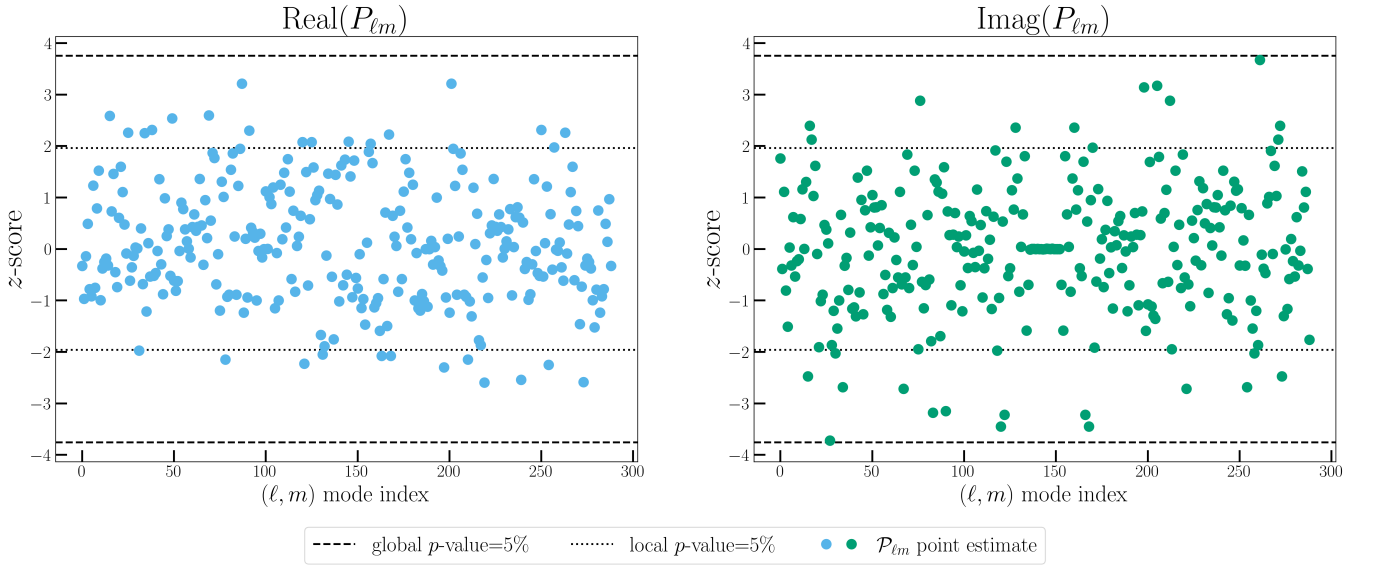


FIG. 11.  $z$ -score distribution of  $\alpha = 3$  case for the combined O1-O4a data.

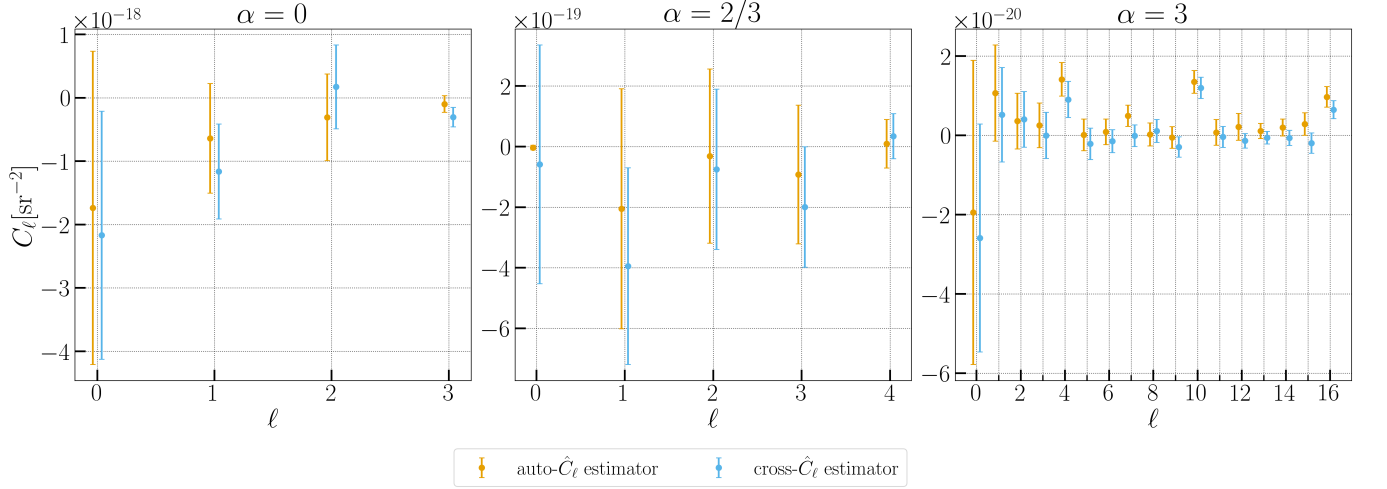


FIG. 12.  $C_\ell$  point estimates using either type of the estimators mentioned above for each power-law spectrum model with the combined O1+O2+O3+O4a data.

defined as

$$\begin{aligned} \Sigma_{\text{RR}} = \frac{1}{4} \{ & \Sigma_{lm'l'm'} + (-1)^m \Sigma_{l-ml'm'} \\ & + (-1)^{m'} \Sigma_{lm'l'-m'} + (-1)^{m+m'} \Sigma_{l-ml'-m'} \}, \end{aligned} \quad (\text{E14})$$

$$\begin{aligned} \Sigma_{\text{II}} = \frac{1}{4} \{ & \Sigma_{lm'l'm'} - (-1)^m \Sigma_{l-ml'm'} \\ & - (-1)^{m'} \Sigma_{lm'l'-m'} + (-1)^{m+m'} \Sigma_{l-ml'-m'} \}, \end{aligned} \quad (\text{E15})$$

$$\begin{aligned} \Sigma_{\text{RI}} = \Sigma_{\text{IR}}^\top \\ = \frac{-i}{4} \{ & \Sigma_{lm'l'm'} + (-1)^m \Sigma_{l-ml'm'} \\ & - (-1)^{m'} \Sigma_{lm'l'-m'} - (-1)^{m+m'} \Sigma_{l-ml'-m'} \}. \end{aligned} \quad (\text{E16})$$

- 
- [1] T. Regimbau, The astrophysical gravitational wave stochastic background, *Res. Astron. Astrophys.* **11**, 369 (2011), arXiv:1101.2762 [astro-ph.CO].
- [2] C. Wu, V. Mandic, and T. Regimbau, Accessibility of the Gravitational-Wave Background due to Binary Coalescences to Second and Third Generation Gravitational-Wave Detectors, *Phys. Rev. D* **85**, 104024 (2012), arXiv:1112.1898 [gr-qc].
- [3] X.-J. Zhu, E. Howell, T. Regimbau, D. Blair, and Z.-H. Zhu, Stochastic Gravitational Wave Background from Coalescing Binary Black Holes, *Astrophys. J.* **739**, 86 (2011), arXiv:1104.3565 [gr-qc].
- [4] X.-J. Zhu, E. J. Howell, D. G. Blair, and Z.-H. Zhu, On the gravitational wave background from compact binary coalescences in the band of ground-based interferometers, *Mon. Not. Roy. Astron. Soc.* **431**, 882 (2013), arXiv:1209.0595 [gr-qc].
- [5] P. A. Rosado, Gravitational wave background from binary systems, *Phys. Rev. D* **84**, 084004 (2011), arXiv:1106.5795 [gr-qc].
- [6] S. Marassi, R. Schneider, G. Corvino, V. Ferrari, and S. Portegies Zwart, Imprint of the merger and ring-down on the gravitational wave background from black hole binaries coalescence, *Phys. Rev. D* **84**, 124037 (2011), arXiv:1111.6125 [astro-ph.CO].
- [7] K. Crocker, V. Mandic, T. Regimbau, K. Belczynski, W. Gladysz, K. Olive, T. Prestegard, and E. Vangioni, Model of the stochastic gravitational-wave background due to core collapse to black holes, *Phys. Rev. D* **92**, 063005 (2015), arXiv:1506.02631 [gr-qc].
- [8] K. Crocker, T. Prestegard, V. Mandic, T. Regimbau, K. Olive, and E. Vangioni, Systematic study of the stochastic gravitational-wave background due to stellar core collapse, *Phys. Rev. D* **95**, 063015 (2017), arXiv:1701.02638 [astro-ph.CO].
- [9] V. Ferrari, S. Matarrese, and R. Schneider, Gravitational wave background from a cosmological population of core collapse supernovae, *Mon. Not. Roy. Astron. Soc.* **303**, 247 (1999), arXiv:astro-ph/9804259.
- [10] C.-J. Wu, V. Mandic, and T. Regimbau, Accessibility of the stochastic gravitational wave background from magnetars to the interferometric gravitational wave detectors, *Phys. Rev. D* **87**, 042002 (2013).
- [11] S. Marassi, R. Ciolfi, R. Schneider, L. Stella, and V. Ferrari, Stochastic background of gravitational waves emitted by magnetars, *Mon. Not. Roy. Astron. Soc.* **411**, 2549 (2011), arXiv:1009.1240 [astro-ph.CO].
- [12] P. D. Lasky, M. F. Bennett, and A. Melatos, Stochastic gravitational wave background from hydrodynamic turbulence in differentially rotating neutron stars, *Phys. Rev. D* **87**, 063004 (2013), arXiv:1302.6033 [astro-ph.HE].
- [13] V. Ferrari, S. Matarrese, and R. Schneider, Stochastic background of gravitational waves generated by a cosmological population of young, rapidly rotating neutron stars, *Mon. Not. Roy. Astron. Soc.* **303**, 258 (1999), arXiv:astro-ph/9806357.
- [14] X.-J. Zhu, X.-L. Fan, and Z.-H. Zhu, Stochastic Gravitational Wave Background from Neutron Star r-mode Instability Revisited, *Astrophys. J.* **729**, 59 (2011), arXiv:1102.2786 [astro-ph.CO].
- [15] T. Regimbau and J. A. de Freitas Pacheco, Cosmic background of gravitational waves from rotating neutron stars, *Astron. Astrophys.* **376**, 381 (2001), arXiv:astro-ph/0105260.
- [16] C. Caprini and D. G. Figueroa, Cosmological Backgrounds of Gravitational Waves, *Class. Quant. Grav.* **35**, 163001 (2018), arXiv:1801.04268 [astro-ph.CO].
- [17] A. A. Starobinskiĭ, Spectrum of relict gravitational radiation and the early state of the universe, *Soviet Journal of Experimental and Theoretical Physics Letters* **30**, 682 (1979).
- [18] R. Bar-Kana, Limits on direct detection of gravitational waves, *Phys. Rev. D* **50**, 1157 (1994), arXiv:astro-ph/9401050.
- [19] M. S. Turner, Detectability of inflation produced gravitational waves, *Phys. Rev. D* **55**, R435 (1997), arXiv:astro-ph/9607066.
- [20] T. Damour and A. Vilenkin, Gravitational radiation from cosmic (super)strings: Bursts, stochastic background, and observational windows, *Phys. Rev. D* **71**, 063510 (2005), arXiv:hep-th/0410222.
- [21] T. W. B. Kibble, Topology of Cosmic Domains and Strings, *J. Phys. A* **9**, 1387 (1976).
- [22] S. Sarangi and S. H. H. Tye, Cosmic string production towards the end of brane inflation, *Phys. Lett. B* **536**, 185 (2002), arXiv:hep-th/0204074.
- [23] X. Siemens, V. Mandic, and J. Creighton, Gravitational wave stochastic background from cosmic (super)strings, *Phys. Rev. Lett.* **98**, 111101 (2007), arXiv:astro-ph/0610920.
- [24] L. Marzola, A. Racioppi, and V. Vaskonen, Phase transition and gravitational wave phenomenology of scalar conformal extensions of the Standard Model, *Eur. Phys. J. C* **77**, 484 (2017), arXiv:1704.01034 [hep-ph].
- [25] B. Von Harling, A. Pomarol, O. Pujolàs, and F. Rompineve, Peccei-Quinn Phase Transition at LIGO, *JHEP* **04**, 195, arXiv:1912.07587 [hep-ph].
- [26] A. C. Jenkins, J. D. Romano, and M. Sakellariadou, Estimating the angular power spectrum of the gravitational-wave background in the presence of shot noise, *Phys. Rev. D* **100**, 083501 (2019), arXiv:1907.06642 [astro-ph.CO].
- [27] A. C. Jenkins and M. Sakellariadou, Shot noise in the astrophysical gravitational-wave background, *Phys. Rev. D* **100**, 063508 (2019), arXiv:1902.07719 [astro-ph.CO].
- [28] D. Alonso, G. Cusin, P. G. Ferreira, and C. Pitrou, Detecting the anisotropic astrophysical gravitational wave background in the presence of shot noise through cross-correlations, *Phys. Rev. D* **102**, 023002 (2020), arXiv:2002.02888 [astro-ph.CO].
- [29] G. Cusin, I. Dvorkin, C. Pitrou, and J.-P. Uzan, Properties of the stochastic astrophysical gravitational wave background: astrophysical sources dependencies, *Phys. Rev. D* **100**, 063004 (2019), arXiv:1904.07797 [astro-ph.CO].
- [30] K. Z. Yang, V. Mandic, C. Scarlata, and S. Banagiri, Searching for Cross-Correlation Between Stochastic Gravitational Wave Background and Galaxy Number Counts, *Mon. Not. Roy. Astron. Soc.* **500**, 1666 (2020), arXiv:2007.10456 [astro-ph.CO].
- [31] K. Z. Yang, J. Suresh, G. Cusin, S. Banagiri, N. Feist,

- V. Mandic, C. Scarlata, and I. Michaloliakos, Measurement of the cross-correlation angular power spectrum between the stochastic gravitational wave background and galaxy overdensity, *Phys. Rev. D* **108**, 043025 (2023), arXiv:2304.07621 [gr-qc].
- [32] G. Cusin, I. Dvorkin, C. Pitrou, and J.-P. Uzan, First predictions of the angular power spectrum of the astrophysical gravitational wave background, *Phys. Rev. Lett.* **120**, 231101 (2018), arXiv:1803.03236 [astro-ph.CO].
- [33] G. Capurri, A. Lapi, C. Baccigalupi, L. Boco, G. Scelfo, and T. Ronconi, Intensity and anisotropies of the stochastic gravitational wave background from merging compact binaries in galaxies, *JCAP* **11**, 032, arXiv:2103.12037 [gr-qc].
- [34] D. Alonso, M. Nikjoo, A. I. Renzini, E. Bellini, and P. G. Ferreira, Tomographic constraints on the production rate of gravitational waves from astrophysical sources, *Phys. Rev. D* **110**, 103544 (2024), arXiv:2406.19488 [astro-ph.CO].
- [35] D. Bertacca, A. Ricciardone, N. Bellomo, A. C. Jenkins, S. Matarrese, A. Raccanelli, T. Regimbau, and M. Sakellariadou, Projection effects on the observed angular spectrum of the astrophysical stochastic gravitational wave background, *Phys. Rev. D* **101**, 103513 (2020), arXiv:1909.11627 [astro-ph.CO].
- [36] B. Allen and A. C. Ottewill, Detection of anisotropies in the gravitational wave stochastic background, *Phys. Rev. D* **56**, 545 (1997), arXiv:gr-qc/9607068.
- [37] G. Cusin and G. Tasinato, Doppler boosting the stochastic gravitational wave background, *JCAP* **08** (08), 036, arXiv:2201.10464 [astro-ph.CO].
- [38] L. Valbusa Dall'Armi, A. Ricciardone, and D. Bertacca, The dipole of the astrophysical gravitational-wave background, *JCAP* **11**, 040, arXiv:2206.02747 [astro-ph.CO].
- [39] A. K.-W. Chung, A. C. Jenkins, J. D. Romano, and M. Sakellariadou, Targeted search for the kinematic dipole of the gravitational-wave background, *Phys. Rev. D* **106**, 082005 (2022), arXiv:2208.01330 [gr-qc].
- [40] G. Mentasti, C. R. Contaldi, and M. Peloso, Strong scale-dependence does not enhance the kinematic boosting of gravitational wave backgrounds (2025), arXiv:2507.16901 [astro-ph.CO].
- [41] S. Dhurandhar, H. Tagoshi, Y. Okada, N. Kanda, and H. Takahashi, The cross-correlation search for a hot spot of gravitational waves, *Phys. Rev. D* **84**, 083007 (2011), arXiv:1105.5842 [gr-qc].
- [42] N. Mazumder, S. Mitra, and S. Dhurandhar, Astrophysical motivation for directed searches for a stochastic gravitational wave background, *Phys. Rev. D* **89**, 084076 (2014), arXiv:1401.5898 [gr-qc].
- [43] D. Agarwal, J. Suresh, V. Mandic, A. Matas, and T. Regimbau, Targeted search for the stochastic gravitational-wave background from the galactic millisecond pulsar population, *Phys. Rev. D* **106**, 043019 (2022), arXiv:2204.08378 [gr-qc].
- [44] F. De Lillo, J. Suresh, and A. L. Miller, Stochastic gravitational-wave background searches and constraints on neutron-star ellipticity, *Mon. Not. Roy. Astron. Soc.* **513**, 1105 (2022), arXiv:2203.03536 [gr-qc].
- [45] D. Talukder, E. Thrane, S. Bose, and T. Regimbau, Measuring neutron-star ellipticity with measurements of the stochastic gravitational-wave background, *Phys. Rev. D* **89**, 123008 (2014).
- [46] B. Abbott *et al.* (LIGO Scientific), Upper limit map of a background of gravitational waves, *Phys. Rev. D* **76**, 082003 (2007), arXiv:astro-ph/0703234.
- [47] J. Abadie *et al.* (LIGO Scientific), Directional limits on persistent gravitational waves using LIGO S5 science data, *Phys. Rev. Lett.* **107**, 271102 (2011), arXiv:1109.1809 [astro-ph.CO].
- [48] B. P. Abbott *et al.* (LIGO Scientific, Virgo), Upper Limits on the Stochastic Gravitational-Wave Background from Advanced LIGO's First Observing Run, *Phys. Rev. Lett.* **118**, 121101 (2017), [Erratum: *Phys.Rev.Lett.* 119, 029901 (2017)], arXiv:1612.02029 [gr-qc].
- [49] B. P. Abbott *et al.* (LIGO Scientific, Virgo), Search for the isotropic stochastic background using data from Advanced LIGO's second observing run, *Phys. Rev. D* **100**, 061101 (2019), arXiv:1903.02886 [gr-qc].
- [50] R. Abbott *et al.* (KAGRA, Virgo, LIGO Scientific), Upper limits on the isotropic gravitational-wave background from Advanced LIGO and Advanced Virgo's third observing run, *Phys. Rev. D* **104**, 022004 (2021), arXiv:2101.12130 [gr-qc].
- [51] B. P. Abbott *et al.* (LIGO Scientific, Virgo), Directional Limits on Persistent Gravitational Waves from Advanced LIGO's First Observing Run, *Phys. Rev. Lett.* **118**, 121102 (2017), arXiv:1612.02030 [gr-qc].
- [52] B. P. Abbott *et al.* (LIGO Scientific, Virgo), Directional limits on persistent gravitational waves using data from Advanced LIGO's first two observing runs, *Phys. Rev. D* **100**, 062001 (2019), arXiv:1903.08844 [gr-qc].
- [53] R. Abbott *et al.* (KAGRA, Virgo, LIGO Scientific), Search for anisotropic gravitational-wave backgrounds using data from Advanced LIGO and Advanced Virgo's first three observing runs, *Phys. Rev. D* **104**, 022005 (2021), arXiv:2103.08520 [gr-qc].
- [54] R. Abbott *et al.* (KAGRA, Virgo, LIGO Scientific), All-sky, all-frequency directional search for persistent gravitational waves from Advanced LIGO's and Advanced Virgo's first three observing runs, *Phys. Rev. D* **105**, 122001 (2022), arXiv:2110.09834 [gr-qc].
- [55] S. W. Ballmer, A Radiometer for stochastic gravitational waves, *Class. Quant. Grav.* **23**, S179 (2006), arXiv:gr-qc/0510096.
- [56] S. Mitra, S. Dhurandhar, T. Souradeep, A. Lazzarini, V. Mandic, S. Bose, and S. Ballmer, Gravitational wave radiometry: Mapping a stochastic gravitational wave background, *Phys. Rev. D* **77**, 042002 (2008), arXiv:0708.2728 [gr-qc].
- [57] E. Thrane, S. Ballmer, J. D. Romano, S. Mitra, D. Talukder, S. Bose, and V. Mandic, Probing the anisotropies of a stochastic gravitational-wave background using a network of ground-based laser interferometers, *Phys. Rev. D* **80**, 122002 (2009).
- [58] K. Wette, Searches for continuous gravitational waves from neutron stars: A twenty-year retrospective, *Astropart. Phys.* **153**, 102880 (2023), arXiv:2305.07106 [gr-qc].
- [59] O. J. Piccinni, Status and Perspectives of Continuous Gravitational Wave Searches, *Galaxies* **10**, 72 (2022), arXiv:2202.01088 [gr-qc].
- [60] K. Riles, Searches for continuous-wave gravitational radiation, *Living Rev. Rel.* **26**, 3 (2023), arXiv:2206.06447 [astro-ph.HE].
- [61] R. Abbott *et al.* (LIGO Scientific, Virgo, KAGRA),

- All-sky search for gravitational wave emission from scalar boson clouds around spinning black holes in LIGO O3 data, *Phys. Rev. D* **105**, 102001 (2022), arXiv:2111.15507 [astro-ph.HE].
- [62] D. Jones, L. Sun, N. Siemonsen, W. E. East, S. M. Scott, and K. Wette, Methods and prospects for gravitational-wave searches targeting ultralight vector-boson clouds around known black holes, *Phys. Rev. D* **108**, 064001 (2023), arXiv:2305.00401 [gr-qc].
- [63] Directed searches for gravitational waves from ultralight vector boson clouds around merger remnant and galactic black holes during the first part of the fourth LIGO-Virgo-KAGRA observing run (2025), arXiv:2509.07352 [gr-qc].
- [64] A. G. Abac *et al.* (LIGO Scientific, VIRGO, KAGRA), Upper Limits on the Isotropic Gravitational-Wave Background from the first part of LIGO, Virgo, and KAGRA's fourth Observing Run (2025), arXiv:2508.20721 [gr-qc].
- [65] Ligo scientific, virgo, kagra collaborations, (in prep.).
- [66] J. D. Romano and N. J. Cornish, Detection methods for stochastic gravitational-wave backgrounds: a unified treatment, *Living Reviews in Relativity* **20**, 2 (2017).
- [67] P. A. R. Ade *et al.* (Planck), Planck 2015 results. XIII. Cosmological parameters, *Astron. Astrophys.* **594**, A13 (2016), arXiv:1502.01589 [astro-ph.CO].
- [68] A. Lazzarini and J. Romano, Use of Overlapping Windows in the Stochastic Background Search, <https://dcc.ligo.org/LIGO-T040089/public> (2004).
- [69] A. Ain, P. Dalvi, and S. Mitra, Fast Gravitational Wave Radiometry using Data Folding, *Phys. Rev. D* **92**, 022003 (2015), arXiv:1504.01714 [gr-qc].
- [70] P. F. Michelson, On detecting stochastic background gravitational radiation with terrestrial detectors, *Monthly Notices of the Royal Astronomical Society* **227**, 933 (1987), <https://academic.oup.com/mnras/article-pdf/227/4/933/3926536/mnras227-0933.pdf>.
- [71] N. Christensen, Measuring the stochastic gravitational-radiation background with laser-interferometric antennas, *Phys. Rev. D* **46**, 5250 (1992).
- [72] E. E. Flanagan, The Sensitivity of the laser interferometer gravitational wave observatory (LIGO) to a stochastic background, and its dependence on the detector orientations, *Phys. Rev. D* **48**, 2389 (1993), arXiv:astro-ph/9305029.
- [73] J. Suresh, A. Ain, and S. Mitra, Unified map-making for an anisotropic stochastic gravitational wave background, *Phys. Rev. D* **103**, 083024 (2021), arXiv:2011.05969 [gr-qc].
- [74] A. Ain, J. Suresh, and S. Mitra, Very fast stochastic gravitational wave background map making using folded data, *Phys. Rev. D* **98**, 024001 (2018), arXiv:1803.08285 [gr-qc].
- [75] K. M. Górski, E. Hivon, A. J. Banday, B. D. Wandelt, F. K. Hansen, M. Reinecke, and M. Bartelman, HEALPix - A Framework for high resolution discretization, and fast analysis of data distributed on the sphere, *Astrophys. J.* **622**, 759 (2005), arXiv:astro-ph/0409513.
- [76] P. D. Lasky, Gravitational Waves from Neutron Stars: A Review, *Publ. Astron. Soc. Austral.* **32**, e034 (2015), arXiv:1508.06643 [astro-ph.HE].
- [77] S. Panda, S. Bhagwat, J. Suresh, and S. Mitra, Stochastic gravitational wave background mapmaking using regularized deconvolution, *Phys. Rev. D* **100**, 043541 (2019).
- [78] A. I. Renzini and C. R. Contaldi, Gravitational Wave Background Sky Maps from Advanced LIGO O1 Data, *Phys. Rev. Lett.* **122**, 081102 (2019), arXiv:1811.12922 [astro-ph.CO].
- [79] A. Renzini and C. Contaldi, Improved limits on a stochastic gravitational-wave background and its anisotropies from Advanced LIGO O1 and O2 runs, *Phys. Rev. D* **100**, 063527 (2019), arXiv:1907.10329 [gr-qc].
- [80] D. Agarwal, J. Suresh, S. Mitra, and A. Ain, Upper limits on persistent gravitational waves using folded data and the full covariance matrix from Advanced LIGO's first two observing runs, *Phys. Rev. D* **104**, 123018 (2021), arXiv:2105.08930 [gr-qc].
- [81] L. Xiao, A. I. Renzini, and A. J. Weinstein, Model-independent search for anisotropies in stochastic gravitational-wave backgrounds and application to ligo-virgo's first three observing runs, *Phys. Rev. D* **107**, 122002 (2023).
- [82] B. Allen and J. D. Romano, Detecting a stochastic background of gravitational radiation: Signal processing strategies and sensitivities, *Phys. Rev. D* **59**, 102001 (1999), arXiv:gr-qc/9710117.
- [83] N. Kouvatsos, A. C. Jenkins, A. I. Renzini, J. D. Romano, and M. Sakellariadou, Unbiased estimation of gravitational-wave anisotropies from noisy data, *Phys. Rev. D* **109**, 103535 (2024).
- [84] J. Aasi *et al.* (LIGO Scientific), Advanced LIGO, *Class. Quant. Grav.* **32**, 074001 (2015), arXiv:1411.4547 [gr-qc].
- [85] B. P. Abbott *et al.*, Sensitivity of the Advanced LIGO detectors at the beginning of gravitational wave astronomy, *Phys. Rev. D* **93**, 112004 (2016), [Addendum: *Phys. Rev. D* **97**, 059901 (2018)], arXiv:1604.00439 [astro-ph.IM].
- [86] L. Nuttall *et al.*, Improving the Data Quality of Advanced LIGO Based on Early Engineering Run Results, *Class. Quant. Grav.* **32**, 245005 (2015), arXiv:1508.07316 [gr-qc].
- [87] B. P. Abbott *et al.* (LIGO Scientific, Virgo), Effects of data quality vetoes on a search for compact binary coalescences in Advanced LIGO's first observing run, *Class. Quant. Grav.* **35**, 065010 (2018), arXiv:1710.02185 [gr-qc].
- [88] P. B. Covas *et al.* (LSC), Identification and mitigation of narrow spectral artifacts that degrade searches for persistent gravitational waves in the first two observing runs of Advanced LIGO, *Phys. Rev. D* **97**, 082002 (2018), arXiv:1801.07204 [astro-ph.IM].
- [89] J. C. Driggers *et al.* (LIGO Scientific), Improving astrophysical parameter estimation via offline noise subtraction for Advanced LIGO, *Phys. Rev. D* **99**, 042001 (2019), arXiv:1806.00532 [astro-ph.IM].
- [90] D. Davis, T. J. Massinger, A. P. Lundgren, J. C. Driggers, A. L. Urban, and L. K. Nuttall, Improving the Sensitivity of Advanced LIGO Using Noise Subtraction, *Class. Quant. Grav.* **36**, 055011 (2019), arXiv:1809.05348 [astro-ph.IM].
- [91] A. Buikema *et al.* (aLIGO), Sensitivity and performance of the Advanced LIGO detectors in the third observing run, *Phys. Rev. D* **102**, 062003 (2020), arXiv:2008.01301 [astro-ph.IM].
- [92] M. Tse *et al.*, Quantum-Enhanced Advanced LIGO De-

- tectors in the Era of Gravitational-Wave Astronomy, *Phys. Rev. Lett.* **123**, 231107 (2019).
- [93] D. Davis *et al.* (LIGO), LIGO detector characterization in the second and third observing runs, *Class. Quant. Grav.* **38**, 135014 (2021), arXiv:2101.11673 [astro-ph.IM].
- [94] L. Sun *et al.*, Characterization of systematic error in Advanced LIGO calibration, *Class. Quant. Grav.* **37**, 225008 (2020), arXiv:2005.02531 [astro-ph.IM].
- [95] F. Acernese *et al.* (VIRGO), Advanced Virgo: a second-generation interferometric gravitational wave detector, *Class. Quant. Grav.* **32**, 024001 (2015), arXiv:1408.3978 [gr-qc].
- [96] F. Acernese *et al.* (Virgo), Increasing the Astrophysical Reach of the Advanced Virgo Detector via the Application of Squeezed Vacuum States of Light, *Phys. Rev. Lett.* **123**, 231108 (2019).
- [97] F. Acernese *et al.* (Virgo), Virgo detector characterization and data quality: results from the O3 run, *Class. Quant. Grav.* **40**, 185006 (2023), arXiv:2210.15633 [gr-qc].
- [98] F. Acernese *et al.* (Virgo), Virgo detector characterization and data quality: tools, *Class. Quant. Grav.* **40**, 185005 (2023), arXiv:2210.15634 [gr-qc].
- [99] S. Soni *et al.* (LIGO), LIGO Detector Characterization in the first half of the fourth Observing run, *Class. Quant. Grav.* **42**, 085016 (2025), arXiv:2409.02831 [astro-ph.IM].
- [100] E. Capote *et al.*, Advanced LIGO detector performance in the fourth observing run, *Phys. Rev. D* **111**, 062002 (2025), arXiv:2411.14607 [gr-qc].
- [101] D. Ganapathy *et al.* (LIGO O4 Detector), Broadband Quantum Enhancement of the LIGO Detectors with Frequency-Dependent Squeezing, *Phys. Rev. X* **13**, 041021 (2023).
- [102] W. Jia *et al.* (members of the LIGO Scientific<sup>†</sup>), Squeezing the quantum noise of a gravitational-wave detector below the standard quantum limit, *Science* **385**, 1318 (2024), arXiv:2404.14569 [gr-qc].
- [103] E. Thrane, S. Mitra, N. Christensen, V. Mandic, and A. Ain, All-sky, narrowband, gravitational-wave radiometry with folded data, *Phys. Rev. D* **91**, 124012 (2015), arXiv:1504.02158 [astro-ph.IM].
- [104] L. S. Collaboration, V. Collaboration, and K. Collaboration, Folded data for first three observing runs of advanced ligo and advanced virgo, 10.5281/zenodo.6326656 (2022).
- [105] C. Messenger, Understanding the sensitivity of the stochastic radiometer analysis in terms of the strain tensor amplitude, LIGO Document T1000195-v1 (2010).
- [106] C. Messenger *et al.*, Gravitational waves from Scorpius X-1: A comparison of search methods and prospects for detection with advanced detectors, *Phys. Rev. D* **92**, 023006 (2015), arXiv:1504.05889 [gr-qc].
- [107] R. Abbott *et al.* (LIGO Scientific, KAGRA, VIRGO), Narrowband Searches for Continuous and Long-duration Transient Gravitational Waves from Known Pulsars in the LIGO-Virgo Third Observing Run, *Astrophys. J.* **932**, 133 (2022), arXiv:2112.10990 [gr-qc].
- [108] A. G. Abac *et al.* (LIGO Scientific, VIRGO, KAGRA), Search for Continuous Gravitational Waves from Known Pulsars in the First Part of the Fourth LIGO-Virgo-KAGRA Observing Run, *Astrophys. J.* **983**, 99 (2025), arXiv:2501.01495 [astro-ph.HE].
- [109] R. Abbott *et al.* (KAGRA, LIGO Scientific, VIRGO), All-sky search for continuous gravitational waves from isolated neutron stars using Advanced LIGO and Advanced Virgo O3 data, *Phys. Rev. D* **106**, 102008 (2022), arXiv:2201.00697 [gr-qc].
- [110] R. Abbott *et al.* (KAGRA, VIRGO, LIGO Scientific), All-sky search for continuous gravitational waves from isolated neutron stars in the early O3 LIGO data, *Phys. Rev. D* **104**, 082004 (2021), arXiv:2107.00600 [gr-qc].
- [111] B. J. Owen, L. Lindblom, L. S. Pinheiro, and B. Rajbhandari, Improved Upper Limits on Gravitational-wave Emission from NS 1987A in SNR 1987A, *Astrophys. J. Lett.* **962**, L23 (2024), arXiv:2310.19964 [gr-qc].
- [112] R. Abbott *et al.* (KAGRA, LIGO Scientific, VIRGO), Search for continuous gravitational wave emission from the Milky Way center in O3 LIGO-Virgo data, *Phys. Rev. D* **106**, 042003 (2022), arXiv:2204.04523 [astro-ph.HE].
- [113] R. Abbott *et al.* (KAGRA, VIRGO, LIGO Scientific), Search for gravitational waves from Scorpius X-1 with a hidden Markov model in O3 LIGO data, *Phys. Rev. D* **106**, 062002 (2022), arXiv:2201.10104 [gr-qc].
- [114] R. Abbott *et al.* (LIGO Scientific, KAGRA, VIRGO), Model-based Cross-correlation Search for Gravitational Waves from the Low-mass X-Ray Binary Scorpius X-1 in LIGO O3 Data, *Astrophys. J. Lett.* **941**, L30 (2022), arXiv:2209.02863 [astro-ph.HE].
- [115] J. T. Whelan *et al.*, Search for Gravitational Waves from Scorpius X-1 in LIGO O3 Data with Corrected Orbital Ephemeris, *Astrophys. J.* **949**, 117 (2023), arXiv:2302.10338 [astro-ph.HE].
- [116] A. F. Vargas and A. Melatos, Search for gravitational waves from Scorpius X-1 with a hidden Markov model in O3 LIGO data with a corrected orbital ephemeris, *Phys. Rev. D* **111**, 084040 (2025), arXiv:2310.19183 [gr-qc].
- [117] E. Floden, V. Mandic, A. Matas, and L. Tsukada, Angular resolution of the search for anisotropic stochastic gravitational-wave background with terrestrial gravitational-wave detectors, *Phys. Rev. D* **106**, 023010 (2022).
- [118] R. Abbott *et al.* (LIGO Scientific, Virgo, KAGRA), Supplement– All-sky, all-frequency directional search for persistent gravitational waves from advanced LIGO’s and advanced Virgo’s first three observing runs (2021).
- [119] A. C. Jenkins, M. Sakellariadou, T. Regimbau, and E. Slezak, Anisotropies in the astrophysical gravitational-wave background: Predictions for the detection of compact binaries by LIGO and Virgo, *Phys. Rev. D* **98**, 063501 (2018), arXiv:1806.01718 [astro-ph.CO].
- [120] A. C. Jenkins, R. O’Shaughnessy, M. Sakellariadou, and D. Wysocki, Anisotropies in the astrophysical gravitational-wave background: The impact of black hole distributions, *Phys. Rev. Lett.* **122**, 111101 (2019).
- [121] G. Cusin, I. Dvorkin, C. Pitrou, and J.-P. Uzan, First predictions of the angular power spectrum of the astrophysical gravitational wave background, *Phys. Rev. Lett.* **120**, 231101 (2018).
- [122] A. C. Jenkins and M. Sakellariadou, Shot noise in the astrophysical gravitational-wave background, *Phys. Rev. D* **100**, 063508 (2019).
- [123] A. C. Jenkins and M. Sakellariadou, Anisotropies in the stochastic gravitational-wave background: Formalism

- and the cosmic string case, *Phys. Rev. D* **98**, 063509 (2018).
- [124] S. Venikoudis, F. De Lillo, K. Janssens, J. Suresh, and G. Bruno, Impact of correlated magnetic noise on directional stochastic gravitational-wave background searches, *Phys. Rev. D* **111**, 082005 (2025), arXiv:2411.11746 [gr-qc].
- [125] A. M. Knee, H. Du, E. Goetz, J. McIver, J. B. Carlin, L. Sun, L. Dunn, L. Strang, H. Middleton, and A. Melatos, Search for continuous gravitational waves directed at subthreshold radiometer candidates in O3 LIGO data, *Phys. Rev. D* **109**, 062008 (2024), arXiv:2311.12138 [gr-qc].
- [126] Z. Šidák and, Rectangular confidence regions for the means of multivariate normal distributions, *Journal of the American Statistical Association* **62**, 626 (1967), <https://doi.org/10.1080/01621459.1967.10482935>.
- [127] R. Kuehl, *Design of experiments: statistical principles of research design and analysis*, 2nd ed. (Pacific Grove (Calif.): Duxbury Press, 2000).
- [128] A. Matas and J. D. Romano, Frequentist versus Bayesian analyses: Cross-correlation as an approximate sufficient statistic for LIGO-Virgo stochastic background searches, *Phys. Rev. D* **103**, 062003 (2021), arXiv:2012.00907 [gr-qc].
- [129] J. Yousuf, S. Kandhasamy, and M. A. Malik, Effects of calibration uncertainties on the detection and parameter estimation of isotropic gravitational-wave backgrounds, *Phys. Rev. D* **107**, 102002 (2023), arXiv:2301.13531 [gr-qc].
- [130] J. T. Whelan, E. L. Robinson, J. D. Romano, and E. H. Thrane, Treatment of Calibration Uncertainty in Multi-Baseline Cross-Correlation Searches for Gravitational Waves, *J. Phys. Conf. Ser.* **484**, 012027 (2014), arXiv:1205.3112 [gr-qc].
- [131] J. Abadie *et al.* (LIGO Scientific, VIRGO), Upper limits on a stochastic gravitational-wave background using LIGO and Virgo interferometers at 600-1000 Hz, *Phys. Rev. D* **85**, 122001 (2012), arXiv:1112.5004 [gr-qc].
- [132] Y. Zhang, M. A. Papa, B. Krishnan, and A. L. Watts, Search for Continuous Gravitational Waves from Scorpius X-1 in LIGO O2 Data, *Astrophys. J. Lett.* **906**, L14 (2021), arXiv:2011.04414 [astro-ph.HE].
- [133] J. Papaloizou and J. E. Pringle, Gravitational radiation and the stability of rotating stars, *Mon. Not. Roy. Astron. Soc.* **184**, 501 (1978).
- [134] L. Bildsten, Gravitational radiation and rotation of accreting neutron stars, *Astrophys. J. Lett.* **501**, L89 (1998), arXiv:astro-ph/9804325.
- [135] S. Galaudage, K. Wette, D. K. Galloway, and C. Messenger, Deep searches for X-ray pulsations from Scorpius X-1 and Cygnus X-2 in support of continuous gravitational wave searches, *Mon. Not. Roy. Astron. Soc.* **509**, 1745 (2021), arXiv:2105.13803 [astro-ph.HE].
- [136] A. Mukherjee, C. Messenger, and K. Riles, Accretion-induced spin-wandering effects on the neutron star in Scorpius X-1: Implications for continuous gravitational wave searches, *Phys. Rev. D* **97**, 043016 (2018), arXiv:1710.06185 [gr-qc].
- [137] V. Dergachev, M. A. Papa, B. Steltner, and H.-B. Eggenstein, Loosely coherent search in LIGO O1 data for continuous gravitational waves from Terzan 5 and the galactic center, *Phys. Rev. D* **99**, 084048 (2019), arXiv:1903.02389 [gr-qc].
- [138] O. J. Piccinni, P. Astone, S. D'Antonio, S. Frasca, G. Intini, I. La Rosa, P. Leaci, S. Mastrogiovanni, A. Miller, and C. Palomba, Directed search for continuous gravitational-wave signals from the Galactic Center in the Advanced LIGO second observing run, *Phys. Rev. D* **101**, 082004 (2020), arXiv:1910.05097 [gr-qc].
- [139] L. Sun, A. Melatos, P. D. Lasky, C. T. Y. Chung, and N. S. Darman, Cross-correlation search for continuous gravitational waves from a compact object in SNR 1987A in LIGO Science Run 5, *Phys. Rev. D* **94**, 082004 (2016), arXiv:1610.00059 [gr-qc].
- [140] C. Chung, A. Melatos, B. Krishnan, and J. T. Whelan, Designing a cross-correlation search for continuous-wave gravitational radiation from a neutron star in the supernova remnant SNR 1987A, *Mon. Not. Roy. Astron. Soc.* **414**, 2650 (2011), arXiv:1102.4654 [gr-qc].
- [141] C. Fransson *et al.*, Emission lines due to ionizing radiation from a compact object in the remnant of Supernova 1987A, *Science* **383**, 898 (2024), arXiv:2403.04386 [astro-ph.HE].
- [142] E. Vitral and G. A. Mamon, Does ngc 6397 contain an intermediate-mass black hole or a more diffuse inner subcluster?, *Astronomy & Astrophysics* **646**, A63 (2021).
- [143] E. Vitral, K. Kremer, M. Libralato, G. A. Mamon, and A. Bellini, Stellar graveyards: clustering of compact objects in globular clusters NGC 3201 and NGC 6397, *Mon. Not. Roy. Astron. Soc.* **514**, 806 (2022), arXiv:2202.01599 [astro-ph.GA].
- [144] R. N. Manchester, G. B. Hobbs, A. Teoh, and M. Hobbs, The australia telescope national facility pulsar catalogue, *The Astronomical Journal* **129**, 1993 (2005).
- [145] T. D. Abbott *et al.* (LIGO Scientific, VIRGO), Search for continuous gravitational waves from neutron stars in globular cluster NGC 6544, *Phys. Rev. D* **95**, 082005 (2017), arXiv:1607.02216 [gr-qc].
- [146] B. P. Abbott *et al.* (LIGO Scientific, Virgo), Supplement–directional limits on persistent gravitational waves from advanced ligo’s first observing run, LIGO Document LIGO-P1600259 (2017).
- [147] B. J. Owen, L. Lindblom, and L. S. Pinheiro, First Constraining Upper Limits on Gravitational-wave Emission from NS 1987A in SNR 1987A, *Astrophys. J. Lett.* **935**, L7 (2022), arXiv:2206.01168 [gr-qc].
- [148] V. Mandic, Marginalizing over calibration uncertainties with gaussian priors, *Stochastic-alog* (2006).
- [149] J. Romano, Marginalizing over calibration uncertainty when there are multiple baselines, *Stochastic-alog* (2006).
- [150] E. Thrane and J. D. Romano, Sensitivity curves for searches for gravitational-wave backgrounds, *Phys. Rev. D* **88**, 124032 (2013).
- [151] M. W. Eastwood, M. M. Anderson, R. M. Monroe, G. Hallinan, B. R. Barsdell, S. A. Bourke, M. A. Clark, S. W. Ellingson, J. Dowell, H. Garsden, L. J. Greenhill, J. M. Hartman, J. Kocz, T. J. W. Lazio, D. C. Price, F. K. Schinzel, G. B. Taylor, H. K. Vedantham, Y. Wang, and D. P. Woody, The radio sky at meter wavelengths: m-mode analysis imaging with the ovro-lwa, *The Astronomical Journal* **156**, 32 (2018).
- [152] Sardarabadi, Ahmad Mouri, Leshem, Amir, and van der Veen, Alle-Jan, Radio astronomical image formation using constrained least squares and krylov subspaces, *A&A* **588**, A95 (2016).

- [153] F. S. Kitaura and T. A. Enßlin, Bayesian reconstruction of the cosmological large-scale structure: methodology, inverse algorithms and numerical optimization, *Monthly Notices of the Royal Astronomical Society* **389**, 497 (2008), <https://academic.oup.com/mnras/article-pdf/389/2/497/2942479/mnras0389-0497.pdf>.